University of Alberta

Characterization of the *cag* Type IV Secretion System and Unique Filaments of *Helicobacter pylori*

By

Marc Roger Couturier

A thesis submitted to the Faculty of Graduate Studies and Research in partial fulfillment of the requirements for the degree of Doctor of Philosophy

in

Bacteriology

Department of Medical Microbiology and Immunology

Edmonton, Alberta
Fall, 2008

Your file Votre référence
ISBN: 978-0-494-46301-7
Our file Notre référence
ISBN: 978-0-494-46301-7

"I preferred to believe my eyes, not the medical textbooks of the medical fraternity."

– Dr. Robin Warren, in regards to identifying *Helicobacter pylori*

Abstract

Helicobacter pylori is a human gastric pathogen with world-wide infection rates approaching 50%. The organism is responsible for gastritis, ulcers, and gastric cancers. *H. pylori* produces several surface structures including type IV secretion systems (T4SS), pilus-like structures that are ancestrally derived from the conjugation apparatus. The *cag* T4SS is implicated in severe disease development *via* secretion of the CagA cytotoxin into eukaryotic cells. Unlike most T4SSs, the *cag* system appears more complex, requiring several additional proteins that show no similarity to any sequenced proteins. Basic biochemical analysis was employed to characterize and assign preliminary function to a subset of these unknown *cag* T4SS proteins.

The CagF protein encoded in the CagI region of the *cag* pathogenicicty island is an inner membrane and cytosolic protein that is required for CagA translocation. CagF interacts with both termini of the effector protein CagA at the inner membrane and likely acts to deliver CagA to the T4SS in a chaperone-like manner. CagF further interacts with a coupling protein and it is not required for pilus structural assembly. CagF therefore has been assigned a modified chaperone-like function.

CagD, also a CagI region protein, is absolutely necessary for CagA secretion and is involved in pilus assembly. CagD localizes to the cytoplasm/periplasm and inner membrane as well as the eukaryotic cell membrane and culture supernatant. CagD is also detected by immunofluorescence microscopy as punctuate foci around the bacterial membrane. The crystal structure of CagD reveals a dimer stabilized by two separate disulphide bonds. The structure is unique, with limited similarity toward other solved structures and therefore no tentative function has been assigned to CagD.

Immunofluorescence and scanning electron microscopy were used to investigate and describe bacterial filaments observed during *H. pylori* infection of eukaryotic cells. Neither the T4SS nor flagellum could be attributed to the filaments. Filaments increase in number as bacteria progressively convert from helicoid to coccoid morphology. The filaments are partially composed of mannose-linked carbohydrates and recognition by convalescent human serum suggests *in vivo* relevance. In conclusion, this thesis characterizes two unique *cag* proteins as well as a unique surface structure in *H. pylori*.

Acknowledgments

I would like the thank my supervisor Dr. Markus Stein for not only taking a chance on a microbial ecology student with no molecular biology experience, but also for showing a great deal of patience in teaching me the this overwhelming field. I also want to thank Dr. Stein for giving me the guidance in the early stages to learn, and then trusting me to work autonomously once I felt comfortable in such a capacity. I felt throughout my tenure in the lab that I worked with Dr. Stein and not under him, and this was an environment which I am grateful to him for promoting in his laboratory.

I would also like to thank my advisory committee (past and present): Dr. Hien Huynh, Dr. Bart Hazes, Dr. Larry Guilbert, and Dr. Diane Taylor. Your insight and advice was always helpful and made me think outside of my *Helicobacter*/type IV secretion system mindset. I also appreciate the patience and open-mindedness you showed whenever I decided to change the direction of my project on a bi-annual basis. To Dr. Taylor; your guidance and advice throughout all aspects of my degree were invaluable and I cannot thank you enough for your support. I would also like to thank Dr. Judy Gnarpe for her friendship and advice in both teaching philosophy and clinical microbiology. I always enjoyed our discussions and value your honesty and integrity. I would also like to thank Dr. Stefan Pukatzki and Dr. Francis Nano for joining the examining committee for the final step in this academic journey.

To all my friends back east (especially Kyle Morgan, Jeremy Wentzell, and Stephen Winfield) who helped guide me through undergraduate studies, I thank you for all your friendship, support, and motivation. To my friends in Edmonton who made life bearable, your social therapy cannot go unnoticed, you know who you are. I especially want to thank James Gunton for taking me under his wing in both the lab and in life. I learned a great deal from you as both a researcher and a father.

To my family; there are multiple facets. The Wagner family who took me in when I arrived in Edmonton and for making me feel like part of the family, words cannot express how deeply touched I am to be a part of such a wonderful family. No matter how far my journey takes me, I will always know where my Edmonton home lies. To Margaret Wallwin, who took me in as not only a son-in-law, but as a great friend: thank you for all your support, care, and trust. To the Couturier family, especially my parents Roger and Lucille, I cannot begin to thank you enough for all your support and understanding over the past 9 years. With each successive move I have pushed further from the home I love and the people I care about. There were days I wasn't sure I would even live to see my high school graduation; but your support gave me the strength and optimism to get where I am today. I love you all so much, and know that all my accomplishments are a reflection of your support.

Finally, to my wife Brianne. How can I begin to even put in words how happy you have made me? My love for you is immeasurable. I am so grateful to have a wife and best friend who understands, encourages, and helps guide me when I'm losing my way. You have a beautiful soul, body, and mind that inspire me and make me a better man. Without you, I am a lost…but with you, all things seem possible. The future is bright and exciting for us. I look forward to the next step in our adventure…wherever it may lead. I hope you know; I am truly proud of you, and proud to have you as my wife.

TABLE OF CONTENTS

LIST OF TABLES

LIST OF FIGURES

List of Abbreviations

ANOVA	analysis of variance
Ap/amp	ampicillin
ATP	adenosine-5'-triphosphate
ATPase	adenosine-5'-triphosphate dephosphorylase
BB	Brucella broth
BME	β-mercaptoethanol
Bp	base pair
BSA	bovine serum albumin
BLAST	Basic Local Assignment Search Tool
C-	carboxy
cag	cytotoxicity associated gene
$CagA^{PY}$	phosphorylated CagA
Cm/cam	chloramphenicol
ConA	concanavalin A
CV	column volume
DBA	*Dolichos biflorus* agglutinin
DC-SIGN	dendritic cell-specific surface receptor C-type lectin ICAM-3-grabbing nonintegrin
DNA	deoxyribonucleic acid
DSP	dithiobis (succinimidyl propionate)
EDTA	ethylene diamine tetraacetic acid
FAK	focal adhesion kinase
FBS	fetal bovine serum
GDP	guanosine-5'-diphosphate
GSK	glycogen synthase kinase
GTPase	guanosine-5'-triphosphate hydrolase
HEPES	4-(2-hydroxyethyl)-1-piperazineethanesulfonic acid
HRP	horseradish peroxidase
HP-NAP	neutrophil activating protein

IL	interleukin
INF	interferon
IP	immunoprecipitation
JAM	junctional adhesion molecule
Km/kan	kanamycin
kan/sac	kanamycin levansucrase gene cassette
LB	Luria Bertani broth
MALT	mucosa-associated lymphoid tissue
MOI	multiplicity of infection
N-	amino
NF-κB	nuclear factor kappa B
NP-40	nonyl phenoxylpolyethoxylethanol 40
NTP	nucleotide triphosphate
OD	optical density
orf	open reading frame
PAI	pathogenicity island
PBS	phosphate buffered saline
PCR	polymerase chain reaction
PET	polyethylene terehthalate
pI	isoelectric point
PMN	polymorphonuclear leukocyte
PNA	Peanut agglutinin
PMSF	phenylmethanesulphonyl fluoride
PVDF	polyvinylidene fluoride
RCA_{120}	*Ricinus communis* agglutinin 120
RIPA	radio immunoprecipitation assay
RPM	revolutions per minute
RPMI	Roswell Park Memorial Institute
SBA	Soy bean agglutinin
SDS-PAGE	sodium dodecyl sulfate polyacrylamide gel electrophoresis
SEM	scanning electron microscopy

SH2	Src homology domain 2
SFK	Src family kinase
Tc	tetracycline
T_h	T-cell helper
TLR	toll-like receptor
TNF	tumor necrosis factor
T3SS	type III secretion system
T4SS	type IV secretion system
UEAI	*Ulex europaeus* agglutinin I
VBNC	viable-but-not-culturable
WGA	Wheat germ agglutinin
WT	wild type
ZO-1	zonula occludens protein 1

Chapter 1

General Introduction

1. Introduction

1.1 *Helicobacter pylori*

In 1875, scientists in Germany documented spiral shaped bacteria in the human stomach that were unable to be cultured in the laboratory (29, 122). This observation may have served as the first meeting between scientific researchers and *Helicobacter pylori* (*H. pylori*). Over the course of the next century, scientists across the world documented findings of spirochete-like organisms associated with human, canine, and primate stomachs (122). *H. pylori* was later identified and cultured from the stomach of patients with gastritis and peptic ulcers in 1984; a discovery that culminated in a Nobel Prize in Medicine and Physiology for Dr.'s Barry Marshall and Robin Warren (136). A global subject of intense ongoing research, *H. pylori* is thought to infect roughly half of the world's population, with disproportionately high infection rates in Asia, Africa, and South America (62, 98).

H. pylori is a Gram-negative, microaerophilic bacteria which belongs to the Epsilonproteobacteria class of bacteria and the order Campylobacterales. Originally misidentified as a *Campylobacter* species (*Campylobacter pyloridis* and *Campylobacter pylori*), genome sequencing lead to the reclassification of *H. pylori* into its own genus, *Helicobacter* (174). *H. pylori* is largely considered a human-only pathogen, however it does infect other primates as well (129). It is unknown whether a true zoonotic/environmental reservoir exists or whether transmission occurs directly from host-to-host. Several other species of *Helicobacter* have been identified to date and can cause varying disease symptoms within the human host (*e.g. H. fennelliae, H. cinaedi, H. heilmannii, H. pullorum, H. canadensis*), while others are awaiting final classification as

distinct species (39, 88, 137, 203, 217). A major complication with the classification of *Helicobacter* species is the overall genetic diversity of the organisms. *H. pylori* genomes show immense plasticity, resulting in significant polymorphisms occurring among strains, as well as isolates of a single strain (178). In fact, it is suggested that each isolate of *H. pylori* represents a unique strain due to non-clonal microevolution within a host (30). This strain variant diversity has been implicated in the overall ability of *H. pylori* to colonize and establish persistent infections within a host over long periods of time (30).

1.2 Morphological states of *H. pylori*

H. pylori is typically described as a spiral-shaped organism or a "helicoid". As a result of this morphology, early investigators mistook the bacteria for spirochete type organisms or *Vibrio* species (122). Helicoid bacteria are considered to comprise the "normal" morphology of the organism and predominate in exponential culture growth and gastric biopsy samples (151). Helicoid organisms are typically between one and three micrometers in length, possess a cluster of polar flagella, and are visibly motile in liquid media, moving in a "cork-screw" motion (152). Helicoid bacteria are commonly attributed to the disease state due to their abundance both *in vitro* and *in vivo*.

The second morphological manifestation of *H. pylori* is termed the "coccoid" morphology, designated as such by its drastically different spherical morphology in comparison to the helicoids. Coccoid bacteria are one or two micrometers in diameter, sometimes possess flagella (which wrap around the bacteria), are generally considered non-motile, and can be found both *in vitro* and *in vivo* (51, 56, 177, 180). When visualized in a culture, the two morphologies are hardly recognizable as the same

organism. Conversion to the coccoid morphology is achieved through a rearrangement of the membranes as well as a change in the lipid profile that is still poorly understood (24, 177, 198). This dramatic conversion process has been documented over time using electron microscopy, revealing a stepwise invagination of the membrane followed by loss of helicoid morphology, and eventual formation of a spherical body (177). The coccoid conversion process has been observed during stationary growth phase as well as during conditions of stress (177, 180). Stress conditions such as temperature downshift (47, 149, 169), nutrient starvation (47), osmotic stress (16, 169), oxygen tension (76, 159), nitric oxide increase (59), and certain antibiotics (196) can contribute to the development of coccoids. Coccoid forms of *H. pylori* cannot currently be revived in standard laboratory culture and as a result are referred to as viable-but-not-culturable (VBNC). However, several lines of investigation have suggested that coccoid *H. pylori* can colonize and cause infection in mice (46, 195).

Two proteins have been directly linked to the coccoid conversion process: AmiA and SpoT. The AmiA protein was identified as an essential factor for coccoid conversion and immune evasion. In the absence of AmiA, the coccoid morphology was not detected (53). The SpoT protein was identified as a stress-response regulator that was necessary for the coordinated conversion of helicoids to coccoids (144). In the absence of SpoT, coccoid conversion is rapid and uncontrolled, leading to cell death. These observations lead to the hypothesis that coccoids represent a persistant state of *H. pylori*. Therefore, it is plausible that the coccoid state serves as a "spore-like" stress-induced survival mechanism for transmission between hosts and/or a factor contributing to long-term

survival and persistence in the stomach. Both morphologies likely play distinct roles in the development of colonization and disease in the host.

1.3 Disease implications

1.3.1 Disease states

Chronic infection with *H. pylori* has been associated with a wide variety of human diseases. In a majority of infected individuals (often over 90%), low level inflammation or no symptoms are detected, and therefore the infection largely goes undiagnosed (7). A second subset of infected individuals displays chronic inflammation of the gastric mucosa and/or duodenal ulceration. This disease state is characterized primarily by antral gastritis, elevated gastrin, and uncontrolled (elevated) acid secretion (83). The third state of *H. pylori*-related disease is directly related to gastric cancer development. Both gastric adenocarcinoma and mucoid associated lymphoid tissue (MALT) type lymphoma have been associated with *H. pylori* infection, however less than one percent of chronically infected patients develop these severe conditions (160, 225). This disease state is typically characterized by corpus gastritis, multi-focal atrophic gastritis, high gastrin, and hypo- or achlorhyrdia (82). The chronic inflammation and duodenal ulceration state is thought to be protective against development of gastric cancer since achlorydia (a major risk factor for gastric cancer) cannot typically develop (129).

1.3.2 Immune response

Infection with *H. pylori* is combated primarily with a cell-mediated immune response rather than a humoral immune response seen with most mucosal pathogens

(Figure 1-1). Initial recognition of the bacterium is thought to be achieved by toll-like receptors (TLR) 2, 4, and 5 (129). Recognition by these receptors induces NF-κB activation which leads to the recruitment of neutrophils and monocytes (including macrophages and dendritic cells) (150). Chemokine expression is also upregulated through TLR signaling, including IL-8 which is implicated in specifically recruiting neutrophils to the site of infection, an effect amplified by the HP-NAP protein (see section 1.4.2) and CagA (see section 1.4.3). The recruitment of macrophages in particular, results in massive TNF-α, IL-1β, IL-12, and IL-23 induction (167). TNFα and IL-1β both drive a proinflammatory environment as they are potent proinflammatory cytokines. IL1β is also the most potent inhibitor of acid production, and therefore elevated IL-1β levels function to increase inflammation at the site of infection as well as induce hypochlorhydria (129). Elevated IL-12 production stimulates IFN-γ release in T helper cells, which inhibits the release of IL-4 from T helper cells, and blocks the development of T_h2 cells (129). Compounding this effect, elevated IL-23 (released by macrophages and neutrophils) further drives an inflammatory response through T-cell activation in a proinflammatory nature (41). This overwhelming bias of T_h1 cytokines results in a polarized T_h1 environment (129). As a result of the increased proinflammatory cytokine production, chronic inflammation with decreased acid production is achieved. This environment plays a key role in determining the fate of the disease progression.

H. pylori is also thought to interfere with antigen presentation by dendritic cells, possibly by binding DC-SIGN with Lewis Antigens on the LPS (see section 1.4.1 for

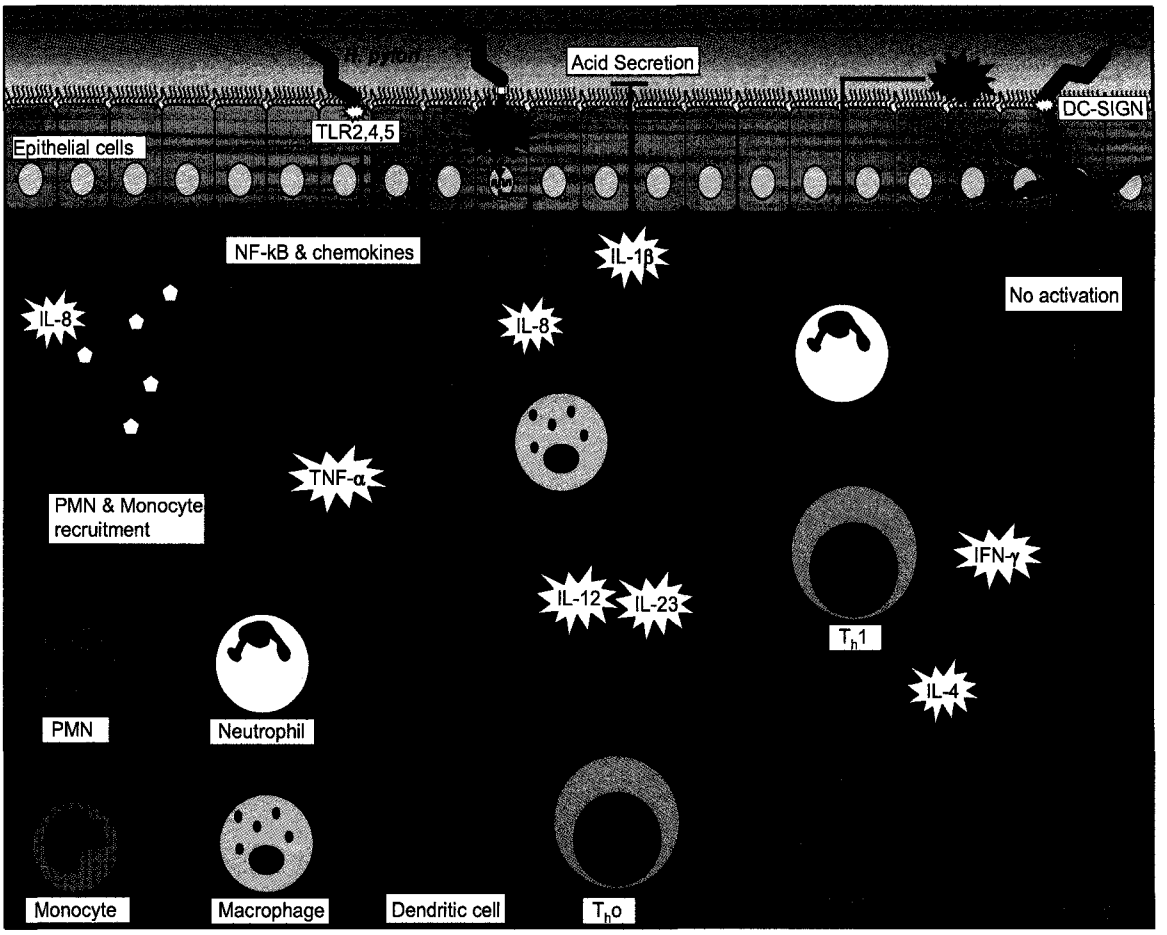

Figure 1-1. The proinflammatory immune response induced and maintained by *H. pylori*. Through direct contact and secreted proteins, *H. pylori* induces proinflammatory effects on gastric epithelial cells. PMNs and monocytes are recruited to the site of infection, which leads to the production of potent proinflammatory cytokines such as IL-8, IL-1β, IL-12, IL-23, and TNFα. The proinflammatory environment, combined with modulation of T-cell, B-cell, and dendritic cell activity leads to a polarized T_h1 response and an impaired humoral response. This overall response yields chronic inflammation in the stomach.

Lewis Antigens) (26). As a result, T and B cells are not activated by the dendritic cells. As a result, the humoral response is often limited in *H. pylori* infections. Due to the skewed proinflammatory response, sterilizing immunity does not occur, antigen recognition is impaired, and as a result the infection is allowed to persist long after the immune assault ceases.

1.3.3 Risk factors

Host polymorphisms, in addition to environmental factors such as smoking and dietary deficiencies have also been implicated in the development of the more severe pathology (7). For example IL-1β polymorphisms resulting in high levels of IL-1β expression have been associated with an increased risk for gastric cancer development when compounded with chronic *H. pylori* infection (129). VacA and/or *cag* pathogenicity island (*cag*-PAI) positive strains of *H. pylori* have also been implicated in the development of more severe pathology, especially when combined with specific host polymorphisms (7, 50, 227). Due to this severe pathology state associated with chronic *H. pylori* infection, the World Health Organization has designated *H. pylori* the only bacterial carcinogen (1).

1.4 Virulence factors

H. pylori possesses an array of virulence-associated factors including, flagella, acid neutralizing enzymes (urease operon), adhesins (BabA, SabA), lipopolysacharide (LPS, Lewis antigens), the neutrophil activating protein (HP-NAP), vacoulating cytotoxin (VacA), CagA, and the *cag*-PAI (66, 129).

1.4.1 Colonization factors

The three to five micrometer flagella represent the first bacterial surface structure identified on *H. pylori* (96). The flagella provide a rotational force to mediate movement through the viscous gastric mucosa (152). The structures appear in mono-polar clusters of two to six and are coated in a sheath-like structure composed of proteins and LPS (97). The sheath is thought to be a continuation of the outer membrane and sometimes covers the entire flagellum (97). There are two flagellin subunits, each immunogenic, however due to the sheath, *H. pylori* is weakly recognized by the highly specific TLR5 (9, 80). At the distal end of *H. pylori* flagella is a paddle-like structure that has yet to be identified, but appears unique to the *H. pylori* flagellum (152). Flagella are thought to use hydrogen ions for proton motive force and subsequent chemotaxis toward the mucosa (233). The urease operon encodes functional urease enzymes that indirectly neutralize hydrochloric acid. This occurs *via* urease-mediated breakdown of urea into carbon dioxide and ammonia, the latter which functions to neutralize the hydrochloric acid, allowing survival in the acidic lumen of the stomach (129).

Once bacteria reach the gastric epithelium, the BabA and SabA outer membrane proteins (adhesins) facilitate binding to the eukaryotic cell (129). The LPS of *H. pylori* displays fucosylated oligosaccharide antigens (Lewis antigens) that structurally and immunologically resemble the human blood group antigens and may also be involved in cell binding (26, 129). The LPS of *H. pylori* as a result is a poor antagonist of the innate immune response, and likely the Lewis antigens act to evade the immune response rather

than antagonize an autoimmune response (129). This short-term immune evasion may play a role in the immediate colonization process, however it remains unclear.

1.4.2 HP-NAP and VacA: Pro-inflammatory molecules

HP-NAP is a dodecameric protein with a total molecular weight of 150 kDa. The protein possesses a large central cavity, similar to bacteriferritin, with iron binding detected *in vitro* (66, 216). As the name would suggest (neutrophil activating protein), neutrophils as well as monocytes and dendritic cells are attracted/activated by HP-NAP. The activation leads to dramatic mRNA upregulation and secretion of cytokines, including IL-12, IL-23, and TNFα. It is thought that activation of neutrophils and monocytes in this manner further leads to a skew toward a polarized Th1 immune response (66). HP-NAP is a key factor in inflammation by *H. pylori* and its activity is likely compounded by both bacterial and host polymorphisms.

The vacuolating cytotoxin is one of the best described virulence factors of *H. pylori* and is present in roughly 50% of cultured strains. The toxin is implicated in peptic ulceration and forms massive vacuolation of tissue culture cells *in vitro* (13, 64, 129). This vacuolation is mediated by the activation of the small GTPase rab7 (158). The VacA toxin also plays other roles including: forming membrane channels that lead to the release of nutrients to the extracellular space, interfering with endosomal and lysosomal activity, inducing apoptosis, inhibiting T-cell activation and proliferation, and initiating the proinflammatory response (129). VacA and HP-NAP together enhance the effects of inflammation induced by *H. pylori* during infection.

1.4.3 The effector molecule: CagA

CagA remains the only known effector molecule translocated by the *cag* T4SS. CagA was first described as a 128 kDa antigenic protein from *H. pylori* that caused cytotoxic effects in eukaryotic cells as well as duodenal ulceration (63). Subsequent investigations determined the protein was varied in size and was injected into the host cells by a T4SS encoded in the *cag*-PAI (12, 185, 205). After translocation into the host cells, CagA is phosphorylated on multiple tyrosine residues contained in repetitive EPIYA motifs (19, 204). Different strains of *H. pylori* possess different CagA polymorphisms in the EPIYA regions, leading to variable effects on the host (105). The number and arrangement of motifs has been directly linked to pathogenic state and further led to the grouping of CagA into western and eastern types (varying in the third EPIYA motif). CagA phosphorylation is of paramount importance as it elicits a wide array of effects on the host. CagA phosphorylation is mediated by Src family kinase (SFK) and Abl kinase (c-Abl and Arg) (166, 188, 204, 209). Independent of phosphorylation, the EPIYA motifs also act as membrane targeting motifs for the protein when inside the eukaryotic cell (108). The major functions of CagA typically depend on phosphorylation state. Actin cytoskeleton effects elicited by CagA are largely dependent on phosphorylated CagA ($CagA^{PY}$), whereas the non-phosphorylated CagA affects tight and adherens junctions, cell polarity, and the proinflammatory response.

CagA modulates cytoskeletal rearrangement and cell morphology in the phosphorylated form by interacting with phosphotyrosine-binding domains such as the Src homology domain 2 (SH2). Three SH2 class proteins (SHP-2, Csk, and Crk) are known to interact with $CagA^{PY}$, leading to cytoskeletal rearrangement and the hallmark

"hummingbird phenotype", characterized by cell scattering, cytoskeletal rearrangement, and elongation (106, 185, 208, 218). The hummingbird phenotype is thought to be largely triggered by SHP-2 phosphatase (a cellular oncogene) activated by $CagA^{PY}$, which leads to induction of the MAP/MEK/ERK signaling pathways (171). The $CagA^{PY}$-SHP-2 interaction further contributes to eukaryotic cellular elongation by inactivating and dephosphorylating focal adhesion kinase (FAK) (219). Furthermore, $CagA^{PY}$ induces cytoskeletal elongation by dephosphorylating the actin binding proteins ezrin, vinculin, and cortactin (140, 187, 189).

Tight junctions and adherens junctions are both disrupted by CagA, independent of phosphorylation, and depend on several proteins. First, the tight junction scaffolding protein, zonula occludens protein 1 (ZO-1) and the transmembrane protein, junctional adhesion molecule (JAM) associate with CagA (though a direct interaction has not been reported), leading to tight junction assembly at the site of *H. pylori* attachment rather than the lateral cell-cell boundary (8). This in turn leads to disruption of the apical junction complex of the cells. CagA also interacts directly with E-cadherin at the adherens cell junctions, leading to disassociation of the junction integrity. Importantly, CagA indirectly activates nuclear translocation of β-catenin which when accumulated, leads to transcriptional upregulation of mitogenic genes that are implicated in carcinogenesis (89). Adherens junction disruption and mitogenic upregulation can be linked in CagA mediated carcinogenesis, as β-catenin is released from E-cadherin at adherens junctions by CagA (89). These effects of CagA result in pools of cytoplasmic and nuclear β-catenin which act to amplify the mitogenic response (146).

CagA binds the polarity associated kinase, PAR1, and inhibits its activity, leading to a subsequent loss in cell polarity (175, 237). PAR1 is a multimeric membrane protein and CagA as a result of binding PAR1 multimerizes within the host cell membrane. It is thought that CagA multimerization is conferred by a domain proximal to the EPIYA motifs (170).

As was described in section 1.3, *H. pylori* can activate NF-κB in gastric epithelial cells, leading to PMN recruitment and a proinflammatory environment. CagA can further amplify this basal effect by binding directly to Grb-2, an effector of the small GTPase H-Ras (35). This in turn leads to signaling through the Ras,Raf, MEK, ERK pathway for NF-κB activation and further PMN recruitment (35). CagA is also thought to induce cyclin D1 expression, further interrupting the natural cell cycle (52). Pairing the *in vitro* role of CagA in both cellular morphologic and transcriptional effects with the *in vivo* evidence that transgenic expression of CagA causes neoplasms in mice (156); the pre-cancerous lesions commonly associated with gastric carcinogenesis strongly implicate an *H. pylori* CagA-dependent carcinogenic effect (102).

The final virulence factor of *H. pylori* that is of particular interest is the *cag* type IV secretion system (T4SS), encoded by the *cag*-PAI. The *cag*-PAI encodes a functional T4SS as well as the cytotoxic effector molecule CagA, which is implicated in more severe gastric pathology such as peptic ulcers and gastric cancer (7). This virulence factor is the major focus of this study and will be described in detail in section **1.8**.

1.5 T4SS

Gram-negative bacteria possess a unique cell envelope that is comprised of a semi-permeable outer membrane, impermeable inner membrane, and a periplasmic space. This envelope maintains the structural support of the bacterial cell and does not allow passage of large macromolecules. For this reason, Gram-negative bacteria have developed complex machinery with which they translocate larger virulence factors in the form of DNA, proteins (termed effector molecules), and nucleoprotein complexes (44, 55, 229). Unlike the type III secretion systems (T3SS) which are assembled from the core components of the flagella (31), the T4SS is composed of the core components of the conjugation apparatuses (sex pilus) (44, 45, 55). The first T4SS was identified by Lederberg and Tatum in 1946 in the form of the F-plasmid coding the conjugative F-pilus (44, 133). With this initial discovery, the conjugation apparatus was further investigated and incorporated into the more recent type IV secretion family. The type-IV secretion systems have been divided into two subgroups based on genetic arrangement rather than function. The first group (type IVA) includes systems that resemble the *Agrobacterium. tumefaciens* (*A. tumefaciens*) VirB/VirD4 system and the pKM101 Tra systems (55). The second grouping (type IVB) includes systems that resemble the *Legionella pneumophila* Icm/Dot system and the IncI plasmids Tra/Trb system (*e.g.* R64) (55). However, the entire T4SS family can be better broken into three conceptual groups based upon the function employed by the subgroups as described below.

1.5.1 Conjugation T4SSs

The first and largest group of T4SSs is the "conjugation" subfamily, which are present in most species of Gram-negative and Gram-positive organisms. These systems facilitate direct transfer of DNA between two cells in close contact. This leads to genome plasticity and as a result increased fitness through the acquisition of (for example) genes conferring antibiotic resistance (55, 134, 191). Evidence for direct DNA transfer via a conjugation-like system has been documented in *H. pylori*, however a genetic locus has yet to be linked to this function (127, 157).

1.5.2 DNA uptake T4SSs

The second subfamily is the "DNA uptake" subfamily, which acquires DNA independent of cell-to-cell contact. There are very few examples of this system known, however *Campylobacter jejuni* and *Helicobacter pylori* each possess one of these systems. In *H. pylori*, the system has been termed "ComB", and functions for DNA uptake as well as natural competence (110, 111). The natural uptake system in *Campylobacter jejuni* (Cjp/VirB) was identified on a plasmid, based on its sequence similarity to the *H. pylori* ComB genes (20).

1.5.3 Effector translocation T4SSs

The third subfamily is the "effector translocation" group. This subgroup contains several prominent plant and animal pathogens which deliver effector molecules to their target eukaryotic cell via what is thought to be a needlelike organelle similar to the T3SS (31, 44, 229). Prominent pathogens, which belong to the effector translocator subgroup,

include *Agrobacterium tumefaciens*, *Bartonella henselae*, *Bordetella pertussis*, *Brucella suis*, *Coxiella burnetii*, *Helicobacter pylori*, *Legionella pneumophila,* and *Rickettsia prowazekii* (44, 55, 229). The effector translocation subgroup is of particular interest to *H. pylori* research, as CagA translocation is mediated by such a secretion system.

1.6 T4SS structural assembly

The effector translocation T4SS structural assembly is best described for the plant pathogen *A. tumefaciens*. The *A. tumefaciens* VirB/VirD4 type IV secretion system translocates the Ti-plasmid (T-DNA) as well as the VirE2, VirE3, MobA, VirF, and VirD2 proteins into plant cells, leading to crown gall tumor formation (44, 54). The subcellular localization and function of the 12 structural components of the VirB/VirD4 system (VirB1-VirB11 and VirD4) have been well characterized, making *A. tumefaciens* the current model for most other effector translocator systems (Figure 1-2). The proteins of the *A. tumefaciens* T4SS can be grouped according to the subcellular localization and/or the molecular function that the protein exhibits within the apparatus.

1.6.1 Energetic inner membrane components

The energetic components of the T4SS are made up of three cytoplasmic facing inner membrane-associated proteins (Figure 1-2). These proteins are VirB4, VirD4 and VirB11. VirB4 in *A. tumefaciens* is a large inner membrane protein with four transmembrane domains and multiple conserved motifs, including a DNA binding motif and Walker A motif (NTP binding domain). VirB4 is a homodimer with ATPase activity and therefore acts as the energy generator for the system (67, 68, 200). The dimerization

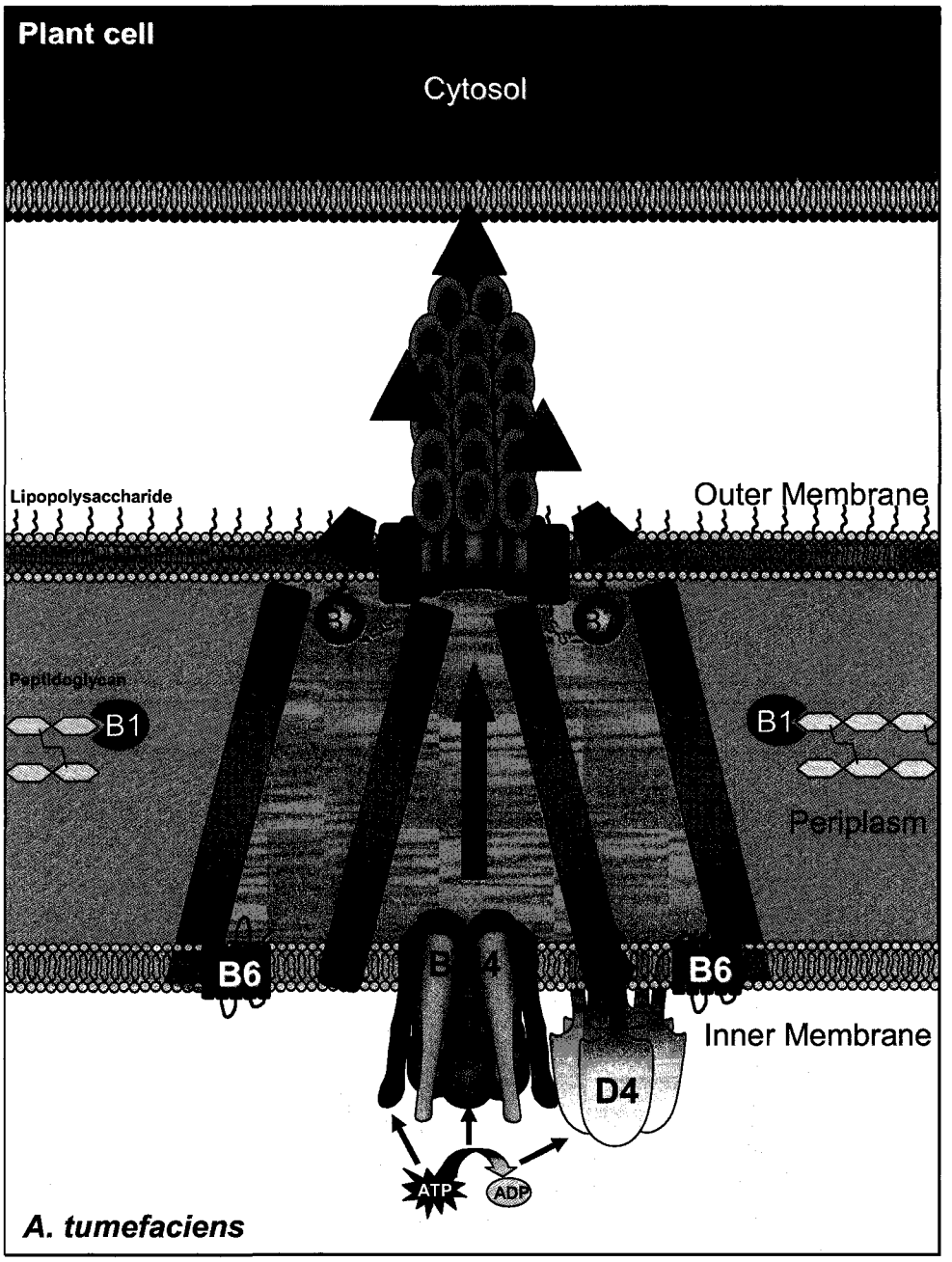

Figure 1-2. Structural model of the VirB/VirD4 T4SS of *A. tumefaciens*. The current structural assembly model of the VirB/VirD4 T4SS is characterized by three distinct groupings of components. The inner membrane energetic components are VirB4, VirB11, and VirD4. The core channel complex-forming proteins are VirB6, VirB7, VirB8, VirB9, and VirB10. The pilus components are VirB2 and VirB5. The accessory proteins are VirB1 and VirB3.

is thought to provide structural integrity to the inner membrane complex, while structural analysis and prediction suggests that the dimers further assemble into a hexamer that docks around VirB11 in the inner membrane (Figure 1-2) (77, 138). The ATP binding function of VirB4 is thought to provide the energy to shuttle effectors through the T4SS (68).

The VirB11 protein has been studied in great depth and has highly conserved hydrophilic domains and both Walker A and Walker B boxes for nucleotide binding (124, 125). These characteristics suggest the localization to be the inner membrane and cytoplasm (likely anchored into the inner membrane and highly exposed to the cytoplasm) (Figure 1-2) (124, 125). VirB11 has high sequence homology to the PulE class of ATPases, suggesting like VirB4, it acts as an energy generator for effector transport (229). VirB11 has also been suggested to play a role in molecular assembly of the actual secretion apparatus, providing the energetic means to move proteins through the membrane leaflets and disassemble the structures (181).

VirD4 also forms a hexameric ring in the inner membrane and is proposed to act as a coupling protein between the relaxosome (a nucleoprotein complex necessary for plasmids to transfer) and the T4SS (Figure 1-2). The hexamer binds DNA in a non-specific manner and an ATPase activity has been suggested, as mutations in the Walker A domain abolished transfer of T-DNA to other T4SS components and to plant cells (14, 128). Interestingly, several T4SSs known to translocate only proteins also possess coupling protein orthologs with Walker A domains including: the Vir systems of *B. henselae* and *R. prowazeckii*, the Dot/Icm system of *L. pneumophila*, and the *cag* system of *H. pylori* (183). Though VirD4 in *A. tumefaciens* may retain a role in DNA transfer

similar to conjugation apparatuses, the presence and necessity for VirD4 orthologs in protein translocation systems is perplexing.

1.6.2 Core complex

A second group of proteins form the core complex of the secretion system, spanning the inner membrane, periplasmic space, and outer membrane. There are five proteins in *A. tumefaciens* that comprise the core complex: VirB6, VirB7, VirB8, VirB9, and VirB10. VirB6 in *A. tumefaciens* is a polytopic and hydrophobic inner membrane protein characterized by 5 transmembrane domains and a periplasmic exposed N-terminus and cytoplasmic exposed C-terminus (Figure 1-2) (116). VirB6 was also shown to form a dynamic channel at the inner membrane above VirB11, to bind T-DNA upon exit from the cytoplasm, to aid in assembly of the VirB9 and VirB7 complex, and to transfer the T-DNA to VirB8 (116, 117).

VirB8 contains one transmembrane domain located near the N-terminus of the protein, though it is considered a bitopic membrane protein by biochemical analysis (116, 229). VirB8 is thought to form an additional segment of the secretion channel, spanning from the inner to the outer membrane (Figure 1-2) (116). VirB8 further binds T-DNA in the periplasmic space after transfer from VirB6, and facilitates transfer of the nucleoprotein complex to the outer membrane complex (116).

The putative secretin protein (PulD family of proteins) VirB9 is an outer membrane protein characterized by a highly conserved N-terminal hydrophilic region, sequence variable central region, and a conserved C-terminal hydrophobic region (115). The N and C terminus have been suggested to be involved in substrate selection and

transfer, as well as regulation of T-pilus biogenesis (115). The central variable region is thought to span the outer membrane, and in addition to the C-terminus, may form a channel through the outer membrane (Figure 1-2) (115, 117). The C-terminus also contains a conserved hydrophobic pocket and cysteine residue that is thought to act as the interaction site for VirB7 (23).

VirB7 is a small lipoprotein that forms homodimers through conserved N-terminal cysteine residues (23). VirB7 has been shown to form higher order complexes with VirB9 via a disulphide bond conferred between conserved C-terminal cysteine residues on VirB9 and VirB7 (Figure 1-2). It is thought that these non-covalent and covalent binding abilities of VirB9 and VirB7 provide stability to the outer membrane complex (23, 117).

The VirB10 protein in *A. tumefaciens* shows significant similarity to the TonB class of proteins, known for their transduction ability of proton motive force from the inner membrane to outer membrane (168). VirB10 is a bitopic membrane-spanning protein that interacts with VirD4 at the inner membrane (Figure 1-2) and undergoes conformational change when VirB11 and VirD4 adopts the ATP bound state (42). VirB10's conformational change is essential for its interaction with the VirB9:VirB7 outer membrane complex, and therefore is thought to act as an energy sensor to allow a bridge between the inner and outer membrane (42).

1.6.3 Pilus complex

The third group of proteins involved in structural assembly of the T4SS are the pilus associated proteins; VirB2 and VirB5. VirB2 is a small protein that is processed at

both the N- and C-termini yielding a 7.2 kDa protein that has been identified as the major pilus subunit (118, 132). VirB2 forms pilus structures by multimerizing in a cyclic fashion to form a tube-like structure through which effector molecules are delivered to the host cell (Figure 1-2) (81). This pilus represents the terminal end of the secretion channel.

The VirB5 protein was only recently ascribed a role in pilus formation, though its association with the pilus was well established. VirB5 associates with the tip of the pilus as well as the shaft during infection and *in vitro*, suggesting it may act as the adhesion component of the pilus (Figure 1-2) (6).

1.6.4 Accessory proteins

Two additional proteins are involved in the T4SS of *A. tumefaciens*, though neither fit in the above three classifications. VirB1 is a lytic transglycosylase required for deconstruction of the peptidoglycan in the periplasmic space (Figure 1-2) (113, 235). Deconstruction of the peptidoglycan is essential for the membrane spanning T4SS to properly form, though secretion can still be detected at very low levels in the absence of this component (25).

The VirB3 protein has been localized to both inner and outer membrane fractions (Figure 1-2) (199). This protein remains the enigmatic component of the prototypical T4SS, though it has been seen to form a complex with VirB2 and VirB5, and interacts with VirB5 *in vitro* (193, 234). To date this protein has not definitively been shown to be a component of the pilus, and may instead provide stability to the VirB2 and VirB5 subunits or act as a chaperone for the pilus components.

1.7 *cag*-PAI

The term "pathogenicity island" is typically used to describe a region of a pathogen's genome that encodes virulence factors and is absent in the non-pathogenic strain or closely related species (92). Consistent with this definition, strains of *H. pylori* that contain an in tact *cag*-PAI are associated with increased virulence and severe disease presentation (50, 227). The *cag*-PAI of *H. pylori* is a 40 kbp gene island inserted at the distal end of the glutamate racemase gene (*glr*) and is comprised of between 27 and 31 genes (depending on the strain) (Figure 1-3) (2, 3, 50). The genetic composition of the pathogenicity island is 35% G+C content in contrast to the genome, which has a G+C of 39%. This difference is consistent with other known pathogenicity islands (74). Flanking the *cag*-PAI are two 31 bp inverted repeats which are indicative of transposon activity and supports the hypothesis that the entire *cag*-PAI was acquired as a single genetic unit (50). The gene island is partitioned into a left (CagII) and right (CagI) segment by an insertion sequence (IS605), which also shows transposon activity and origin (3, 50). Some strains of *H. pylori*, however, have a continuous *cag*-PAI with no IS605 intervening DNA region (50). The aforementioned characteristics, as well as findings in other pathogenicity islands which echo these traits, suggest that the gene islands are a result of acquired DNA through horizontal transmission, for which thus far there is no donor identified (50, 63, 74, 101, 220). As *cag*-PAI positive strains are found across the world, and human pan-migration patterns (predating 12,000 years) have been modeled by *H. pylori* genome sequencing, it is logical to assume that the horizontal

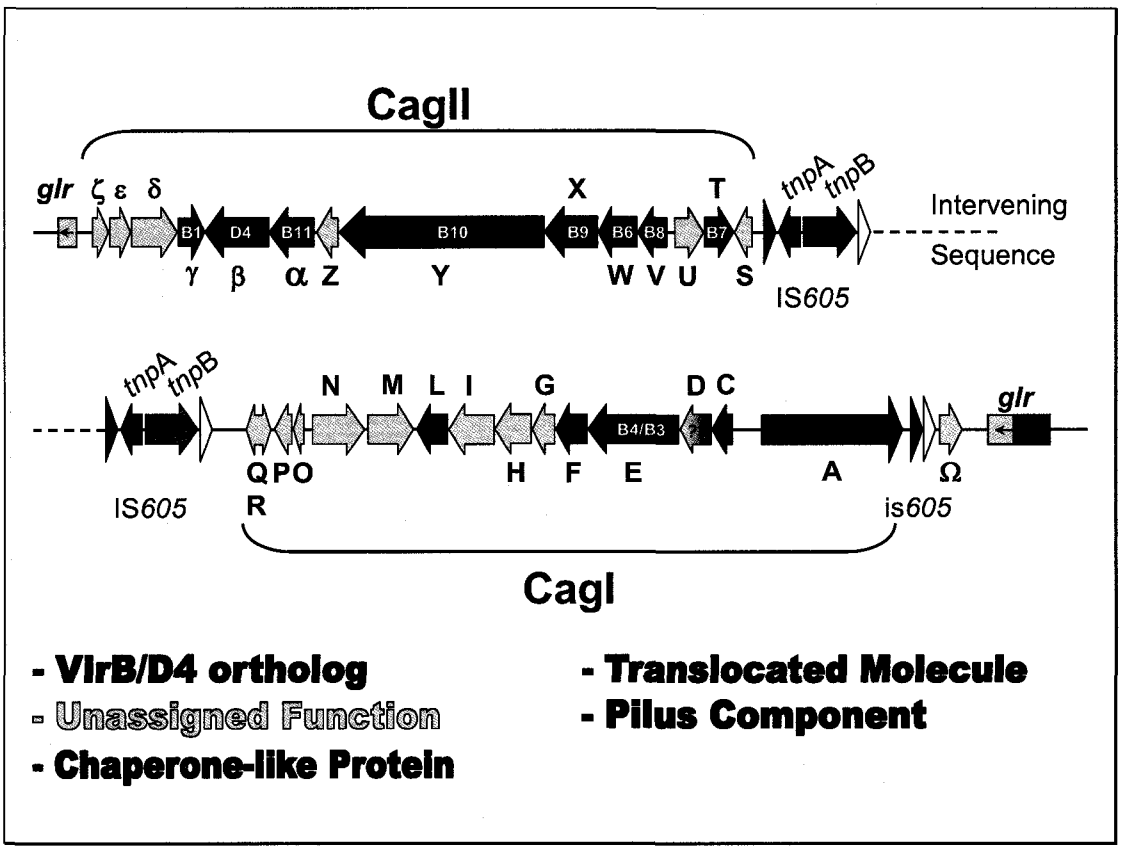

Figure 1-3. Genetic arrangement of the *cag*-PAI. The *cag*-PAI integration site in the glutamate racemase gene is represented by the light blue box. IS605 sequences start and stop at black and white arrowheads respectively. Dotted lines represent variable length intervening DNA sequence. Block arrows represent the ORFs of the *cag*-PAI. The name of each ORF is indicated by the bold-face letter (*e.g.* F indicates CagF). Names placed above the ORF signify those proteins with predicted signal peptides. Green arrows indicate those proteins that are presumed orthologs of the VirB/VirD4 T4SS (orthologous nomenclature in white text on the block arrow). Pink arrows indicate pilus components. Red arrows are chaperone-like proteins. Translocated proteins are indicated by baby blue arrows.

acquisition of the *cag*-PAI predated human pan-migration and possibly human existence (84).

1.8 *H. pylori cag* T4SS

The *cag*-PAI is known to encode a T4SS within its 27-31 genes, including a single known effector molecule, CagA. In addition to CagA, there are ten orthologs to the VirB/VirD4 T4SS of *A. tumefaciens* (3, 6, 10, 22, 38, 50, 113, 130, 172, 210, 229, 238, 239). Furthermore, the ten known VirB/VirD4 orthologs in *H. pylori* are absolutely required for translocation of CagA, and all but Cagβ are required for IL-8 induction (Table 1-1). IL-8 induction is thought to be a host response to the fully assembled *cag* T4SS making contact with eukaryotic cells (87). The remaining proteins of the *cag*-PAI are unique to *H. pylori* although several are also implicated in either CagA translocation and/or IL-8 induction (Table 1-1).

1.8.1 VirB/VirD4 orthologs

The VirB1 ortholog in the *cag*-PAI is Cagγ, identified by sequence as well as *in vitro* transglycosylase activity (235). The VirB2 pilus subunit is CagC. CagC was identified based on secondary structure prediction, molecular weight, N- and C- terminal processing, and surface localization (10, 130). However, CagC has not been directly visualized in association with a pilus structure to date. VirB3 and VirB4 are thought to be encoded by the same gene, *cag*E. CagE possesses limited predicted secondary structure in the N terminus of the protein to VirB3, while the ATPase function is inferred by the characteristic Walker motifs on the C-terminal region of the protein (50, 130).

Table 1-1. *Cag* proteins involved in CagA translocation and IL-8 induction.

Protein	CagA translocation	IL-8 Induction
CagΩ	-	-
CagA	+	-
CagC	+	+
CagD	+	-
CagE	+	+
CagF	+	-
CagG	+	-
CagH	+	+
CagI	+	-
CagL	+	+
CagM	+	+
CagN	-	-
CagO	-	-
CagP	-	-
CagQ	-	-
CagR	-	-
CagS	-	-
CagT	+	+
CagU	+	+
CagV	+	+
CagW	+	+
CagX	+	+
CagY	+	+
CagZ	-	-
Cagα	+	+
Cagβ	+	-
Cagγ	+	+
Cagδ	+	+
Cagε	-	-
Cagζ	-	-

VirB5 has no identified ortholog to date. CagW resembles VirB6 based on five strongly predicted transmembrane domains (116, 130). CagT is a predicted lipoprotein and likely plays the role of VirB7 in the *cag* T4SS. CagT possesses a typical signal sequence, as well as two conserved cysteine residues thought to mediate dimer formation and interaction with a VirB9-like protein (50). CagT was also visualized on the outer membrane surface of the bacteria in a ring-like orientation and associated with a surface structure (172, 210). One protein, CagM, has been identified as interacting directly with CagT. The VirB8 ortholog was identified based on membrane topology of the CagV protein expressed in *E. coli* (38). Though the secondary structure is suggestive, VirB8 and CagV share little or no protein sequence similarity. CagX was readily identified as a VirB9 ortholog based on the primary sequence of the protein (50). Like the VirB9 protein, CagX shares a similar predicted secondary structure and a conserved C-terminal cysteine residue. This cysteine is predicted to mediate the interaction with the lipoprotein CagT (130). CagX was also observed to be associated with unique surface organelles similar to CagT, aggregating at the base of the pilus, reminiscent of secretin channels (210). Two proteins are currently known to directly interact with CagX: CagM and CagY. CagY is the ortholog of VirB10, however it is considerably larger, and only shows similarity at the distal C-terminus (11, 50). The large central region of the protein possesses tandem α-helical repeats, which may be involved in the formation of a surface-localized sheath-like structure (70, 172). Cagα is a VirB11 ortholog and shares overall sequence similarity, Walker domain conservation, as well as structural similarity (50, 230). Cagα is localized in the inner membrane and likely forms a hexameric ring (61, 230). Furthermore, Cagα ATPase activity is inhibited by the compound CHIR-1, a

member of the thiadiazolidine-3,5-diones (109). CHIR-1 has potential as a therapeutic compound since its inhibition is specific to the Cagα ATPase of *H. pylori* and does not affect human ATPases. The final VirB/VirD4 ortholog is Cagβ, which shows high overall sequence similarity, Walker A box domain conservation, and predicted secondary structure to VirD4 (50, 183).

1.8.2 Unique Cag proteins

In addition to the ten VirB/VirD4 orthologs, there are nine additional Cag proteins that are required for CagA translocation and for which there is no detectable sequence similarity to any other proteins as determined by BLAST search (5, 87). These proteins are CagD (established in this work), CagF, CagG, CagH, CagI, CagL, CagM, CagU, and Cagδ (87). All but CagD, CagF, CagG, and CagI were also required for IL-8 induction (Table 1-1). Of these proteins only CagF and CagL were described. CagF was originally identified as an immunogenic outer membrane protein that was common in most clinical isolates (the results in these studies refute the CagF membrane localization findings) (61, 192). The CagL protein was identified as a tip subunit for the T4SS pilus, as well as a structural "covering" component of the pilus, though not the major subunit (131). Importantly, this protein was shown to bind specifically to the host integrin $\alpha_5\beta_1$, in an RGD motif dependent manner and triggers CagA secretion as well as activation and phosphorylation of FAK and Src kinase (131). Interestingly, with the recent identification of VirB5 at the tip of the T-pilus in *A. tumefaciens* as well as the shaft, convergent evolution may suggest that CagL is analogous to VirB5, while not having any obvious sequence or predicted secondary structure similarity (6).

Analysis of ten additional proteins showed them to be nonessential for CagA translocation or IL-8 induction: CagΩ, CagN, CagO, CagP, CagQ, CagR, CagS, CagZ, Cagε, and Cagζ (Table 1-1) (87). These proteins also show no sequence similarity to any sequenced proteins as determined by BLAST search (5). Very little information has been derived concerning the functions of these proteins. The crystal structure of two of the proteins that are not required for CagA translocation or IL-8 induction have been solved, CagZ and CagS (48, 49). These proteins were thought to be potential effector molecules, however the structures of these two proteins revealed nothing about the potential function of these proteins. A third protein not involved in T4SS function, CagN, was preliminarily described as a C-terminally processed inner membrane protein (34). No additional work has been published on this protein to date. Given the limited information currently available about the *cag* T4SS, Figure 1-4 depicts the accepted subcellular localization and interaction scheme. This model depicts a T4SS pilus that extends from the bacterial surface, serving as one of two known surface structures in *H. pylori.*

1.9 Objectives

CagA has been aggressively studied by several major research labs worldwide, leading to its identification and assignment as an oncoprotein translocated to gastric cells by *H. pylori.* Interestingly, there has been very little study of the complex mechanism in which *H. pylori* delivers the molecule into the host. One particular study served as the initial description of those *cag* proteins necessary for translocation and IL-8 induction, however few of these results have been further investigated or confirmed (87). As described above, the T4SS of *A. tumefaciens* has been well described and

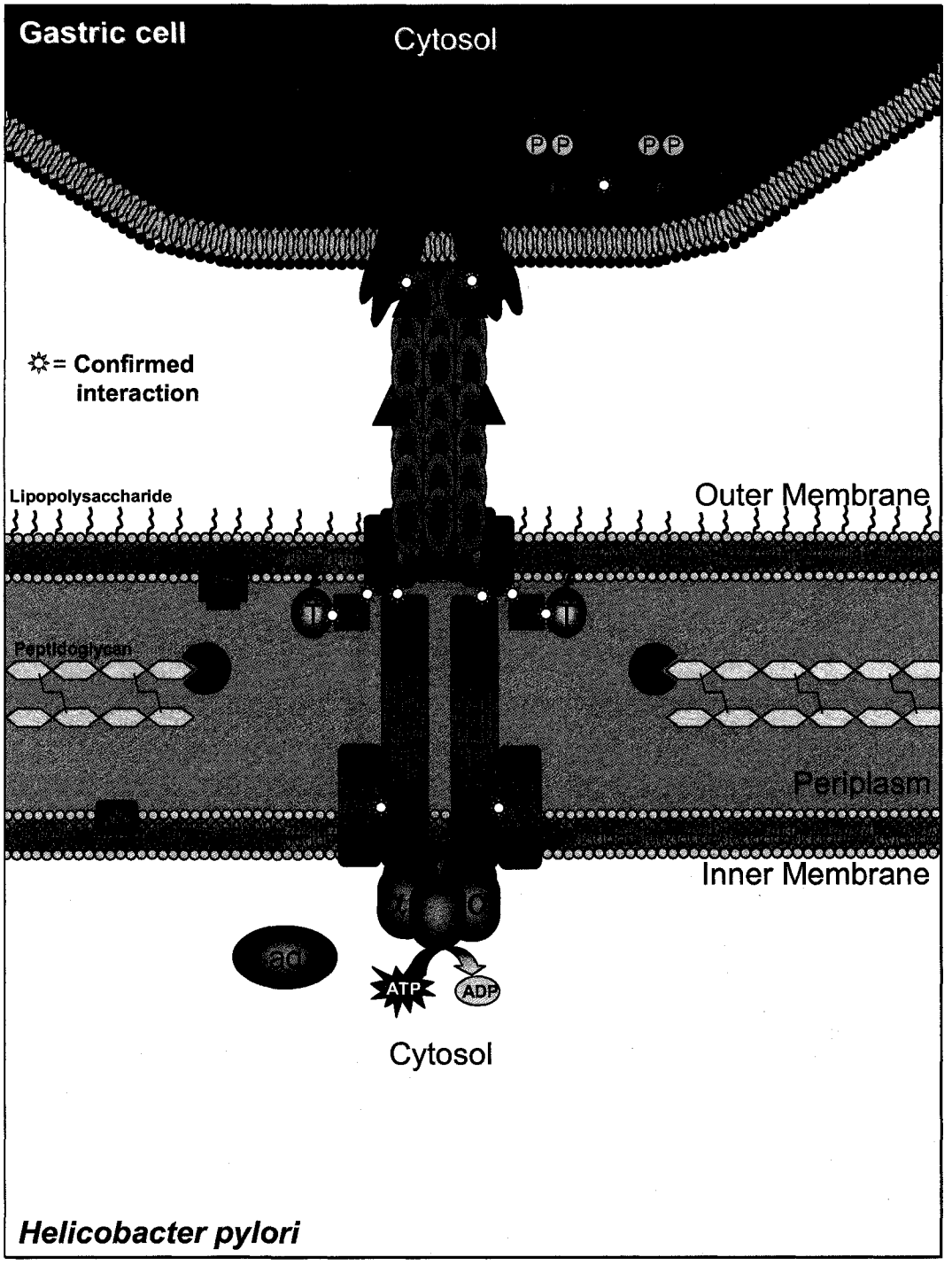

Figure 1-4. Schematic model of the *cag* T4SS in *H. pylori*. All documented subcellular localizations for Cag proteins are depicted in a schematic model. Confirmed protein-protein interactions are indicated by yellow starbursts. Only proteins with documented interactions or localizations are included in this model.

characterized, leading to an intricate understanding of the T-DNA translocation process in that pathogen. However, unlike *A. tumefaciens*, *H. pylori* possesses several enigmatic proteins that are involved in effector translocation that have not been characterized.

The primary objective of this study was to characterize proteins in the CagI region of the *cag*-PAI (Figure 1-3). In particular CagD and CagF were chosen for this study based on their ease of expression and potential involvement in CagA translocation. Through interaction studies, subcellular localization assays, functional translocation assays, and structural analysis, a preliminary characterization of these two proteins has been achieved. CagF was assigned a chaperone-like function in the translocation of CagA at the inner membrane, is not involved in pilus assembly, and represents the first confirmed *cag-cag* protein interaction within the *cag*-PAI to be reported. Although CagD has not yet been assigned a function from these studies, the crystal structure has been solved and the biochemical characterization has described a complex dimeric protein that is not only necessary for CagA translocation within the bacteria (previously not reported), but is also localized outside of the bacteria and with eukaryotic membranes *in vitro*. These studies have provided the foundations for future investigation into the *cag* T4SS assembly and translocation process, specifically for determining the precise role and mechanism for CagD and CagF.

The second goal of these studies was to characterize a previously undescribed bacterial surface structure in *H. pylori* that could not be attributed to either of the previously identified surface structures (flagella or T4SS). These structures were termed "filaments", and were observed during *in vitro* infection and morphologic conversion to coccoids. Filaments are composed partially of antigenic D-mannose linked carbohydrate

residues and are implicated *in vivo* by convalescent human serum recognition. These filaments likely represent a unique bacterial appendage that is involved in *H. pylori* homeostasis and/or pathogenesis. This study represents the first description of filaments and will likely lead to further biochemical analysis and a greater focus on the morphologic conversion *in vitro*.

Chapter 2

Materials and Methods

2 Materials and methods

2.1 Bacterial strains and growth conditions

All *H. pylori* and *E. coli* strains used in this work are listed in Table 2-1. *E. coli* was grown on Luria Bertani (LB) solid medium (Difco Laboratories, Detroit, MI) at 37°C for 18 hours. The following antibiotics were used in LB agar and broth for *E. coli* growth and selection: kanamycin (50 μg/ml), chloramphenicol (50 μg/ml), and ampicillin (100 μg/ml). *E. coli* in LB liquid medium was grown at 37°C for 18 hours with shaking at 220 RPM.

H. pylori was grown on Brucella broth (BB) media (Difco Laboratories, Detroit, MI) supplemented with 10% fetal bovine serum (FBS) (PAA Laboratories GmbH, Pasching, Austria) and the following antibiotics were added for selection in the indicated final concentrations: trimethoprim (10 μg/ml), vancomycin (5 μg/ml), amphotericin B (8 μg/ml), and cycloheximide (100 μg/ml). BB solid media supplemented with kanamycin (25 μg/ml) was used to grow strains possessing kanamycin resistance (Table 2-1). *H. pylori* strains were incubated at 37°C for 48 hours in an anaerobic jar containing a gas mixture composed of 5% CO_2, 5% H_2 and 90% N_2. Liquid cultures of *H. pylori* were grown in BB liquid medium (10% FBS and antibiotics listed previously) in an anaerobic jar containing a Campygen gas pack (Oxoid, Cambridge,UK) (5% O_2, 10% CO_2 and 85% N_2). Cultures were incubated at 37°C for 18 hours with 160 RPM rotation.

Table 2-1. Strains and plasmids used in these studies.

Bacterial Strain or plasmid	Relevant genotype, phenotype, or characteristics	Source or reference
E. coli		
DH5α	*sup*E44 *lac*U169 (Φ80*lacZ*ΔM15) *hsd*R17 *rec*A1 *end*A1*gry*A96 *thi*-1 *rel*A1	Invitrogen
DH5αAF	Cm^r, Ap^r; pSK+*cag*A and pACYC184x*cag*F	This study
DH5αA	Ap^r; pSK+*cag*A	This study
F-F/F-S	Cm^r, Ap^r, Km^r; pSK+recx*cag*F-Strep and pACYC184x*cag*F	This study
F-S	Ap^r, Km^r;pSK+recx*cag*F-Strep	This study
H. pylori		
G27	Wild-type clinical isolate strain	(227)
G27Δ*cag*Y	kan^r: deletion of *hp*0527 gene	(205)
G27Δ*com*B	kan^r: interuption of *hp*0034 (VirB8), *hp*0035 (VirB9), and *hp*0036 (VirB10)	This study
G27/A-FL	kan^r, *cag*A^{PR}-*cag*A-FLAG-kanamycin resistance cassette inserted at *recA*	This study
G27/F-FL	kan^r, *cag*A^{PR}-*cag*F-FLAG-kanamycin resistance cassette inserted at *recA*	This study
G27/8-FL	kan^r, *cag*A^{PR}-*orf*8-FLAG-kanamycin resistance cassette inserted at *recA*	This study
G27Δ*cag*A	kan^r, deletion of *hp*0547 CagA translocation defficient	(204)
G27Δ*cag*F	deletion of *hp*0543, sucrose resistant, CagA translocation deficient, type IV secretion pilus assembly deficent	This study
ΔF/F-FL	kan^r, insertion at *recA*	This study
ΔF/F10N	kan^r, insertion at *recA*	This study
ΔF/F50N	kan^r, insertion at *recA*	This study
ΔF/F100N	kan^r, insertion at *recA*	This study
ΔF/F10C	kan^r, insertion at *recA*	This study
ΔF/F50C	kan^r, insertion at *recA*	This study
ΔF/F75C	kan^r, insertion at *recA*	This study
G27Δ*cag*X	deletion of *hp*0528 gene, CagA translocation deficient	A. Covacci
G27Δ*cag*D	deletion of *hp*0545 gene, sucrose resistant, CagA translocation deficient	This study
Δ*cag*D/D-FL	kan^r, insertion at *recA,* reduced CagA translocation	This study
Δ*cag*D/Dwt	kan^r, insertion at *recA,* reduced CagA translocation	This study
D*	Sucrose resistant, rescued mutant, CagA tranlocation positive	This study
ΔF/F-Strep	kan^r, insertion at *recA*	This study
G27/GapDH-Strep	kan^r, insertion at *recA*	This study
G27/CagD-Strep	kan^r, insertion at *recA*	This study

N6	Wild-type clinical isolate	(86)
N6Δ*fla*AB	kan^r, cat^r: deltion of *fla*A and *fla*B genes, flagella negative	(120)
87A300	Wild-type clinical isolate	(186)
J99	Wild-type clinical isolate: sequenced strain	(4)
26695	Wild-type clinical isolate: sequenced strain	(214)
Plasmids		
pBluescript SK(+)	Ap^r	Stratagene
pSK+recx*orf*8	Km^r, Ap^r; vector for *H. pylori* transformation of *orf*8-FLAG	This study
pSK+recx*cag*A	Km^r, Ap^r; vector for *H. pylori* transformation of *cag*A-FLAG	This study
pSK+recx*cag*F	Km^r, Ap^r; vector for *H. pylori* transformation of *cag*F-FLAG	This study
pSK+recx*cag*F-10N	Km^r, Ap^r; vector for *H. pylori* transformation of *cag*F-10N-FLAG	This study
pSK+recx*cag*F-50N	Km^r, Ap^r; vector for *H. pylori* transformation of *cag*F-50N-FLAG	This study
pSK+recx*cag*F-100N	Km^r, Ap^r; vector for *H. pylori* transformation of *cag*F-100N-FLAG	This study
pSK+recx*cag*F-10C	Km^r, Ap^r; vector for *H. pylori* transformation of *cag*F-10C-FLAG	This study
pSK+recx*cag*F-50C	Km^r, Ap^r; vector for *H. pylori* transformation of *cag*F-50C-FLAG	This study
pSK+recx*cag*F-75C	Km^r, Ap^r; vector for *H. pylori* transformation of *cag*F-75C-FLAG	This study
pSK+recx*cagD*	Km^r, Ap^r; vector for *H. pylori* transformation of *cag*D-FLAG	This study
pSK+recx*cag*Dwt	Km^r, Ap^r; vector for *H. pylori* transformation of *cag*D	This study
pSK+recx*cag*D-Strep	Km^r, Ap^r; vector for *H. pylori* transformation of *cag*D-*Strep*II	This study
pSK+recx*cag*F-Strep	Km^r, Ap^r; vector for *H. pylori* transformation of *cagF-Strep*II	This study
pSK+recx*gap*DH-Strep	Km^r, Ap^r; vector for *H. pylori* transformation of *gap*DH-*Strep*II	This study
pACYC184	Tc^r, Cm^r	New England Biolabs
pACYC184x*cag*F	Cm^r; vector for expression of CagF-FLAG in *E. coli* under control of *cag*A^{PR} (insertion of gene product at *Xho*1 and *Bam*H1 restriction sites)	This study
pSK+*cag*A	Ap^r; *cag*A^{PR} and *cag*A gene (insertion of gene product at *Xho*1 and *Xba*1 restriction sites)	This study
pMA1	pSK+ vector with CagF up and downstream sequences (upstream region cloned into *Kpn*1 and *Xho*1, downstream cloned *Xba*1 and *Not*1)	This study
pMA2	pMA1; Km^r and *sac*B insertion (insertion between up and downstream regions of *cag*F at *Xho*1 and *Xba*1 restriction sites)	This study
pSK+DUP	Ap^r; pSK+recx*orf*8 replacing recA upstream with CagD upstream fragment (*Kpn*1/*Xho*1)	This study
pSK+DKAN	Ap^r, Km^r; pSK+DUP with kan/sac construct inserted *Xho*1/*Xba*1	This study

pSK+DKO	Ap^r, Km^r; pSK+DKAN with recA downstream replaced with CagD downstream at *Not*1/*Sac*1 digestion sites	This study
pDKO	Ap^r; pSK+DKO digested *Sal*1 to remove kan/sac	This study
pSK+CMUP	Ap^r; pSK+recx*orf*8 replacing recA upstream with ComB upstream fragment (*Kpn*1/*Xho*1)	This study
pSK+CMKAN	Ap^r, Km^r; pSK+CMUP with kan/sac construct inserted *Xho*1/*Xba*1	This study
pSK+CMKO	Ap^r, Km^r; pSK+CMKAN with *rec*A dowstream replaced with ComB downstream at *Not*1/*Sac*1	This study

2.2 Molecular genetic methods

2.2.1 Expression plasmid construction

Standard recombinant DNA methodology was used as described previously (179). All plasmid work was performed in *E. coli* strain DH5α (Invitrogen) (Table 2-1). DNA was amplified by polymerase chain reaction (PCR) using oligonucleotides containing unique restriction enzyme recognition sequences at the terminal ends (Table 2-2). Amplified DNA was extracted from agarose gels using a QIAquick gel extraction kit (QIAGEN, Valencia, CA) and digested with appropriate enzymes for direct subcloning into appropriate vectors (Table 2-1).

The plasmid pBluescript SK(+) (Stratagene) was modified to yield the plasmid pSK+recx*orf*8. A 1,500-base-pair region upstream of the recombinase gene in *H. pylori* (*rec*A) was amplified using the oligonucleotides recUp+ and recUp− and cloned into the *Kpn*I/*Xho*I sites of the pBluescript SK(+) vector. The *rec*A downstream fragment was amplified using the oligonucleotides recD+ and recD− and enzymatically digested with appropriate enzymes (Table 2-2). The resulting vector was digested with *Not*I/*Sac*I, and the 750-base-pair *rec*A downstream region was inserted by ligation. A kanamycin resistance gene cassette (*aph*A) was introduced between the *rec*A upstream and downstream regions using the *Bam*HI and *Not*I restriction sites. The *cag*A promoter was amplified (CagA^{Pr}+ and CagA^{Pr}−) and digested with the appropriate enzymes (Table 2-2). *orf8* was amplified (orf8FL+ and orf8FL−), which introduced a FLAG sequence flanked by *Xba*I and *Bam*HI restriction sites at the 3′ end of the gene. Both fragments, the *cagA* promoter and *orf8*-FLAG, were simultaneously inserted between the *kan* cassette and the *recA* upstream region.

Table 2-2. Oligonucleotides used in these studies

Gene/target DNA	Oligonucleotide name	Sequence 5' - 3'[a]
		TATCTCGAG
*cag*A	AF+	CATATGACTAACGAAACCATTAACCA
	AF-	TATTCTAGAAGATTTTTGGAAACCACCTTTTG
*cag*A^{PR}	CagA^{Pr}+	TATCTCGAGTAGAACGCTTCATGCACTCACC
	CagA^{Pr}-	TTTCATATGTTCTCCTTACTATACCTAGTT
*cag*F	FF+	TATATATCATATGAAACAAAATTTGCGTGAAC
	FF-	TATTCTAGAATCGTTATTTTTGTTTTGATTTTT
*rec*A upstream	recUP+	AAGGTACCGGTTTGTGGCGAGCGTGCGTTTG
	recUP-	AACTCGAGCTTATCCCCAAGGCGCACCAACG
*rec*A downstream	recDN+	AAGCGGCCGCGATGACCCTTTAGAAGAAATGGA
	recDN-	AAGAGCTCGCCACTAGCCATGCTTAAACAAC
*orf*8-FLAG	orf8-FL+	ATAATACATATGTTTAGAAAACTAGCAACC
	orf8-FL-	ATAGGATCCTCACTTGTCATCGTCGTCCTTGTAAT CTCTAGACTTTGAATCTTTCAGTAACGC
*cag*F upstream	FUp+	TATGGTACCCTTGCGACTCAAAGCATCACTGAT
	FUp-	TTAATCTCGAGTTGTTCACGCAAATTTTGTTTCAT
*cag*F downstream	FD+	AAAATCTAGAGATGAAGTAACAAACAAAATGCTC
	FD-	ATATATATGCGGCCGCTGCAACACCACTTGTGCTT GAGAT
*cag*D	DF+	TATATATCATATGTTGATCAACAATAATAATAATA G
	DF-	TATTCTAGATAGATATACCGCTTCACATGTAAT
cagD 5' upstream region	DUP+	TATAGGTAACTGGTTAATGGTTTCGTTAGTCAT TATATCTCGAG
	DUP-	GTCGACCTTTCAAGAGAATTCAGAGCAAC TATATATAGCGGCCGC
*cag*D 3' downstream region	DDN+	GTCGACTATACGATTACATGTGAAGCG
	DDN-	TCTTCTATGAGCTCTATCCTA
*com*B8 5' upstream region	ComBUP+	TATAGGTACCAAGCCGTTCAATAGCGAGCAG TATATCTCGAG
	ComBUP-	GAATTCTTCAGTGATGCTGTAGCGAGT TATATATAGCGGGCCGC
*com*B10 3' downstream region	ComBDN+	GAATTCATTACAACCTTTTCTTTAATCTAC
	ComBDN-	TTTGAGCTCTTCATTCTC TCTGGGTATAGG
*cag*D (wild-type)	CagD-	ATAGGATCCTTATAGATATACCGCTTCACATGT
*cag*D-StrepII	D-Strep-	ATAGGATCCTCATTTTTCAAATTGTGGATGACTCC ATGCACTAGTTAGATATACCGCTTCACATGTATT
*cag*F-StrepII	F-strep-	ATAGGATCCTCATTTTTCAAATTGTGGATGACTCC ATGCACTAGTATCGTTATTTTTGTTTTGATTTTT
*gap*DH-StrepII	Gap-Strep+	ATACATATGACTATCAAAGTAGGTATCAAC

	Gap-Strep-	ATAGGATCCTCATTTTTCAAATTGTGGATGACTCC ATGCACTTTTGGAGATGTGAGCGATCAG
*cag*F minus 10 codons from N-teminus	F10N+	TATATATCATATGTTGAAAATTTTAGAAAATGAT
*cag*F minus 50 codons from N-teminus	F50N+	TTTTTTTCATATGAACCTTACCACTCTTTATGAT
*cag*F minus 100 codons from N-teminus	F100N+	TTTTTTTCATATGTCATTTCTCAGTAATCAGGAT
*cag*F minus 10 codons from C-teminus	F10C-	TTTTCTAGAGAGCATTTTGTTTGTTACTTC
*cag*F minus 50 codons from C-teminus	F50C-	TTTTCTAGAATGCGTGAAGTCATAGGCATG
*cag*F minus 75 codons from C-teminus	F75C-	TATTCTAGAAAAAAAATTCACTATATCGCT

[a] Underlined sequences denote restriction digest recognition site

The resulting vector was designated pSK+recx*orf*8. To create pSK+recx*cag*A, pSK+recx*cag*F, pSK+recx*cag*F-10N, pSK+recx*cag*F-50N, pSK+recx*cag*F-100N, pSK+recx*cag*F-10C, pSK+recx*cag*F-50C, pSK+recx*cag*F-75C, pSK+recx*cag*D, and pSK+recx*cag*Dwt (Table 2-1), the *orf*8 gene was excised with from the vector and replaced by one of the respective genes, which were amplified excluding the stop codons, using the oligonucleotide pairs AF+/AF−, FF+/FF−, F10N+/FF-, F50N+/FF-, F100N+/FF-, FF+/F10C-, FF+/F50C-, FF+/F75C-, and DF+/DF- (Table 2-2).

To express the CagF-FLAG fusion from pACYC184 (New England Biolabs, Ipswich, MA), *cag*F-FLAG including the *cag*A promoter was excised by using XhoI/BamHI from pSK+recx*cag*F and cloned into pACYC184 digested with SalI/BamHI. To express CagA without the FLAG tag, *cag*A was amplified with its natural promoter using the oligonucleotides cagA^{Pr}+ and cagAD− (Table 2-2) and cloned into pBluescript SK(+) (Table 2-1).

To express *Strep*II-tag constructs of *H. pylori* CagF and CagD, and *E. coli* GAPDH, genes were amplified with C-terminal *Strep*II tags and ligated into pSK+recx*orf*8. *cag*F, *cag*D, and *gap*DH were amplified with the appropriate oligonucleotides (Table 2-2) and digested with *Nde*1 and *Bam*H1. pSK+recx*orf*8 was digested with *Nde*1 and *Bam*H1 to remove the *orf*8 gene and Flag tag. The resulting plasmids were termed pSK+recxD-Strep, pSK+recxF-Strep, and pSK+recxGapDH-Strep (Table 2-1).

2.2.2 Knockout plasmid construction

G27Δ*cag*F was generated as described previously (60). Short regions of the *cag*F 5′ upstream region (oligonucleotides FUp+ and FUp−) or 3′ downstream region (oligonucleotides FD+ and FD−)(Table 2-2) were amplified by PCR containing several hundred base pairs of flanking sequences. Products were successively cloned after digestion into pBluescript SK(+) to create pMA1 (Table 2-1). A cassette containing a kanamycin resistance gene and the *sac*B gene (kan/sac) was then cloned between the two amplified regions, resulting in vector pMA2.

The *cag*D deleted mutant (G27Δ*cag*D) was created by homologous recombination as described (60). The *cag*D gene was disrupted by amplifying regions proximal to the 5' end of *cag*E and the 3' end of CagA. The upstream fragment (DUP) was amplified using the oligos DUP+ containing the restriction site *Kpn*1 and DUP- containing the restriction sites *Xho*1 and *Sal*1 (Table 2-2). The downstream fragment (DDN) was amplified using the oligos DDN+ containing the restriction sites *Not*1 and *Sal*1 and DDN- containing the restriction site *Sac*1 (Table 2-2). The DUP fragment was cloned into pSK+recx*orf*8 (Table 2-1) to create pSK+DUP using the restriction sites *Kpn*1 and *Xho*1. A kan/sac casette (60) was cloned downstream of the DUP fragment using the restriction sites *Xho*1 and *Xba*1 resulting in the plasmid pSK+DKAN (Table 2-1). Finally, the DDN fragment was amplified and cloned downstream of the kan/sac cassette using the restriction sites *Not*1 and *Sac*1. The resulting plasmid was named pSK+DKO. pSK+DKO was further digested with *Sal*1, which removed the kan/sac cassette. The resulting plasmid was named pDKO (Table 2-1).

The same procedure was used to create a knockout plasmid for the ComB system. The *com*B8 (hp0034), *com*B9 (hp0035), and *com*B10 (hp0036) genes were disrupted by amplifying regions proximal to the 5' region of *com*B8 and the 3' region of *com*B10. The ComUP fragment was amplified using the oligos ComBUP+ containing the restriction site *Kpn*1 and ComBUP- containing the restriction sites *Xho*1 and *Eco*R1 (Table 2-2). The downstream fragment (ComDN) was amplified using the oligos ComDN+ containing the restriction sites *Not*1 and *Eco*R1 and ComBDN- containing the restriction site *Sac*1 (Table 2-2). The downstream fragment (ComUP) was cloned into pSK+recx*orf*8 to create pSK+CMUP using the restriction sites *Kpn*1 and *Xho*1 (Table 2-1). The kan/sac gene construct was cloned downstream of the ComBUP fragment using the restriction sites *Xho*1 and *Xba*1 resulting in the plasmid pSK+CMKAN (Table 2-1). Finally, the ComBDN fragment was cloned downstream of the kan/sac cassette using the restriction sites *Not*1 and *Sac*1. The resulting plasmid was named pSK+CMKO (Table 2-1).

2.2.3 *H. pylori* transformation/mutant construction

H. pylori strain G27 was transformed using natural plate transformation (223). *H. pylori* was streaked for competence by spreading bacteria from dense to sparse using a standard dilution streak method. Non-selective plates were incubated at 37°C for 18 hours in an anaerobic jar containing a gas mixture composed of 5% CO_2, 5% H_2 and 90% N_2. Bacterial growth was examined for competence based on visual and consistence confirmation. Competent bacteria were light yellow in color, maintained low viscosity, and did not readily adhere to inoculation loops. Competent bacteria were streaked to

fresh non-selective media in 2-3 cm circles, and incubated for four hours at the previously listed incubation conditions. Ten micrograms of purified plasmid DNA was then added directly on the competent bacteria and mixed carefully with a sterile inoculation loop. The transformations were then incubated 18 hours as described above and streaked to Brucella Broth plates containing kanamycin. Successful homologous recombination events were selected by kanamycin resistance and sucrose sensitivity when applicable. Potential transformants were screened by PCR to confirm recombination in the correct gene locus and immunoblot where appropriate.

G27 was transformed with pMA1 (Table 2-1) resulting in the *cag*F mutant which was selected for kanamycin resistance. The corresponding DNA region was amplified by PCR to confirm recombination. To create a non-polar *cag*F deletion strain that was lacking artificially introduced genes, the *cag*F mutant was transformed with pMA2 (Table 2-1) and mutants selected on BB plates containing 10% sucrose. G27Δ*cag*F colonies were confirmed by PCR and sensitivity to kanamycin. pSK+recx*cag*F (Table 2-1) was transformed into G27Δ*cag*F, resulting in the strain G27Δ*cag*F/F-FL. Colonies were screened by PCR, western blot, and kanamycin resistance.

G27 was transformed with the plasmid pSK+DKO (Table 2-1) to yield the strain G27Δ*cag*D. Colonies were selected on kanamycin and screened for expression loss of CagD by western blot as well as PCR. A non-polar deletion was made in the same method as for CagF, using the plasmid pDKO to transform G27Δ*cag*D. Colonies were selected on sucrose and confirmed by western blot, PCR, and kanamycin sensitivity. pSK+recx*cag*D and pSK+recx*cag*Dwt were each transformed separately into G27Δ*cag*D

(Table 2-1), resulting in the strains Δ*cag*D/D-FL and Δ*cag*D/Dwt. Colonies were screened by PCR, western blot, and kanamycin resistance.

The ComB mutant was also created using the same methodology as for CagD and CagF. The plasmid pCMKO (Table 2-1) was transformed into G27 and plated on BB containing kanamycin. Colonies were selected by kanamycin resistance and sucrose sensitivity. Colonies were also confirmed by PCR. The resulting strain was termed G27Δ*com*B.

The plasmids pSK+recx*orf*8, pSK+recx*cag*F, and pSK+recx*cag*A were each transformed into G27 separately (Table 2-1), resulting in the strains G27/8-FL, G27/F-FL, and G27/A-FL respectively. Transformants were plated on kanamycin and screened for resistance. Recombinations were confirmed by PCR and Flag expression confirmed by immunoblot.

The plasmids pSK+recxD-Strep and pSK+recxGapDH-Strep were each transformed into G27 while pSK+recxF-Strep was transformed into G27Δ*cag*F (Table 2-1). The resulting strains were named G27/D-Strep, G27/GapDH-Strep, and ΔF/F-Strep respectibely (Table 2-1).

2.3 Antibodies

2.3.1 Antibody applications

All antibody dilutions for immuofluorescence miscropy or western blotting are listed in Table 2-3. The α-*Helicobacter* mouse serum and polyclonal rat-antiserum against full-length CagD was custom-made by Immuno-Precise Antibodies Ltd. (Victoria). CagF was detected with precleared α-CagF rabbit polyclonal serum (192).

CagL, CagX, and Cagα were each detected with α-CagL, α-CagX, and α-Cagα rabbit polyclonal serum respectively (kindly provided by Rainer Haas, Ludwig-Maximilians-University) (172). CagA was detected with rabbit polyclonal α-CagA (kindly provided by Antonello Covacci, Novartis Vaccines, University of Siena). The mouse monoclonal antibody α-HopE was kindly provided by Peter Doig (Astra Zenecca, Boston, MA). h-Met was detected with α-h-Met (C-28) polyclonal rabbit serum (Santa Cruz Biotechnology). Tyrosine phosphorylated proteins were detected with the mouse monoclonal α-PY99 (Santa Cruz Biotechnology). *Strep*II fusion proteins were detected using the Strep classic mouse monoclonal antibody (IBA BioTAGnology, Goettingen, Germany). Sera from *H. pylori* positive patients 5 and 90 were kindly provided by Philip Sherman (University fo Toronto) (27, 69). *H. pylori* negative control sera was kindly provided by Diane Taylor (University of Alberta).

Secondary antibodies for immunoblotting were goat α-rat (Sigma-Aldrich, St. Louis, MO), goat α-rabbit (Sigma-Aldrich), goat α-mouse (Sigma-Aldrich), goat α-mouse F(ab')2 specific, and donkey α-mouse Fcγ (Jackson Laboratories), each conjugated to horseradish peroxidase (HRP). Fluorescent probe secondary antibodies included Alexa Fluor 488 goat α-rat, Alexa Fluor 594 goat α-human, and Alexa Fluor 488 goat α-mouse (Molecular Probes, Eugene, OR).

Table 2-3. Antibodies used in these studies and their dilution factors

Antibody	Immunoblotting	Immunofluorescence	Source	Source
α-CagA	1:2500	N/A	Rabbit	Antonello Covacci
α-CagD	1:2000	1:600	Rat	This Study
α-CagF	1:200	N/A	Rabbit	(192)
α-CagL	1:5000	N/A	Rabbit	(130)
α-CagX	1:5000	N/A	Rabbit	(172)
α-Cagα	1:5000	N/A	Rabbit	(172)
α-h-Met(C28)	1:2000	N/A	Rabbit	Santa Cruz
α-PY99	1:2000	N/A	Mouse	Santa Cruz
α-HopE	1:1000	N/A	Mouse	Peter Doig
α-*Helicobacter*	N/A	1:200	Mouse	This Study
α-Flag-M2	1:3000	N/A	Mouse	Sigma-Aldrich
α-Strep mAb classic	1:1000	N/A	Mouse	IBA
α-Patient 5	N/A	1:100	Human	(27, 69)
α-Patient 90	N/A	1:100	Human	(27, 69)
α-Patient 9	N/A	1:100	Human	Diane Taylor

2.3.2 Antibody production

H. pylori antiserum was raised in mice as follows: *H. pylori* strain 87A300 was harvested from overnight growth on Brucella Broth Agar, washed in 10 mM phosphate buffered saline (PBS), and collected by centrifugation at 8000 X *g*. The bacteria were resuspended in PBS and heat killed by boiling. Mice were injected subcutaneously with the heat-killed bacteria corresponding to approximately 100 μg of total material. The animals were boosted five times subcutaneously every two weeks before the final bleed was taken. Serum specificity was confirmed by western blot.

Purified recombinant CagD was kindly provided by Giuseppe Zanotti (University of Padova) and used to boost rats five times subcutaneously every two weeks as described above. Antibody specificity was confirmed by western blot against wild-type *H. pylori* and the isogenic *cag*D mutant.

2.4 Immunoblotting

All protein samples were prepared with Laemmli's sample buffer (0.125 M Tris-HCl, 20% (v/v) glycerol, 4% (w/v) sodium dodecyl sulfate (SDS), 0.02% (w/v) bromophenol blue, 5% (v/v) β-mercaptoethanol (BME)). Samples were separated by sodium dodecyl sulfate-polyacrylamide gel electrophoresis (SDS-PAGE) at 20 mA through the stacking gel and 30 mA through the separation gel until the desired migration was achieved. Gels were, transferred to Amersham Hybond-P polyvinylidene fluoride (PVDF) (GE Healthcare, Amersham, UK) membranes at 70 V for 90 minutes and blocked in 5% (w/v) skim milk or 3% (w/v) Bovine Serum Albumin (BSA). All primary and secondary antibodies were diluted in 1% (w/v) BSA. Primary antibodies were

incubated at least 12 hours at 4°C. Secondary antibodies were incubated one hour at room temperature with gentle agitation. Four fifteen minute washes with vigorous shaking were conducted with PBS following each antibody incubation. Membranes were developed using the chemiluminescent substrate ECL (GE Healthcare).

2.5 ^{35}S metabolic labeling, cross-linking, and Flag immunoprecipitation

Helicobacter pylori strains were grown under microaerophilic conditions overnight in 90% RPMI-based minimal medium (lacking Cys and Met)-10% BB mixture at 37°C shaking at 160 RPM. Ten microliters of Redivue [^{35}S] methionine (Amersham) was added to each culture and incubated for an additional 5 hours. $6x10^9$ bacteria were collected by centrifugation at 9,000 X *g* for five minutes, washed two times in PBS, and resuspended in 200 µl of 10 mM PBS. Ten microliters of 10% nonyl phenoxylpolyethoxylethanol (NP-40) (Calbiochem) and then 15 µl of 25 mM dithiobis (succinimidyl propionate) (DSP) (Pierce) in dimethyl sulfoxide (DMSO) was added to each sample. Samples were incubated on ice for two hours, and the cross-linking reaction was stopped with 5 µl of 1 M Tris (pH 7.5).

For Flag immunoprecipitation, a three-fold volume of lysis buffer (20 mM PBS, 130 mM NaCl, 7.15% (w/v) sucrose, 1% NP-40, 1 mM phenylmethanesulphonyl fluoride (PMSF), and 227 µg/ml lysosyme) was added to each sample. 100 U of DNase1, RNase-free (Roche Applied Science, Mannheim, Germany) was added to each sample. Cells were frozen in liquid nitrogen and thawed five times in a room temperature water bath, then centrifuged for ten minutes at 16,000 X *g*. The supernatant was removed and added to 30 µl α-Flag-M2 agarose beads (Sigma-Aldrich). Beads were previously equilibrated

with three washes of lysis buffer and blocked with 3% (w/v) bovine serum albumin for six hours to eliminate nonspecific binding. The supernatant and beads were incubated at 4°C for two hours on a rotary beam. Beads were centrifuged at 16,000 X *g*, washed in lysis buffer three times, and resuspended in 50 µl of 1x Laemmli's buffer containing 5% (v/v) BME. All IP's were conducted at least three times.

2.6 Extracellular supernatant immunoprecipitation

Equal numbers of bacteria ($1.5x10^9$) were analyzed for sample collection. Bacteria were centrifuged at 9,000 X *g* for 10 minutes to pellet the organisms. The remaining supernatant was then filtered through a 0.22 µm PVDF filter syringe (Millipore) to ensure all bacteria had been removed from the extracellular supernatants. The supernatants were preabsorbed with 30 µl of Protein G Dynabeads (Invitrogen) for 30 minutes. Beads were first equilibriated with three brief exchanges of IP buffer (20 mM PBS, 130 mM NaCl, 7.17% sucrose, 1 mM PMSF). The extracellular supernatant fractions were then removed to new tubes and 3 µl of α-CagD was added to each sample. Samples were incubated for two hours at 4°C with gentle rotation. Following this incubation, the samples were incubated with 50µl of equilibriated protein G Dynabeads. The samples were allowed to immunoprecipitate for two hours at 4°C with gentle rotation. Beads were washed in IP buffer three times five minutes and boiled in Laemmli's buffer. Extracellular supernatant IPs were performed at least three times.

2.7 StrepII purification

H. pylori strains were grown overnight to suitable OD_{600} (greater than $2x10^9$ bacteria/ml). Approximately $1.8\text{-}2.0x10^{10}$ bacteria were collected by centrifugation at 8000 X *g* at room temperature for five minutes. Bacteria were gently resuspend in 1 ml of sterile PBS and centrifuged at 8000 X *g*, twice. Pelleted bacteria were resuspended in 200 µl of PBS and 600 µl of lysis buffer. Samples were subjected to freeze/thaw in liquid nitrogen 5 times. Samples were centrifuged at 16,000 X *g* for 10 minutes at 4°C. The supernatant was removed to a new tube and the pellet was retained for SDS-PAGE and western blot analysis.

The Strep-Tactin Sepharose column (volume 0.2 ml) was prepared for sample binding as follows. Two column volumes (CV) of wash buffer (100 mM Tris-Cl, 150 mM NaCl, 1 mM EDTA, pH 8) were allowed to pass by gravity flow through the column. The bacterial supernatants were added to the column and allowed to flow through. One CV of wash buffer was loaded on the column the flow-through fraction was collected. Four additional washes were conducted. Samples were eluted by adding 0.5 CV of elution buffer (100 mM Tris·Cl, 150 mM NaCl, 1 mM EDTA, 2.5 mM desthiobiotin, pH 8). A total of six elutions were conducted. Samples were visualized by coomassie stain, western blot, or enzymatically digested with trypsin for liquid chromatography mass spectrometry identification.

2.8 Bacterial subcellular fractionation

Bacterial fractionation was performed as previously described with modifications (95). *H. pylori* was grown overnight in standard conditions. $4x10^9$ bacteria were

centrifuged at 8,000 X *g* and washed in sterile PBS twice. Bacteria were then resuspended in 1 ml of periplasm separation buffer containing 50 mM Tris (pH 7.0), 20% (w/v) sucrose, and 1 mM PMSF. Bacteria were treated with 10 mM EDTA containing 10 μg/ml lysosyme for ten minutes at room temperature. Periplasmic proteins were floated out of the membrane bi-layer by centrifugation at 8,000 X *g* for ten minutes at 4°C. The bacterial fraction was then resuspended in 1 ml of sonication buffer containing 10mM Tris-HCl (pH 7.0) and 1mM PMSF. Samples were sonicated on ice five times for one minute bursts at 35% output (Fisher Sonic Dismembrator, amplitude 1.4). Unlysed bacteria were removed by centrifugation at 16,000 X *g* for two minutes. The supernatant containing membranes and cytosol was centrifuged for one hour at 100,000 X *g* (Optima Max-E Ultracentrifuge, TLA 120.2 rotor) at 4°C. The supernatant containing the cytosol was removed and the membrane pellet was washed three times in sonication buffer. The membrane pellet was resuspended in 0.5 ml of sonication buffer with either 0.1% or 0.2% (w/v) *N*-lauroyl sarcosine (United States Biochemical Corp., Cleveland, OH). *N*-lauroyl sarcosine was optimized for solubility of the inner membrane proteins at 0.1% (w/v) and 0.2% for optimal separation of insoluble outer membrane proteins. Detergent solubility was conducted with rotation at room temperature for 30 minutes. The membrane proteins were then separated by centrifugation at 100,000 X *g* for 30 minutes at room temperature. The supernatant contained the inner membrane proteins, while the outer membrane proteins were located in the pellet. Outer membrane samples were then dissolved in sonication buffer containing 0.1% (w/v) SDS. Equal percentages of each sample were analyzed by immunoblot analysis. The antibodies used to control for membrane fraction

specificity were α-CagF, α-Cagα, and α-HopE (Table 2-3). Fractionations were conducted at least three times.

2.9 Growth and infection of host cells

Gastric epithelial AGS (ATCC# CRL-1739) and NCI-N87 (ATCC# CRL-5822) tissue culture cells were grown and maintained at 37°C in 5% CO_2/95% air in culture medium comprised of RPMI-1640 with 25 mM HEPES buffer and L-glutamine (Invitrogen) supplemented with 10% (v/v) FBS (PAA). For fluorescence microscopy purposes, tissue culture cells were seeded on sterile 12 mm glass coverslips (Fischer Scientific, Swedesboro, NJ) in a 24-well plate (BD Falcon, Franklin Lakes, NJ) at a density of $3x10^5$ cells in culture medium. For eukaryotic membrane fractionation, $5x10^6$ cells were seeded in 10 cm tissue culture dishes. For CagA tyrosine phosphorylation assays $1x10^6$ cells were seeded in 5 cm tissue culture dishes. After 16 hours, confluent monolayers were washed three times with infection medium comprised of RPMI-1640 with 25 mM HEPES and L-glutamine supplemented with 5% (v/v) FBS, and buffered to pH 6.5. An MOI of 10:1 was used for immunofluorescence microscopy and 100:1 for eukaryotic membrane fractionation or CagA tyrosine phosphorylation assays.

2.10 Immunofluorescent microscopy studies

Eukaryotic cells were infected as described and washed briefly to remove unattached bacteria with 37°C wash buffer (PBS + 1% (v/v) FBS). Infected cells were then fixed in 4% (w/v) paraformaldehyde (Sigma-Aldrich) in PBS for ten minutes at room temperature. Paraformaldehyde was removed from samples with three brief

exchanges of wash buffer. Samples were stained with each appropriate antibody (Table 2-3) diluted in wash buffer for one hour at room temperature. Samples were washed with four fifteen-minute washes in wash buffer at room temperature with vigorous shaking at 60 RPM. All secondary antibodies were used in a 1/400 dilution in wash buffer and stained for one hour at room temperature in the dark. Alexa Fluor 568-Phalloidin (Molecular Probes) was used according to manufacturer specifications in a 1/40 dilution in wash buffer. Fluorescein conjugated lectins (Concanavalin A [ConA], *Dolichos biflorus* agglutinin [DBA], Peanut agglutinin [PNA], *Ricinus communis* agglutinin 120 [RCA_{120}], Soy bean agglutinin [SBA], *Ulex europaeus* agglutinin I [UEAI], and Wheat germ agglutinin [WGA]) (Vector Laboratories, Burlingame, CA) were used at a final concentration of 20 μg/ml and stained in the same manner as secondary antibodies. The fluorescent dye Hoechst 33342 (Molecular Probes) at a final concentration of 0.5 μg/ml was used to stain DNA in bacteria and AGS cells. Coverslips were washed four times fifteen-minutes after labeling with secondary antibodies and mounted on glass slides using 1:1 PBS and glycerol containing 20 mg/ml n-propyl gallate (Sigma-Aldrich) as mounting medium and antifade reagent. All immunofluorecent microscopy was performed on a Leica DMI6000 B inverted fluorescence microscope (Leica Microsystems, Wetzlar, Germany) equipped with a Hamamatsu Orca ER camera (Hamamatsu Photonics, Hamamatsu, Japan). Fluorochromes were detected with an A4, L5, or TX2 filter set. Images were processed in OpenLab 5.0.2 (Improvision Incorporated, Waltham, MA) for contrast and Adobe Photoshop 7.0 (Adobe Systems Incorporated, San Jose, CA) for formatting. All immunofluorescence experiments were conducted at least three times.

2.11 Scanning electron microscopy

Infected eukaryotic cells on glass coverslips were fixed with 3% (v/v) gluteraldehyde (Electron Microscopy Sciences, Hatfield, PA) for one hour at room temperature. Samples were washed with PBS (10 mM, pH 7.2) followed by treatment with 2% (w/v) osmium tetroxide (Electron Microscopy Sciences) for one hour at room temperature. Excess osmium was removed by washing with distilled water, taking care to liberate the osmium from beneath the coverslip. Tannic acid (Sigma-Aldrich) was used at 1% (w/v) to crosslink the osmium, followed by careful washes with distilled deionized water (ddH_2O). A second 2% osmium treatment was performed to complete the tannic acid crosslinking reaction. Samples were washed a final time in ddH_2O before dehydration through a graded ethanol series. Samples were passed through a discontinuous series of ice cold ethanol (25, 50, 75, 90, and 100% in ddH_2O) allowing three fifteen-minute treatments for each ethanol solution. Following ethanol dehydration, samples were subjected to critical-point drying with liquid CO_2. Samples were either visualized immediately after drying or lightly coated with gold using an Edwards S150B Sputter Coater. Samples were visualized with a Hitachi model S-2500 SEM operating with an accelerating voltage between 4-8kV. Images were post-processed in Photoshop 7.0 (Adobe Systems Inc.) for formatting.

2.12 Contact dependence assay using tissue culture inserts

24-well Millicell hanging cell culture inserts with polyethylene terehthalate (PET) membranes (0.4 μm) (Millipore, Bedford, MA) were inoculated with *H. pylori* in the

presence or absence of eukaryotic cells as well as conditioned media from active infections. Incubations were conducted for 1-24 hours and each day up to 12 days. AGS cells were seeded in 24-well dishes and treated as described for glass coverslip growth. Inserts were placed inside wells and allowed to equilibrate in infection medium, Brucella broth, or culture medium at 37°C. *H. pylori* were added to the insert well at an MOI of 50:1. Following the necessary incubation time for each experiment, wells and inserts were briefly washed with warm PBS. Inserts were then filled with 4% (w/v) paraformaldehyde and fixed for ten minutes at room temperature. Paraformaldehyde was washed from the inserts three times with wash buffer and the membrane was removed from the hanging insert with a sterile scalpel. Membranes were processed, stained, and mounted for immunofluorescent microscopy using the same technique described for glass coverslips. Contact dependence assays were conducted in triplicate.

2.13 DNA composition analysis

AGS cells infected with G27 on glass coverslips were incubated for the final 30 minutes of a four hour infection with 100 U/ml of RNase-free DNase 1 (Roche Applied Science) based on previous work (37). Samples were stained with Hoechst 33342 and α-*Helicobacter* mouse serum as described above. The assays were repeated at least three times.

2.14 *De novo* protein synthesis assay

Chloramphenicol was added to bacterial growth 30 minutes prior to infection of eukaryotic cells to block protein synthesis. A working concentration of 25 μg/ml was

employed as described previously (206). Chloramphenicol was also added to the tissue culture medium at 25 μg/ml. G27 at an MOI 10:1 was then added to $3x10^5$ AGS cells grown on glass coverslips and allowed to infect for four hours. Samples were fixed and stained with α-*Helicobacter* mouse serum as described above for immunofluorescent microscopic evaluation. Bacterial cultures treated with, or without chloramphenicol were also incubated with 10 μl of Redivue [^{35}S] methionine (Amersham) for four hours. Lysates were separated by SDS-PAGE and exposed to Amersham Hyperfilm ECL (Amersham) to detect ^{35}S incorporation and confirm chloramphenicol activity.

2.15 Periodate oxidation and borohydrate reduction of carbohydrates

Samples were prepared for immunofluorescence microscopy as described above. Periodate oxidation and subsequent borohydrate reduction of carbohydrates was performed as described previously (224). After fixing *H. pylori* infected AGS cells, samples were oxidized with 10 mM periodic acid (Sigma-Aldrich) in PBS pH 4.5 for one hour at room temperature in the dark. Samples were washed twice with PBS pH 4.5 and reduced with 50 mM potassium borohydrate (Sigma-Aldrich) in PBS pH 7.4 at room temperature for 30 minutes. Samples were then washed six times in PBS pH 7.4 to remove all residual periodic acid and borohydrate. Samples were treated with one cycle of degradation for partial oxidation/reduction and twice for complete oxidation/reduction of the carbohydrates. Samples were stained with α-*H. pylori* mouse antiserum as described above and visualized by fluorescence microscopy. Periodate oxidation studies were conducted in triplicate.

2.16 Numerical acquisition and statistical analysis

Samples from time course infections stained with α-*Helicobacter* mouse serum were analyzed visually by immunofluorescence microscopy. *H. pylori* was enumerated and scored based on morphology (coccoid or helicoid), presence of filaments, and connectivity between bacteria by filaments. Samples were carefully examined on multiple planes of focus at 1000X magnification to accurately assign the correct morphology to each bacterium. Each time point was analyzed over multiple fields of view until the total number of bacteria cells examined for each sample was greater than 1000 bacteria. An ANOVA analysis of the data obtained from three independent trials indicated that there was no significant difference between the trials. Therefore, the data was combined to determine standard deviations for the all of the scored parameters. All statistical calculations were conducted using Prizm 5 (GraphPad, La Jolla, CA).

2.17 CagA tyrosine phosphorylation assay

Eukaryotic membranes were solublized as described previously (12). All steps were conducted on ice and in 4°C centrifuges. Cells were washed six times with 5 ml of ice-cold PBS, scraped in 1 ml PBS, and pelleted at 7000 X *g*. The supernatant was discarded and cells were resuspended in 500 µl of saponin lysis buffer (50 mM Tris/Cl, pH 7.4, 1% saponin (Sigma-Aldrich) (w/v), 2 mM sodium ortho-vanadate (Sigma-Aldrich), protease inhibitor cocktail (Complete EDTA-free, Roche)). After five minute incubation on ice, cells were pelleted again at 16,000 X *g* and the supernatant (cytosol) was transferred to a new tube. The pellets containing membranes and the insoluble fraction were solublized in 150 µl of RIPA buffer (25 mM Tris-HCl pH 7.6, 150 mM

NaCl, 1% NP-40, 1% sodium deoxycholate, 0.1% SDS, and Complete EDTA-free, (Roche)). Following five minutes incubation on ice, the insoluble fraction was pelleted and the supernatant (membrane) transferred into a new tube and mixed with 30 µl of 6x Laemmli's buffer. Tyrosine phosphorylation assays were conducted at least three times.

2.18 Fractionation of AGS cells

In vitro infection and fractionation of AGS cells yielding cytosolic, membrane, and insoluble/bacterial fractions was performed as described previously (205). After infection, samples were placed on ice and washed with 10 ml of ice-cold 10 mM PBS supplemented with 2 mM vanadate. All subsequent steps and centrifugations were conducted at 4°C. The infections were scraped in 2 ml of PBS/vanadate. Two dishes of replicate infections were combined and transferred into a 15 ml Falcon-tube (BD Falcon). Samples were centrifuged for five minutes at 200 X *g* (Allegra 64R High-Speed centrifuge, S0410). The supernatant was removed and the remaining cells were resuspended in 4 ml of homogenization buffer (0.5 mM EDTA pH 7.4, 250 mM sucrose, 3 mM imidazole, Complete EDTA-free protease inhibitor). Infected cells were centrifuged for ten minutes at 1,500 X *g* and resuspended in 300 µl of homogenization buffer. Infected cells were lysed by mechanical disruption by gentle aspiration into a 1 ml syringe equipped with a 0.22 gauge needle and expelled forcefully against the sidewall of the 15 ml Falcon tube. The syringe expulsion was repeated five additional times to ensure complete lysis. The cells were then pelleted for ten minutes at 1,500 X *g*. The resulting supernatant was transferred to a new tube. The pellet containing the bacteria, unlysed cells, and the cytoskeletal fraction (Insol) was resuspended in 200 µl of

1X Laemmli's buffer. The remaining supernatant was then centrifuged for 20 minutes at 41,000 X *g* (Optima Max-E Ultracentrifuge, TLA 120.2 rotor). The supernatant from the resulting spin contained the eukaryotic cytosol. The pellet contained the eukaryotic membranes and was resuspended in 1X Laemmli's buffer. All AGS fractionations were conducted at least three times.

2.19 IL-8 ELISA

AGS cells were seeded in 24 well tissue culture dishes ($2x10^5$ cells) and incubated overnight at 37°C in RPMI supplemented with 10% FBS. Cells were washed twice in PBS and infection medium (RPMI with 5% FBS) was added to each well. *H. pylori* was added to each appropriate well at an MOI of 1000 and the infection was incubated for 24 hours at 37°C. Culture supernatants were collected, centrifuged, and the supernatant stored at -80°C until use. Samples were assayed using a Human IL-8 ELISA kit (DIACLONE, France) according to the manufacturer's specifications. Samples were tested as recovered as well as in five-fold dilution. IL-8 was detected using a biotinylated IL-8 antibody, streptavidin-HRP, and chromogen TMB. Plates were read on a Beckman Coulter DTX 880 Multimode detector with 490 nm primary wave length and 620 nm as a reference wave length. All samples were conducted in triplicate except strain Δ*cag*E, which was performed in duplicate.

2.20 Web-based computer programs

Compute pI/Mw Tool (http://ca.expasy.org/tools/pi_tool.html), SignalP v3.0 (http://www.cbs.dtu.dk/services/SignalP/), BLAST – Basic Local Alignment Sequence

Tool (http://blast.ncbi.nlm.nih.gov/Blast.cgi), and "DAS" – Dense Alignment Sequence (http://www.sbc.su.se/~miklos/DAS/) (5, 65, 79, 94, 148)

Chapter 3

Interaction with CagF is Necessary for CagA Translocation Into the Host *via* the *Helicobacter pylori* Type IV Secretion System

Portions of this chapter have been published as:

Couturier, M. R., Tasca, E., Montecucco, C., and Stein, M. (2006) Interaction with CagF is necessary for CagA translocation into the host *via* the *Helicobacter pylori* type IV secretion system. *Infection and Immunity*, 74(1):273-281.

3. Interaction with CagF is necessary for CagA translocation into the host *via* the *Helicobacter pylori* type IV secretion system

3.1 Introduction

Helicobacter pylori (*H. pylori*) is a gram-negative, microaerophilic, spiral shaped bacterium that colonizes the gastric epithelium of the human stomach. *H. pylori* has been implicated in significant gastric maladies such as peptic ulcer disease, chronic gastritis, MALT lymphoma, and adenocarcinoma (142, 154, 155, 165, 207, 221). Strains of *H. pylori* that are typically associated with these severe maladies in infected patients contain an intact *cag* pathogenicity island (PAI) that confers inflammation and ulceration in stomach cells (50, 227).

The *cag*-PAI of *H. pylori* is a 40 kbp chromosomal region that was acquired by horizontal transfer and inserted at the distal end of the glutamate racemase gene (*glr*) (Figure 1-3). Depending on the clinical strain, the *cag*-PAI is comprised of 27-31 genes (2, 3, 50). A portion of these genes encode a type IV secretion system (T4SS), and a single known effector molecule, CagA (50). T4SSs are ancestrally related to conjugation systems and can be grouped according to their function into three categories: i) DNA transfer (best characterized system for DNA transfer between gram-negative bacteria), ii) DNA uptake and release, and iii) effector translocation (44, 72, 110, 111, 133, 229). The *cag* T4SS of *H. pylori* belongs to the effector translocator group of T4SSs. This group contains several prominent plant and animal pathogens that deliver effector molecules to their target eukaryotic cell *via* what is thought to be a needlelike surface organelle. Other examples include *Agrobacterium tumefaciens, Brucella suis, Bartonella henselae,*

Bordetella pertussis, Coxiella burnetii, Legionella pneumophila, and *Rickettsia prowazekii* (44, 55, 229, 240).

The VirB/VirD4 type-IV secretion system of *Agrobacterium tumefaciens* has become the standard reference of comparison for effector translocation T4SSs in gram-negative bacteria. All T4SSs in bacterial pathogens encode genes showing ancestral relation to the genes encoding the VirB/VirD4 apparatus in *A. tumefaciens*. *Helicobacter pylori* possesses orthologs to all the VirB/VirD4 transport system proteins except the pilus coating/tip subunit VirB5 (3, 6, 10, 22, 38, 50, 113, 130, 172, 210, 238). Furthermore, the ten known VirB/VirD4 orthologs in *H. pylori* are absolutely required for translocation of CagA along with eight additional Cag proteins for which there is no detectable sequence similarity in the database (87). As well, there is no evidence for vertical descent for the *H. pylori* T4SS or any other type IV protein transporter system. A likely result of this non-vertical decent is the presence of the additional accessory genes in the *H. pylori* T4SS. Therefore, in-depth molecular analysis of the system, rather than functional inference from the VirB/VirD4 homologues of *A. tumefaciens* is necessary to further our knowledge of this complex system.

To date, considerable attention has been given to the CagA effector protein, expanding our understanding of its function in the eukaryotic cell; however the specific mechanism by which *H. pylori* translocates CagA into the host gastric epithelial cell is largely unknown. CagA remains the only identified effector that is translocated by the T4SS of *H. pylori* into gastric epithelial cells (12, 154, 185, 205). Following translocation, CagA is phosphorylated on multiple EPIYA motifs by Src-family kinases and recruited to the plasma membrane where it interacts with various host cell proteins

including SHP-2 phosphatase (8, 19, 107, 204, 218). Interaction of the SH2 domain of SHP-2 with tyrosine-phosphorylated CagA activates SHP-2 phosphatase activity and induces MAP kinase/MEK/ERK signaling pathways leading to abnormal proliferation of gastric epithelial cells and cell scattering, otherwise known as the "hummingbird phenotype" (171). Other substrates which CagA interacts or localizes with include: ZO-1, JAM, Grb2, c-Src, c-Met, PLCγ, Csk, c-Abl, E-cadherin, Fak, and PAR1 (8, 35, 57, 139, 140, 146, 166, 175, 187, 218, 219, 231, 237).

With the exception of the VirB/VirD4 orthologs, suggested functions for the remaining Cag proteins prove elusive based on the lack of similarity to known proteins. To determine the mechanism of CagA recognition and translocation by the T4SS we attempted to identify proteins that could potentially interact with CagA. These results describe the first interaction between the effector protein CagA and another *cag* encoded protein, CagF. In contrast to a previous report (192) we demonstrate that CagF localizes to both the inner bacterial membrane and cytoplasm and may be a protein with a unique chaperone-like function that recruits CagA to the T4SS.

3.2 Results

3.2.1 CagF interacts directly with two molecular weight species of the CagA antigen in *E.coli*

We sought to screen for Cag protein interactions using an activity reconstitution-based bacterial two-hybrid system because a yeast 2-hybrid assay did not identify any interactions between members of the *cag*-PAI (213). This 2-hybrid system provides

bacterial proteins a prokaryotic environment in which to fold and interact, which may be better suited for detecting interactions than yeast. Our lab previously identified several potential interacting partners, but were unable to obtain reliable and consistent results (unpublished work performed by Sarah Keen). One possible interaction revealed by the bacterial 2-hybrid results involved the CagA antigen and a protein of unknown function, CagF. To test this potential interaction, plasmids expressing Flag-tagged CagF and native CagA were constructed as described in Chapter 2 and co-transformed into *E. coli* strain DH5α. Co-immunoprecipitation of CagA together with the Flag-tagged CagF in *E. coli* supported the interaction between both proteins (Figure 3-1). CagA was not unspecifically precipitated by the α-Flag agarose beads when expressed alone, supporting the specificity of the CagA-CagF interaction. The ability for the two proteins to interact in *E. coli* suggests that the interaction occurs directly and is not conferred by an intermediary Cag protein. CagA is unstable in *E. coli* and breaks down into two major fragments, a 100kDa amino-terminal fragment and a 35kDa carboxy-terminal species as seen in *H. pylori* (141, 153, 227). Both the full length and cleaved 100kDa fragment of CagA co-precipitated with CagF (Figure 3-1). These results suggest that the distal carboxy-terminal portion of CagA is not involved in this direct interaction.

3.2.2 Confirmation of the CagA / CagF interaction in *H. pylori*

A chromosomal insertion of CagF-Flag was made in strain G27. *H. pylori* strains G27 and G27/F-FL were metabolically labeled with ^{35}S, crosslinked with DSP, and cell lysates were applied to α-Flag agarose beads (Sigma). Samples of the immunoprecipitations and supernatants were subjected to SDS-PAGE and transferred to

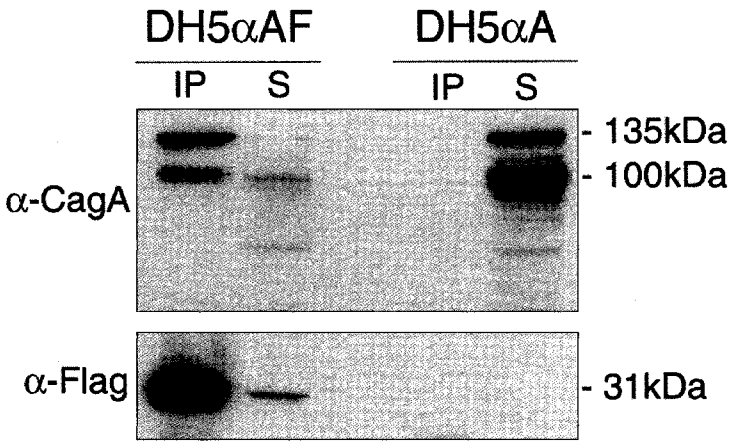

Figure 3-1. CagA co-immunoprecipitates with CagF in *E. coli*. CagF-Flag and CagA were co-expressed in *E. coli* strain DH5α. Proteins interacting with CagF were co-immunoprecipitated from cell lysates with monoclonal anti-Flag antibody coupled to agarose beads. Immunoprecipitates (IP) and supernatants (S) were separated by 9% SDS-PAGE and transferred onto PVDF membranes in duplicate. The membranes were probed with polyclonal CagA antiserum or with monoclonal anti-Flag antibody. Blots were developed with peroxidase-coupled secondary antibodies.

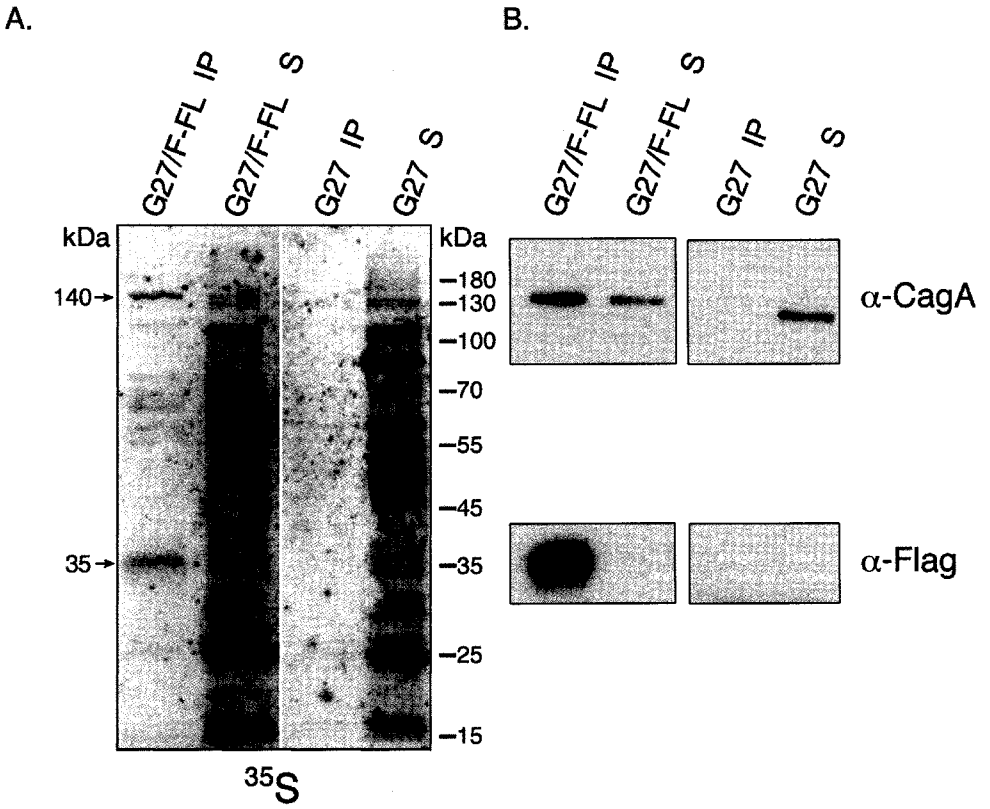

Figure 3-2. Radioactive profile and western blot of proteins that interact with CagF in *H. pylori*. *H. pylori* strains G27 (wild-type) and G27/F-FL were metabolically labeled with ^{35}S for 5h and crosslinked with DSP. Strains were lysed and immunoprecipitated using α-Flag M2 agarose beads. Following SDS-PAGE and transfer onto a PVDF membrane, the ^{35}S labeled proteins in each sample were visualized by exposure of the membrane to radiographic film. Protein identifications of CagF and CagA were confirmed by western blot.

PVDF membranes. The membranes were developed by autoradiography (Figure 3-2A). An intense band running in the 35 kDa range was detected on the radiograph. This band co-migrated with the specific immunoprecipitated CagF-Flag (theoretical molecular mass 32 kDa) and was absent in the control G27 immunoprecipitation. Western blot with the α-Flag antibody confirmed this identity (Figure 3-2B). A second band in the G27/F-FL immunoprecipitation was present at roughly the 140 kDa range (Figure 3-2A). This protein we suspected was CagA and was also not present in the G27 control precipitation. CagA was positively identified using a polyclonal antibody directed against the full-length protein (Figure 3-2B). The lack of discernible IP bands with the G27 control strain suggests that the interaction with CagF was specific and the proteins visualized were in fact co-precipitated. Several other bands were detected by autoradiographic analysis of the immunoprecipitate of G27/F-FL suggesting that other proteins may be involved in a multiprotein complex. Further investigations of the identities of these proteins are described below (**3.2.3**).

The experiment was then modified to determine if this interaction was strong enough to be detected in the absence of the DSP crosslinker. Figure 3-3A shows that both CagA and CagF readily interacted in the absence of a crosslinking agent, suggesting that this interaction is specific, strong enough to allow co-immunoprecipitation, and not artificially induced by the cross-linker. CagA was also Flag-tagged and chromosomally inserted to allow for the reciprocal immunoprecipitation to be screened. The reciprocal immunoprecipitation of CagF with CagA-Flag is illustrated in Figure 3-3B. When Flag-tagged CagA was immunoprecipitated from *H. pylori*, CagF was detected with a rabbit polyclonal CagF antibody. In order to assure that the interaction was due to a specific

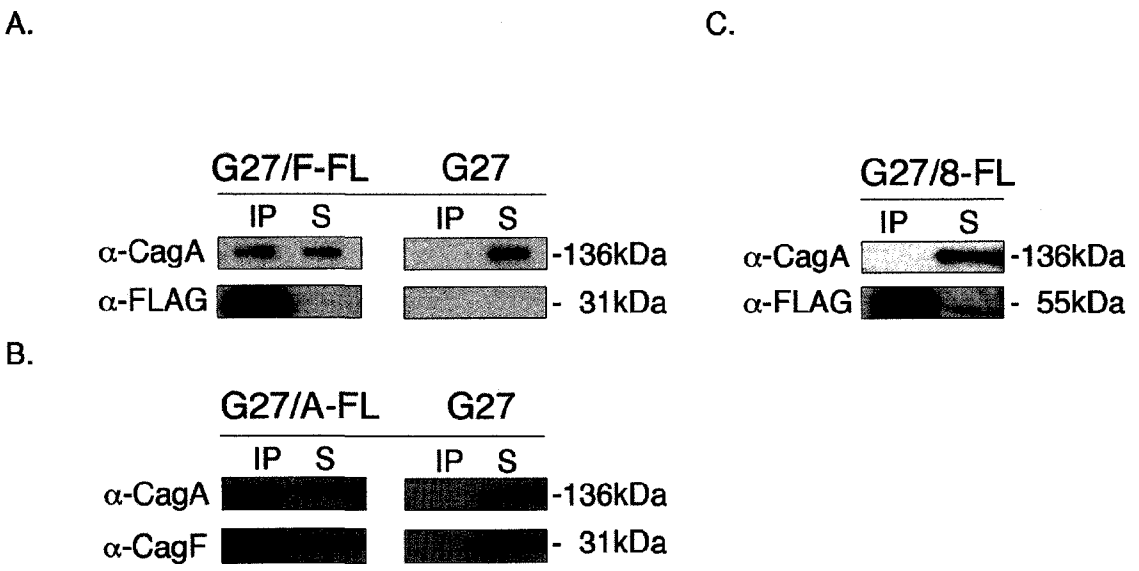

Figure 3-3. CagA and CagF co-immunoprecipitate in *H. pylori*. Lysates of *H. pylori* strains G27, G27/F-FL (A), G27/A-FL (B), and G27/8-FL (C) were immunoprecipitated using α-Flag M2 agarose beads. PVDF membranes were exposed to polyclonal CagA or CagF sera as appropriate. The strains G27 (A and B) and G27/8-FL (C) served as negative controls to test for proteins that might unspecifically bind to the beads or the Flag-tag, respectively.

protein interaction and not conferred directly by the Flag-tag fused to the C-terminus of either CagF or CagA, Orf8, a Cag protein from the distal 3' region of the *cag*-PAI was Flag-tagged and used for immunoprecipitation as described (Figure 3-3C.). CagA was not detected, suggesting that the interaction between CagA and CagF was not an artifact caused by the presence of the Flag-tag. The G27 negative control was clear of unspecific binding of any of the proteins probed by immunoblot (Figure 3-3A & B).

3.2.3 Mass-spectrometry further identifies interacting partners with CagF

The results in Figure 3-2A suggested that additional proteins may interact with CagF. It was of interest to attempt to identify these interacting components by mass-spectrometry. The Flag fusion constructs described above required antibody binding for purification. As the Ig component can often interfere with mass-spectrometry results, we employed *Strep*II fusions to purify CagF on a highly specific column. The *Strep*II tag (biotin analog) was fused to the C-terminus of *cag*F as well as *E. coli gap*DH (strains ΔF/F-Strep and G27/GapDH-Strep) and bound specifically to an optimized resin (Streptactin). The target proteins were then cleaved from the Streptactin using a specific agent (desthiobiotin) and collected in various elution samples. The target protein and interacting partners were then separated by SDS-PAGE and stained by coomassie blue to detect various bands. The CagF sample eluted two obvious bands at approximately 35 kDa and 130 kDa. Based on the previous results, these proteins were expected to be precipitated (Figure 3-4A). The CagF-Strep protein was confirmed by western blot (Figure 3-4B). There were four additional bands (~110 kDa, ~75 kDa, ~65 kDa, and ~55 kDa) detected on the SDS-PAGE gel that were absent in the control GapDH-Strep

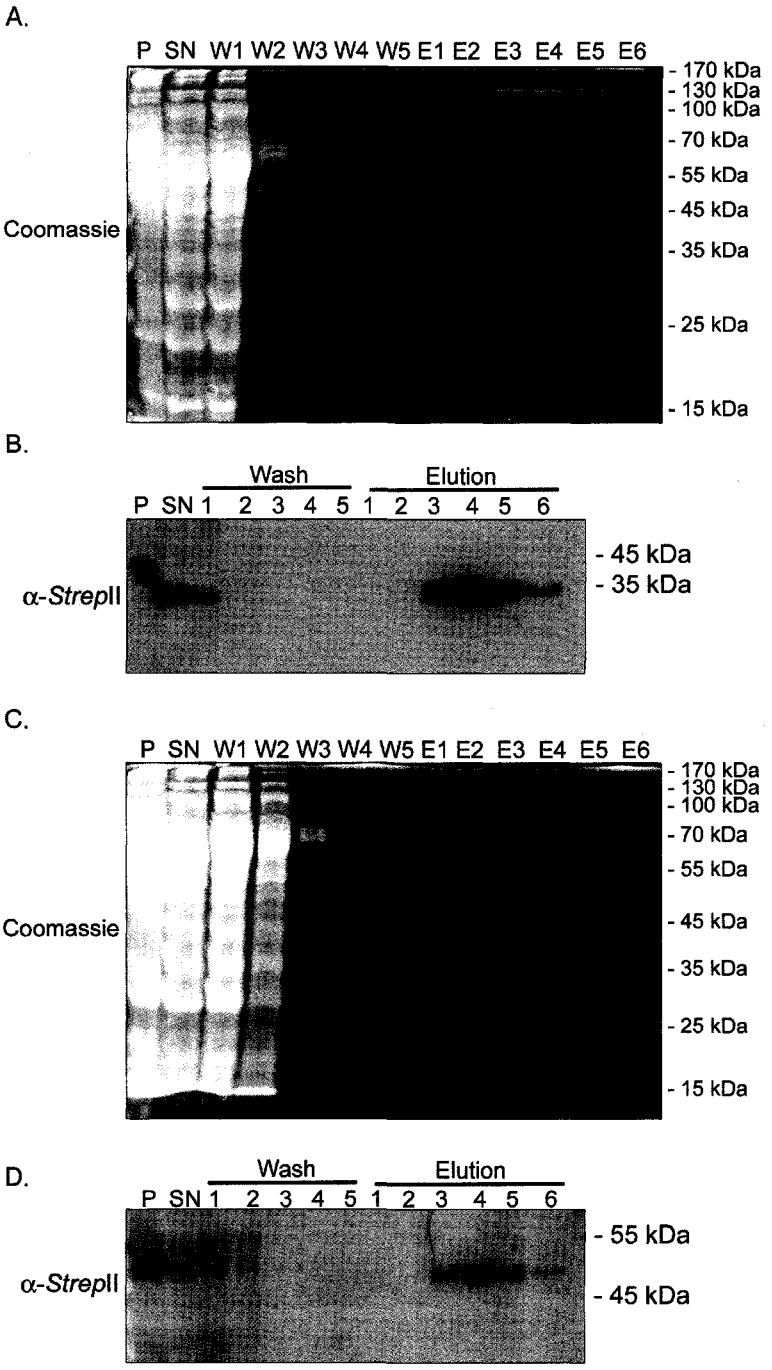

Figure 3-4. CagF-Strep (A and B) and GapDH-Strep (C and D) purifications. Bacteria from overnight cultures of G27Δ*cag*F/F-strep and G27/GapDH-Strep were lysed and the insoluble fraction was separated (P) by centrifugation. The supernatant (SN) was applied to Streptactin columns, washed (W), and eluted (E). Samples were visualized by coomassie stain and western blot using α-StrepII classic antibody. CagF-Strep has an expected electrophoretic mobility of 31 kDa and GapDH-Strep has an expected electrophoretic mobility of 49 kDa.

pulldown (Figure 3-4C). Liquid chromatography mass spectrometry/mass spectrometry (LC-MS/MS) results detected one Cag protein in the various samples. The protein detected in samples 110 and 55 was CagA. This would be expected as the N-terminal breakdown product (approximately 100 kDa) was shown to interact with CagF (Figure 3-1). Several peptides were identified as exact matches to CagA, each assigned to the N-terminal 100 kDa region of CagA (Table 3-1). Though we were unable to detect the 35 kDa fragment of CagA in our previous IP data, the LC-MS/MS results identify CagA in this low molecular weight range as well (though visually not as easily detected as full length CagA, Figure 3-4A). Three distinct peptides were identified in sample 55, corresponding to the extreme C-terminus of the protein (Table 3-1).

A coupling protein was also identified based on peptide identification. The LC-MS/MS output revealed peptides with sequence identity to coupling proteins from F plasmid (TraD) and *E. coli* (VirD4) (Table 3-1). Peptides from coupling proteins were identified in the 110 and 75 samples, with the expected molecular weight of coupling proteins ranging from 80-85 kDa. Though Cagβ is a putative coupling protein in the *cag*-PAI, these peptides did not map to Cagβ or any sequenced *H. pylori* proteins.

Several additional *H. pylori* proteins were identified that were not Cag proteins including: NADH hydrogenase subunit G in sample 110, molecular chaperone DnaK and methyl accepting chemotaxis protein (MCP) in sample 75, heat shock protein 60 (Hsp60) in fraction 65, conserved hypothetical iron-sulfur protein, hypothetical protein HP0086, and protease DO in fraction 55.

Table 3-1. LC-MS/MS protein identification, mass, source organism, peptide sequence, and accession number for protein bands extracted from CagF-Strep purification

Protein Designation	Mass	Organism	Peptide Sequence	Accession	Sample
CagA	44,325	*H. pylori*	INSNIKSGAINEK	gi|7021429	55
CagA	44,325	*H. pylori*	NSALYQSVK	gi|7021430	55
CagA	44,325	*H. pylori*	LGNFNNNNNNGLK	gi|7021431	55
CagA	131,503	*H. pylori*	HDWNATVGYK	gi|2498231	110
CagA	131,503	*H. pylori*	EAEKNGGPT	gi|2498231	110
CagA	131,503	*H. pylori*	NVTLQGNLK	gi|2498231	110
CagA	131,503	*H. pylori*	VDNAVASYDPDQKPIVDK	gi|2498231	110
CagA	131,503	*H. pylori*	VEQALADLK	gi|2498231	110
CagA	131,503	*H. pylori*	IDNLSQAVSEAK	gi|2498231	110
CagA	131,503	*H. pylori*	GVGVTNGVSHLEAGFSK	gi|2498231	110
CagA	131,503	*H. pylori*	DQQGNNVATIINVH	gi|2498231	110
CagA	131,503	*H. pylori*	GINNPSFYLYK	gi|2498231	110
CagA	131,503	*H. pylori*	VENLNAALNEFK	gi|2498231	110
CagA	131,503	*H. pylori*	DLGINPEWISK	gi|2498231	110
CagA	131,503	*H. pylori*	DEIFALINK	gi|2498231	110
Coupling protein TraD	81,489	Plasmid F	NSPAANLVEEK	gi|9507815	110
Coupling protein TraD	81,489	Plasmid F	ASEQYSYGADPVR	gi|9507815	110
Coupling protein TraD	81,489	Plasmid F	SYYDPSIDK	gi|9507815	110
Coupling protein TraD	81,489	Plasmid F	IAEFAAGEIGEK	gi|9507815	110
Coupling protein TraD	81,489	Plasmid F	EDPFWQGSGR	gi|9507815	110
Coupling protein TraD	81,489	Plasmid F	DSEIQNFLHGTVGAGK	gi|9507815	110
Coupling protein TraD	81,489	Plasmid F	YLQGIEHNGEPFTIR	gi|9507815	110
Coupling protein TraD	81,489	Plasmid F	AAASLFDVMNTR	gi|9507815	110
Type IV secretory pathway, VirD4 component	84,387	*Escherichia coli* 53638	NSPAANLVEEK	gi|75512230	75
Type IV secretory pathway, VirD4 component	84,387	*Escherichia coli* 53638	EDPFWQGSGR	gi|75512230	75
Type IV secretory pathway, VirD4 component	84,387	*Escherichia coli* 53638	TLEGMRDLIR	gi|75512230	75
Type IV secretory pathway, VirD4 component	84,387	*Escherichia coli* 53638	QQSENEVTGGR	gi|75512230	75
Type IV secretory pathway, VirD4 component	84,387	*Escherichia coli* 53638	IAEFAAGEIGEK	gi|75512230	75

3.2.4 CagF deletion constructs fail to immunoprecipitate CagA

It was of interest to determine whether the CagA binding region of CagF could be determined by conducting several deletions from the N and C terminus of CagF. Larger deletions were employed since the lack of sequence similarity or conserved motifs rendered the use of specific deletions or mutations useless for our studies. 10, 50, and 100 amino acids were deleted from the N terminus via amplification using specific oligonucleotides (Table 2-2). 10, 50, and 75 amino acid deletions were constructed for the C-terminus. Each construct was fused to a Flag tag at the C-terminus as described previously for full length CagF. The constructs were transformed into G27Δ*cag*F and screened for expression. Though the 10N, 50N, 10C, 50C, and 75C deletion constructs expressed in *E. coli* (albeit the 50N and 75C at barely detectable levels), when recombined into G27Δ*cag*F, the 10N and 10C deletion constructs were detected at similar levels to *E. coli*. Detection of the 50C deletion was greatly reduced, the 75C deletion construct was barely detected, and the 50N deletion was not detected at all. Immunoprecipitations were conducted using the Flag antibody for each strain ΔF/10N, ΔF/10C, ΔF/50C, and ΔF/75C (Figure 3-5). As expected, ΔF/75C was not precipitated, likely due to the low expression levels of the protein or comigrated with the Ig light chain. ΔF/50C was precipitated, however no CagA was detected. The 10N and 10C CagF deletions however rendered puzzling results. Nearly 50% of the trials with these constructs resulted in very low levels of CagA coprecipitation; however the other 50% of the trails were negative for CagA precipitation (representative negative and positive IPs shown in Figure 3-5). Overall the results suggest that CagF deletion constructs are unstable and as a result do not function or are degraded.

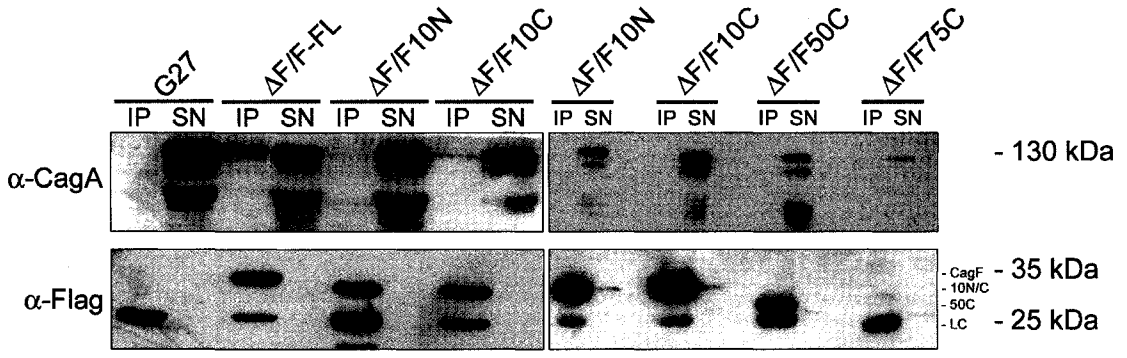

Figure 3-5. CagF truncation analysis. Various N and C-terminal deletion constructs of CagF expressed from the G27Δ*cag*F background strain fail to immunoprecipitate CagA consistently. Representative positive (left frame) and negative trial shown (right frame). Flag-tagged CagF truncation constructs were immunoprecipitated with α-Flag M2 agarose beads and probed by western blot with α-Flag and α-CagA. LC indicates Ig light chain.

3.2.5 Subcellular localization of CagF

We next sought to determine the cellular location of CagF by use of the bacterial fractionation protocol of Gauthier et al. (95). This protocol has been well established in Enteropathogenic *E. coli* and yielded a better fractionation than similar protocols used in *H. pylori* (21, 90, 91, 164, 232). Through prediction software analysis it was suggested that CagF is a 31 kDa protein with a pI of 4.64 (Compute pI/Mw Tool, http://ca.expasy.org/tools/pi_tool.html), contains no signal peptide sequence (SignalP v3.0, http://www.cbs.dtu.dk/services/SignalP/), and has one strongly predicted transmembrane domain proximal to the C-terminus of the protein ("DAS" – Dense Alignment Sequence, http://www.sbc.su.se/~miklos/DAS/)(65, 79, 94, 148). The CagF protein was predicted to localize to the cytoplasm by multiple topographic prediction software. However, the transmembrane domain would suggest that a membrane localization is more likely for this protein than the cytoplasm (28, 93).

As Figure 3-6A shows, the CagF antibody bound to the inner membrane and cytoplasmic fractions of strain G27 of *H. pylori*. The control inner membrane antibody directed toward the VirB11 ortholog (Cagα) was strongly reactive to the inner membrane fractions (Figure 3-6B). Structural analysis suggests an inner membrane localization of Cagα in *H. pylori*, which is consistent with models proposed for *A. tumefaciens* that suggest inner membrane anchoring and cytoplasmic exposure of the majority of the protein (44, 182, 229). A monoclonal antibody directed toward the outer membrane porin HopE was reactive to the outer membrane and the inner membrane (Figure 3-6B)(75). These results suggest that the separation of the inner membrane from the outer

A.

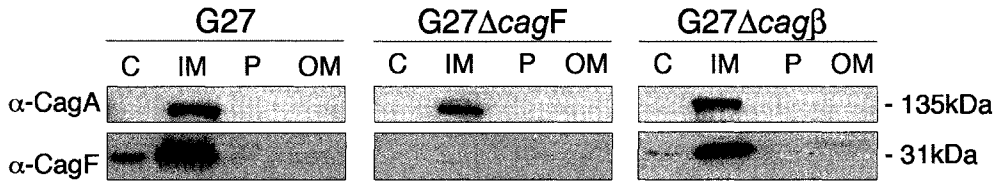

B.

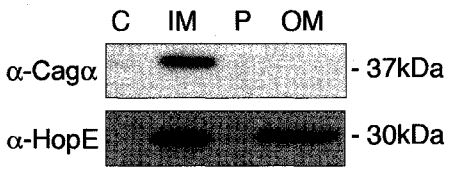

Figure 3-6. Subcellular localization of CagF and CagA. G27, G27Δ*cag*F, and G27Δ*cag*β were fractionated into four major fractions: cytoplasm (C), inner membrane (IM), periplasm (P), and outer membrane (OM). The cytoplasm was purified by ultracentrifugation, periplasm by lysosyme treatment, and inner and outer membranes by differential solubility in 2% wt/vol sodium lauroyl sarcosine. Equal percentages of samples were analyzed. A. Immunodetection of CagF and CagA was facilitated by α-CagF and α -CagA respectively. B. Immunoblots were probed with the control antibodies α-Cagα (inner membrane) and α-HopE (outer membrane) to monitor the purity of the fractions.

membrane is not 100% efficient; however the sarcosine-insoluble outer membrane fraction was free of inner membrane contamination (Figure 3-6B). Since the CagF antibody was not reactive against the outer membrane fraction (Figure 3-6A), this suggests that CagF is not likely outer membrane localized as previously published. The lack of a signal peptide sequence, prediction to associate with the cytoplasm and inner membrane, combined with our results all argue against outer membrane localization. It should be noted that the method employed for bacterial fractionation has potential limitations in *H. pylori*. Results may vary depending on the growth phase and exact protocol used. Multiple detergent-based separation conditions were conducted all yielding similar results (see Chapter 4 for optimized data).

A mutant of the *vir*D4 ortholog (Cagβ) was also used to screen for localization of CagF and CagA. Previous work showed that a mutant of the putative ATP binding and hydrolyzing protein (211) prevents CagA translocation, likely due to an inability to target CagA to the T4SS (87). In the absence of the Cagβ protein, CagF and CagA fractionated similar to the wild-type, suggesting that their localization does not depend on the Cagβ protein or a properly assembled secretion apparatus (Figure 3-6A.).

3.2.6 CagA localization and stability in a CagF mutant.

To investigate a possible function for the CagF-CagA interaction, fractionation experiments were conducted on a Δ*cag*F mutant of G27. The interaction of CagA and CagF paired with the possible inner membrane localization of CagF suggested that CagF might play a role in delivery of CagA to the membrane for transport through the type-IV secretion apparatus. When the fractions of G27 and G27Δ*cag*F were probed with a

polyclonal CagA antibody, CagA was found located in the inner membrane for both samples (Figure 3-6A). These results suggest that localization of CagA to the inner membrane of the bacteria was independent of CagF. However, since CagF is necessary for the successful translocation of CagA we tested whether CagF stabilized CagA in *H. pylori*. CagA did not break down in the absence of CagF, suggesting that the stability of CagA in *H. pylori* is not dependent on the interaction with CagF (Figure 3-6A). The interaction between CagA and CagF is therefore likely to exert function after CagA localizes to the membrane through a mechanism still unknown. However, as visible in Figure 3-1, CagA appeared to be more stable when co-expressed with CagF in *E. coli* compared to CagA expressed alone.

3.2.7 CagF does not form dimers when co-expressed in *E. coli*

These results described CagF as a relatively small (31 kDa), negatively charged (pI 4.64) protein that interacted directly with a translocated effector molecule CagA, and is encoded proximal to CagA. Because this resembles properties of T3SS chaperones, CagF was a likely candidate for chaperone function. Type III secretion systems (T3SS) possess the greatest characterized array of secretion chaperones. In these systems, chaperone proteins typically function as dimers when interacting with the secreted molecule (85, 162). CagF was co-expressed in *E. coli* from separate vectors, each with a C-terminal epitope tag (Flag or *Strep*II). CagF-Flag was immunoprecipitated using the specific Flag antibody, and detected by western blot (Figure 3-7). CagF-Flag readily precipitated in the co-expressed sample. However, CagF-Strep was not detected in the

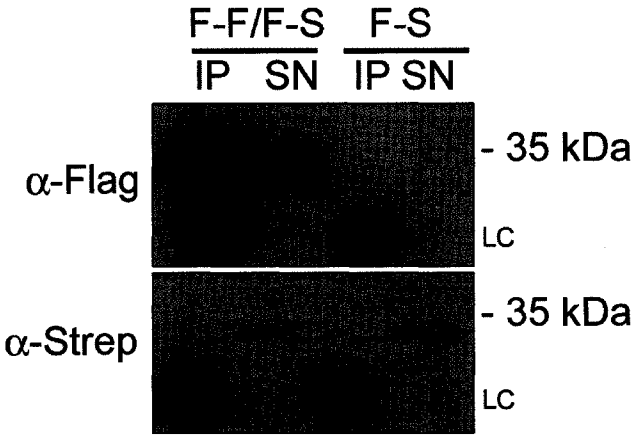

Figure 3-7. CagF does not dimerize when co-expressed in *E. coli*. *E. coli* strains F-F/F-S (expressing CagF-Flag and CagF-Strep) and F-S (expressing CagF-Strep) were immunoprecipitated with α-Flag MS agarose beads and probed by western blot with α-Flag and α-Strep Classic. LC indicated IgG light chain.

precipitation lane when probed with the Strep monoclonal antibody, only the supernatant fraction (Figure 3-7). These results suggest that CagF does not dimerize when the protein is expressed alone. This is in contrast to other published findings which detected CagF dimers during gel filtration chromatography (163).

3.2.8 CagF translocation was not detected in AGS cells

To test the possibility that CagF may translocate with CagA, the strains G27, G27Δ*cag*F, G27Δ*cag*X, and G27Δ*cag*F/F-FL were tested in a translocation assay in which bacteria were incubated with AGS cells for 3h after which the AGS cells were washed and fractionated into soluble, host membrane, and insoluble fractions. The fractions were analyzed for the presence of CagA and CagF-Flag. In both the wild-type and CagF-Flag strain, CagA translocation into the AGS cell membrane was detected by immunoblot (Figure 3-8A), while the G27Δ*cag*F and G27Δ*cag*X strains did not allow for CagA translocation. The Flag antibody was able to detect CagF only in the insoluble fraction containing the bacteria, but not in the host cell membrane (Figure 3-8A). These data suggested that CagF was not translocated with CagA. The requirement of both CagF and CagX for CagA translocation was previously reported by Fischer *et al* (87). However, in that study, the *cag*F mutant was created by insertion of a kanamycin resistance cassette into the *cag*F sequence and thus a polar effect on other genes could not be excluded. Our experiment employed a non-polar in-frame deletion of most of the open reading frame of CagF, which we could use to verify the importance of CagF for CagA translocation. Reintroduction of the *cag*F-Flag gene into the G27Δ*cag*F strain also

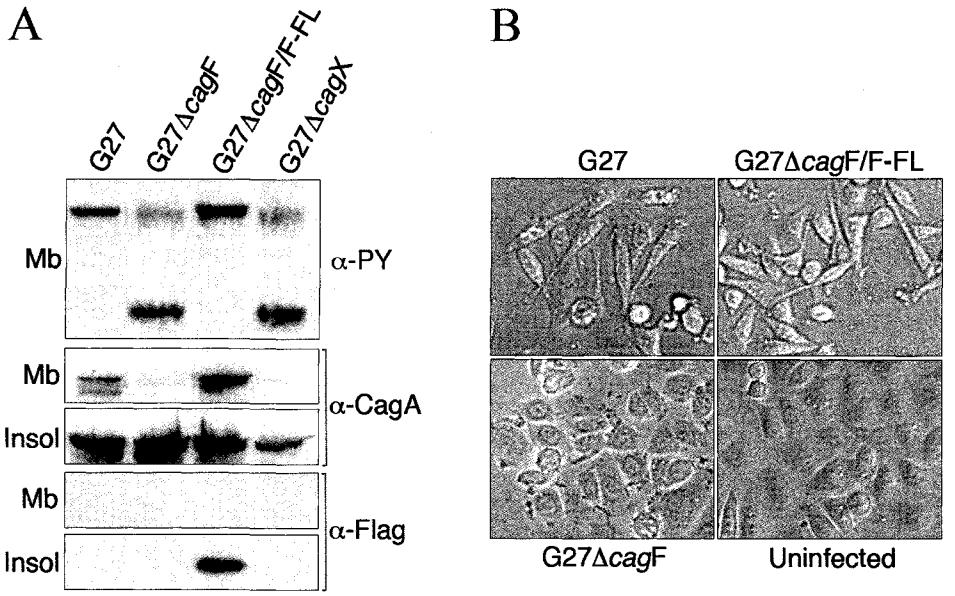

Figure 3-8. CagF is required for CagA host cell translocation, but is not translocated itself. AGS cells were infected with G27, its isogenic mutants G27Δ*cag*X and G27Δ*cag*F, and G27Δ*cag*F/F-FL for 4 hours or left uninfected. Some cells were (A) fractioned by syringe lysis and others (B) visualized by phase contrast microscopy. Host cell cytosol and membrane proteins (Mb) were separated from the cellular fraction containing the bacteria, unlysed cells, and the cytoskeleton proteins (Insol). Samples were separated by SDS-PAGE and analyzed by western blot using α-phosphotryosine (PY), α-CagA, and α-Flag. Estimated mobility for CagA is 136 kDa and a Flag-tagged CagF is 32 kDa.

demonstrated that CagF-Flag is functional and able to restore the wild-type hummingbird phenotype (Figure 3-8B).

3.2.9 CagF not involved in type IV secretion pilus assembly

It was of interest to determine whether CagF is involved in pilus assembly in addition to binding CagA at the inner membrane. CagL was recently shown to be an adhesin of the type IV secretion pilus that binds to host integrin and fractionates with the eukaryotic membrane when using the methodology employed to confirm that CagF was not translocated into the host cell (131). For this purpose, CagL can be used as a reporter of proper pilus assembly and presentation. CagL was detected in the wild-type infected membrane fraction as well as the insoluble fraction as expected when blotting with a CagL antibody (Figure 4-11). Interestingly, CagL was associated with the host cell membrane in the G27Δ*cag*F samples (Figure 4-11). CagL was not detected in the host membrane fraction for the G27Δ*cag*D strain, which suggests the finding with CagF is specific. Antiserum for CagX and CagF were used to control that bacterial membrane components were not contaminating the eukaryotic membrane fraction. H-Met was used as a control to show equal loading as well as a marker of eukaryotic membranes (Figure 4-11). To further confirm this finding, an IL-8 induction assay was used to detect proper pilus assembly, as pilus contact with eukaryotic cells is thought to enhance IL-8 induction. During infection with G27Δ*cag*F and ΔF/F-FL, IL-8 levels were not readily decreased compared to wild-type, confirming that CagF was not involved in pilus assembly (Figure 4-12). This result is in agreement with previously published results (87).

3.3 Discussion

The specific mechanism by which *H. pylori* translocates CagA into the host gastric epithelial cell is largely unknown. Most known T4SSs in bacterial pathogens encode genes showing ancestral relation to the genes encoding the VirB/VirD4 apparatus in *A. tumefaciens*. *Helicobacter pylori* possesses orthologs to all the VirB/VirD4 transport system proteins except the pilus coat/tip subunit VirB5 (3, 10, 22, 38, 50, 113, 130, 172, 210, 238). Some components have only recently been identified by secondary structural similarity and actually possess little detectable sequence similarity at the amino acid or nucleotide level (*e.g.* CagE/VirB3, CagW/VirB6, CagV/VirB8, CagC/VirB2) (10, 22, 130). Additionally, the *cag* pathogenicity island of *H. pylori* contains 28-31 genes (depending on the strain), of which nineteen gene products (ten VirB/VirD4 homologues plus nine novel proteins) seem to be necessary for the successful translocation of CagA (Table 1-1) (87). Though originally published as eighteen required proteins, our results reported in chapter 4 of this work describe the necessity of a nineteenth protein, CagD, for CagA translocation (submitted data). These non-orthologous gene products show no sequence similarity to any sequenced proteins, and because of this, little is known or predicted concerning the role of these proteins in CagA translocation. To date, only CagC, CagL, CagN, and CagF have been characterized in any detail (10, 34, 61, 131, 163).

Very few protein interactions have been confirmed between the components of the *cag* T4SS. Prior to our identification of the CagF and CagA interaction, only two interactions were detected between *cag* proteins and other *H. pylori* proteins of unknown

function. Terradot *et al.* (2004) performed yeast 2-hybrid analysis on a subset of gene products including several Cag and non-Cag proteins. Their analysis identified an interaction between the Cagα and HP1451 as well as CagA and HP0496 (213). They suggested that Cag-Cag interactions are not easily detected with 2-hybrid methods, likely due to its limitation in analyzing interactions of membrane proteins. Our report of the CagF and CagA interaction was confirmed shortly after our publication by the laboratory of Dr. Wolfgang Fischer and Dr. Rainer Haas (163). In addition to this interaction, Dr. Fischer and Haas's group were able to detect several additional interactions using a yeast 2-hybrid system. The following interactions were detected in yeast: CagF:CagY, CagF:CagX, CagF:CagA, CagA:CagY, CagA:CagA, Cagβ:CagY, Cagα:Cagα, CagY:CagY, CagY:CagN, CagX:CagM, CagV:CagN, CagU:CagA, CagT:Cagβ, CagM:CagM, CagL:Cagβ, and CagH:Cagβ (130). Several of these interactions were determined to be indirect when studied in *H. pylori.* The following interactions were confirmed as direct interactions in *H. pylori*: CagX:CagM, CagX:CagY, and CagT:CagM (130).

CagA is the only known effector protein of the *H. pylori* T4SS. Therefore we were especially interested to determine which Cag proteins interact with CagA and to define their role in substrate secretion and translocation. We employed immunoprecipitations to successfully derive the first known interaction between two Cag proteins, CagA and CagF, both in a surrogate *E. coli* host and natural *H. pylori* host. The interaction between CagF and CagA is particularly interesting in *E. coli*, because it shows that the two proteins interact with each other directly without intermediary proteins. Furthermore, the results showed that two CagA species were specifically pulled down.

The first one corresponded to the full-length 135kDa CagA and the second corresponded to the 100kDa carboxy-terminally processed CagA (141). The 35kDa carboxy-terminal fragment of CagA was not co-immunoprecipitated with CagF indicating that CagF interacts with the 100kDa amino-terminal portion of CagA and not the 35kDa carboxy-terminus. Truncation experiments using various N and C-terminal deletions of CagF were inconclusive. Small 10 amino acid deletions from either terminus of CagF were sometimes able to interact with CagA, however this was not consistently reproduced. Additional deletion constructs either were not stable or did not interact with CagA at all. It is possible that the interaction is conferred by overall charge or secondary structural features rather than motif specificity. The charge interaction possibility is supported by the very acidic predicted pI of CagF, while CagA has a very basic predicted pI. If this is the case, any large deletions would possibly disrupt the interaction. These findings were consistent with those of Dr. Wolfgang Fischer who was unable to detect interactions with CagA with any deletion constructs created for CagF (Fischer, Ludwig-Maximilians-University, personal communication).

Our preliminary findings have important implications for the CagA secretion process. The fact that the CagA-CagF interaction is crucial for CagA translocation into AGS cells combined with the finding that the 35 kDa carboxy-terminus of CagA is not involved in this interaction, suggests that at least one CagA secretion and/or translocation motif is located within the amino-terminal 100 kDa of the protein. Recent work also confirmed that a second, C-terminal secretion signal exists in CagA in the 35 kDa C-terminal fragment, and that CagF interacts proximal to this region as well (112). This group however was unable to detect interaction with the 100 kDa N-terminal portion of

CagA (163). It should be noted that each N-terminal CagA fragment tested in this group's studies possessed a GSK tag fused to the N-terminus which may have interfered with the CagF interaction. We were able to immunoprecipitate the unaltered N-terminus of CagA with CagF, which strengthens our findings. However, in the same manner, we immunoprecipitated Flag-tagged CagF to detect CagA, and therefore our C-terminal Flag may have abrogated the interaction with the C-terminus of CagA. The C-terminal fragment of CagA was identified by three different peptides in the mass-spectrometry sample using CagF-Strep to bind interacting partners. Though this finding may indicate that low levels of this fragment were interacting with CagF, it is also possible that the full length CagA was degraded after boiling the samples for SDS-PAGE analysis. Taken together, these findings suggest that like other type IV secretion systems, the C-terminus is involved in secretion; however the N-terminus is also important according to our results. Type IV secretion effector molecules for *A. tumefaciens* (VirE2 and VirF), *Bartonella henselae* (BepsA-G), as well as *Legionella pneumophila* (RalF) display C-terminal secretion motifs despite possessing little sequence similarity (14, 147, 184, 222). Therefore it seems CagA is similar in this sense.

Another important finding of our work is that besides its major interaction with CagA, CagF-Flag also appeared to interact with additional proteins. Using StrepII tag fusions of CagF, we were able to detect an additional interacting protein that appeared to be a coupling protein. The peptide identities were assigned to several VirD4/coupling protein family proteins in conjugation plasmid systems. However based on the sequenced strains of *H. pylori*, there is only one coupling protein in *H. pylori* (Cagβ), and none of the peptides identified are found in Cagβ. Since our samples contained only *H.*

pylori strain G27, it is likely that these peptides were derived from another coupling protein besides Cagβ. The complete sequence of strain G27 has not been completed and annotated, therefore we cannot determine whether G27 possesses additional coupling proteins with sequence identity to the TraD-like coupling proteins; however the presence of these peptides would suggest this is possible. Furthermore, as each strain of *H. pylori* is genetically very diverse, this is a plausible scenario. In addition to these findings, Dr. Wolfgang Fischer also described unpublished findings in his laboratory that detected Cagβ as an interacting partner of CagA in the sequenced strain 26695 (personal communication). Therefore it is possible that CagF interacts with Cagβ or another coupling protein directly or that CagF interacts with a coupling protein *via* a CagA intermediate. Since the Cagβ mutant had no effect on CagA or CagF localization, it is possible that the protein interaction is non-essential for CagA and CagF interaction; however Cagβ is necessary for CagA translocation. Therefore, one possible scenario is that CagA and CagF arrive at the inner membrane independently and then interact. CagF then delivers CagA to a coupling protein, and the putative ATPase provides energy for the first step in secretion at the inner membrane. In this sense, the coupling protein would mediate a bridge between the chaperone complex and the secretion system. In the absence of the coupling protein, CagF and CagA would still arrive in the membrane and interact as seen in Figure 3-6, however CagA would not be secreted due to the absence of the coupling protein.

Yeast 2-hybrid results reported by Dr. Haas and Dr. Fischer indicated that CagX and CagY interact with CagF (130). CagX migrates at approximately 63 kDa and a band on our radiographic exposure appears in this range (Figure 3-2A). We were however

unable to detect CagX in this immunoprecipitation. As well, no band in the 210 kDa size range appears on our radiograph, suggesting that CagY was not one of the unknown bands. It is more likely that the larger band migrating above 70 kDa is Cagβ. As we do not have an antibody to Cagβ, this cannot currently be confirmed. Additional interactions independent of CagF should also be expected for CagA during its passage through the periplasm and the outer membrane. It is likely that each protein interacts with several proteins independent of the other partner, possibly in a transient manner. In this sense, the proteins may interact at different times and locations, as has been recently documented for the VirB/VirD4 system in *A. tumefaciens* (43). Determining when and where CagA and CagF interact will be of particular interest in defining the role of this interaction in effector secretion.

We demonstrated that CagA was located in the bacterial inner membrane fraction, independent of CagF. This would suggest that CagA does not rely on CagF to locate to the membrane, however it is possible that CagF acts as a modified chaperone-like protein by binding CagA once at the membrane and delivering it into the actual secretion apparatus. This would assign a chaperone-like function to CagF that is not based on a cytoplasmic association but rather a subsequent trafficking to the secretion complex. The theoretical pI of CagF was estimated to be 4.64, the lowest of the putative proteins in the *cag*-PAI. Chaperone proteins are typically characterized by a low pI and molecular weight (85, 162). Though the pI of CagF was consistent with a chaperone, the molecular weight was larger than most known chaperones from type three secretion systems, which may suggest CagF has another function conferred by the protein (85, 162). Our results suggesting localization to the cytoplasm and the inner membrane would be in agreement

with our proposed unique chaperone-like function. Furthermore, CagF was not shown to be translocated into AGS cells with CagA and was not required for pilus assembly (IL-8 induction) and CagL presentation (integrin binding), suggesting that CagF may be a chaperone-like protein and a structural inner membrane component of the *H. pylori* T4SS that may be involved in the first steps of substrate recognition. *In vivo* reports of *cag* gene expression using mRNA from *H. pylori* infected rhesus macaques and human biopsies show that CagF is expressed less than any other *cag* gene tested (32, 33). This suggests that even at low expression level, CagF can still maintain its crucial role in type IV secretion.

This work stands as the first documented interaction between CagA and another Cag protein as well as the first direct interaction within *H. pylori cag* T4SS. Further work is required to define the role of CagF in substrate recognition and secretion by the *H. pylori* T4SS as well as the role of the coupling protein in this complex; however we have determined that the protein is necessary for CagA secretion and pilus assembly.

Chapter 4

The *Helicobacter pylori* CagD Protein is Required for CagA Translocation and Type IV Secretion Pilus Assembly

Portions of this chapter have been submitted to *Journal of Molecular Biology* as:

Cendron, L.*, Couturier, M. R.*, Angelini, A., Barison, N., Stein, M., and Zanotti, G. (2008) The *Helicobacter pylori* CagD (HP0545, Cag24) protein is required for CagA translocation and type IV secretion pilus assembly.

* These two authors contributed equally.

The experiments described in 4.2.1-4.2.4 were conducted by Laura Cendron, Alessandro Angelini, Nicola Barison, and Giuseppe Zanotti.

4. The *Helicobacter pylori* CagD protein is required for CagA translocation and type IV secretion pilus assembly

4.1 Introduction

Helicobacter pylori is a human-only gastric pathogen that is thought to infect half of the world's population (98). The pathogen is associated with a spectrum of gastric diseases, ranging from mild gastritis, to peptic ulcer disease, and in extreme cases gastric cancer (62, 102, 165). *H. pylori* strains typically associated with severe maladies in infected patients have been found to possess an intact *cag* pathogenicity island (*cag*-PAI) that has been directly linked to gastric inflammation and ulceration (18, 44, 50, 227).

The *cag*-PAI of *H. pylori* is a 40 kbp chromosomal region inserted at the distal end of the glutamate racemase gene (*glr*) (50). It is thought that this gene island was acquired by horizontal gene transfer. The *cag*-PAI is comprised of approximately 27-31 genes, which is strain specific (2, 3, 50). A large subset of these genes encode a type IV secretion system (T4SS) as well as CagA, the well studied effector molecule (50). T4SSs are ancestrally related to conjugation systems and can be grouped according to their function into three categories: i) DNA transfer (best characterized system for DNA transfer between gram-negative bacteria), ii) DNA uptake and release, and iii) effector translocation (44, 72, 110, 111, 133, 229). The *cag* T4SS of *H. pylori* belongs to the latter group of T4SSs. Several prominent plant and animal pathogens possess effector translocation T4SSs that deliver effector molecules to their target eukaryotic cell *via* a pilus-like organelle. Some of these notorious pathogens include *Agrobacterium*

tumefaciens, Brucella suis, Bartonella henselae, Bordetella pertussis, Coxiella burnetii and *Legionella pneumophila* (44, 55, 229, 240).

To date, CagA remains the only identified effector that is translocated by the *cag* T4SS of *H. pylori* into gastric epithelial cells (12, 154, 185, 205). Following translocation into the host, CagA is tyrosine phosphorylated on multiple EPIYA motifs by Src-family kinases and recruited to the plasma membrane where it can multimerize and interact with various host cell proteins including SHP-2 phosphatase (8, 19, 107, 204, 218). Interaction of the SH2 domain of SHP-2 with tyrosine-phosphorylated CagA activates SHP-2 phosphatase activity and induces MAP kinase/MEK/ERK signaling pathways leading to abnormal proliferation of gastric epithelial cells and cell scattering (171). This cell scattering has been termed the "hummingbird phenotype" due to the long beak-like elongations displayed by infected cells. CagA has been documented as interacting with a myriad of other substrates including: ZO-1, JAM, Grb2, c-Src, c-Met, PLCγ Csk, c-Abl, E-cadherin, Fak, and PAR1 (3, 12, 20, 40-42, 47, 50, 53, 60, 61, 65, 66).

Bioinformatics analysis, mutational and immunological studies, as well as yeast two-hybrid assays have been used in an attempt to better understand the localization and function played by of each individual components of the *cag*-PAI. Each of these *cag* components has particularly been analyzed for their role in CagA translocation and interleukin-8 (IL-8) induction (87, 130). Ten of the *cag*-PAI components (Cagγ, CagC, CagE, CagW, CagT, CagV, CagX, CagY, Cagα, Cagβ) have been proposed to be the orthologs of the T4SS proteins (VirB1, VirB2, VirB3/4, VirB6, VirB7, VirB8, VirB9, VirB10, VirB11, and VirD4) in *Agrobacterium tumefaciens* (3, 10, 22, 38, 50, 113, 130,

172, 210, 238). The only VirB/D4 component that does not have a recognized ortholog in the *cag*-PAI is the enigmatic VirB5 pilus accessory/tip associated component, a protein that is essential in several DNA transfer and effector translocation systems, but is not present in the T4SS of several other pathogens (229). The remaining genes in the *cag*-PAI are instead unique to *H. pylori* and thus far the function has only been proposed for CagC, CagF, and CagL (10, 61, 131, 163). A subset of the non-orthologous Cag proteins are thought to act as unique accessory factors to the secretion system, whereas the function of the remaining proteins remain elusive as they have no noticeable effect on CagA translocation or IL-8 induction (87, 190). A subset of the proteins have been demonstrated to be essential for both CagA delivery and IL-8 induction, while others only are involved in CagA translocation (34, 87, 190).

The *cag*D gene is found in a majority of clinical isolates, but little is known about its role in *H. pylori* disease (176). A kanamycin insertion in the *cag*D gene was reported to only decrease CagA translocation efficiency as well as showing a decrease in IL-8 induction (87). Primary sequence analysis reveals that CagD (mature molecular weight approximately 20 kDa) contains a predicted signal sequence, which suggests it may localize to the periplasmic space and would be expected to show association with the inner membrane (79). A recent proteomic analysis of the bacterial culture supernatant reported only one Cag protein, CagD (201). This finding was not studied in any detail, and currently the mode in which CagD is enriched in the extracellular fraction remains unclear.

The three-dimensional crystal structure of only three *cag*-PAI proteins have been solved to date: Cagα, an ATPase located on the inner membrane (230), CagZ, a 23 kDa

protein involved in the translocation of CagA (48), and CagS, a 23 kDa protein coded by a well conserved gene in the *cag*-PAI whose function remains unknown (49). With the exception of Cagα, the crystal structures for these proteins lack supporting biochemical characterization. Our goal in this study was to crystallize the CagD protein and provide preliminary functional and biochemical analysis. This study reports the structural characterization of CagD, demonstrates that CagD is essential for the CagA toxin secretion and pilus assembly, and characterizes its localization within the bacteria as well as its extracellular localization in the culture supernatant and eukaryotic membrane.

4.2 Results

The results described in 4.2.1-4.2.4 were obtained by Laura Cendron, Alessandro Angelini, Nicola Barison, and Giuseppe Zanotti. Results described in 4.2.5-4.2.9 were conducted by Marc Roger Couturier and Markus Stein.

4.2.1 Protein cloning and expression

Since the full-length CagD sequence (HP0545) was predicted to include a N-terminal secretion signal with high confidence (SignalP 3.0; (79)), the first 32 amino acids were not amplified in the recombinant construct. The amino acid sequence, with the numbering system adopted and secondary structure elements is illustrated in Figure 4-1. Both analytical gel filtration and dynamic light scattering gave results compatible with a species of about 45 kDa, thus confirming that the protein associates to form a dimer in solution. The dimer is characterized by a covalent intermolecular disulfide bridge, as

A.

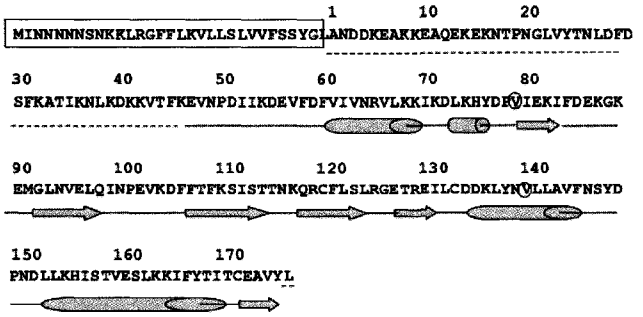

B.

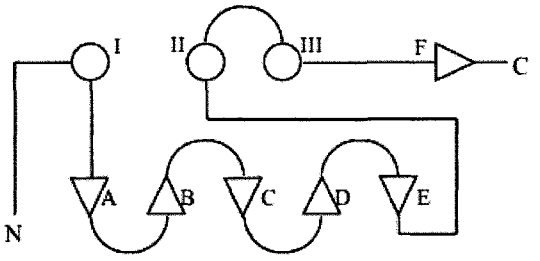

Figure 4-1. Amino acid sequence (A) and schematic topology (B) of CagD. The boxed area represents the predicted N-terminal signal peptide. Underlined residues undergo partial proteolysis and cannot be seen in the structure or may be disordered. The two valine residues that have been mutated to Seleno-methionines in order to solve the phase problem are circled. Secondary structure elements are also shown: α-helices (cylinders) and β-strands (arrows). B. Schematic representation of the topology of the CagD monomer. Circles represent α-helices, triangles β-strands. N and C the N- and C-terminus, respectively.

proven by comparing SDS-PAGE results in denaturing, reducing, and non-reducing conditions. Moreover, the CagD dimer was found to coexist with the corresponding monomer in the cell lysis and first purification steps; however, eventually complete conversion from the monomeric to the dimeric state was achieved.

4.2.2 The molecular model

The crystal structure of CagD has been solved in two different crystal forms, a monoclinic one that diffracts to a maximum resolution of 2.2 Å, and a hexagonal crystal form that diffracts to 2.6 Å. In both cases, CagD is a homo-dimer where the two monomers are covalently linked by a disulphide bridge. In the crystal structure of the monoclinic space group, three monomers are present in the asymmetric unit. Two of the monomers form a dimer, while the third is the member of a dimer generated by the crystallographic two-fold axis. In the hexagonal crystal form, only one monomer constitutes the asymmetric unit, and a crystallographic two-fold axis generates the second half of the dimer.

The electron density for the polypeptide chain of the CagD monomer is clearly visible starting from amino acid 47 to 176. The polypeptide chain folds as a single domain, composed of five β-strands and three α-helices. The five β-strands are organized in an anti-parallel β-sheet, flanked on one side by the three α-helices (Figure 4-1B and 4-2). The five strands, labeled from A to E in Figure 4-2B, are all contiguous and include residues 79-83 (A), 92-98 (B), 107-114 (C), 118-124 (D) and 127-131 (E). The electron density for the strands is very well defined, with the exception of the six residues from 85 to 91, a loop that connects strands A and B. This loop is disordered in the monoclinic

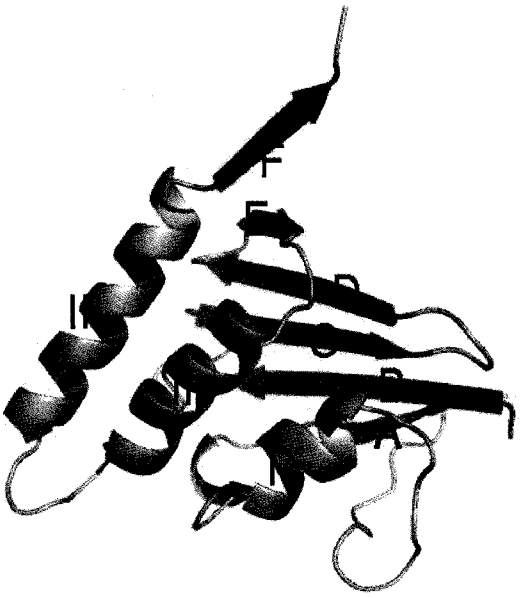

Figure 4-2. Ribbon diagram of the monomer of CagD showing the organization of the secondary structure elements. Helices (yellow) are labeled from I to III, strands (green) from A to F.

space group and is included in the final model only for the hexagonal crystal form. The C-terminal portion of the chain includes two relatively long α-helices (helix II, residues from 135 to 145, and helix III, from 153 to 169), running anti-parallel to each other, and a final strand, F, from 171 to 174 (Figure 4-2). The latter protrudes from the core of the monomer and runs anti-parallel to the same strand of a second monomer, allowing for the formation of the dimer. The surface of interaction also involves a portion of strands D and E of the two monomers, which are held together not only by the S-S bridge between two Cys172, but also by hydrogen bonds between main chain atoms of the two strands. A total of ten H-bonds are detected in this region (Figure 4-3). A second intramolecular disulphide bridge is present between Cys120, belonging to strand D, and Cys133, close to the beginning of the second α-helix. More complex is the architecture of the N-terminal portion of the protein: strand A is connected to the α-helix I (residues 61-68) by a turn and a very short α-helix (residues 73-76). Finally, a long stretch (residues from 51 to 60) reverses the direction of the polypeptide chain in such a way that residues from 47 to 52 form a short strand which runs antiparallel to β-strand A. Electron density stops around residue 46, and for the first ten residues (57 to 56), is not well defined as it is for the rest of the molecule. This suggests a slightly higher mobility of this part of the protein with respect to the molecular core.

Mass spectrometry data of a sample obtained by dissolving some crystals have demonstrated that the protein we have crystallized undergoes a proteolytic cleavage between residues 46 and 47 in one of the two monomers. A low amount of cleavage is also observed in total *H. pylori* cell lysates. Since one third of the monomers in the crystal are equivalent (and they are all equivalent in the hexagonal space group form), we

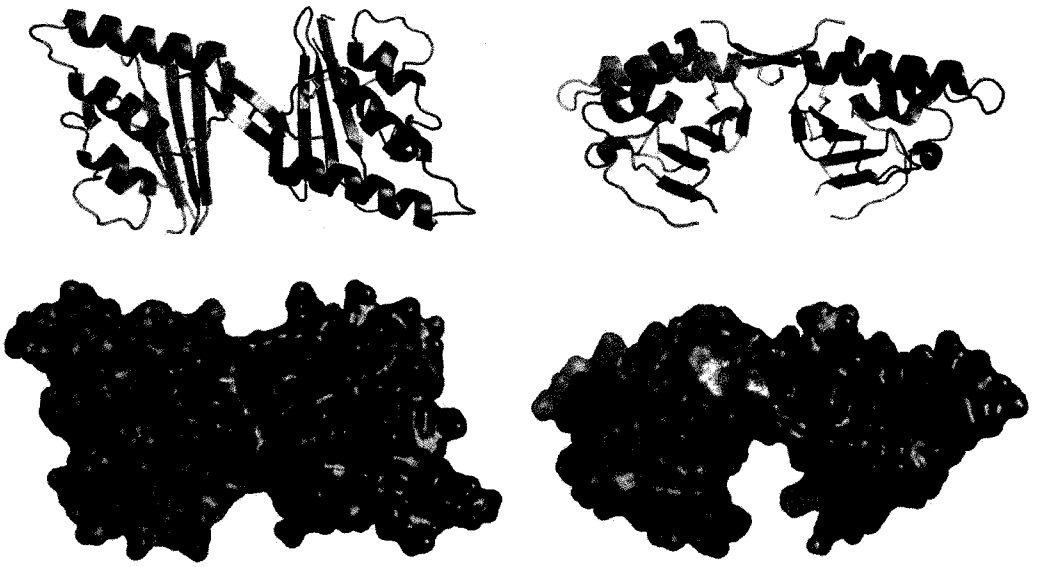

Figure 4-3. Ribbon diagram (top) and surface topology (bottom) of the CagD dimer. The two monomers are shown in green and magenta, residues involved in disulphide bridges in yellow. In the left view, the molecular two-fold axis is perpendicular to the plane of the paper, in the right view the axis runs vertical in the paper plane.

have to conclude that the first 46 amino acids, present in only one of the two monomers, are disordered and cannot be seen in the electron density.

It is interesting to notice that the formation of the dimer produces a large crevice in between the two monomers (Figure 4-3). The truncated N-terminus is on the same side of the model, so we could speculate that these 46 amino acids, when present, could partially fill in this cavity. In fact, some unexplained electron density at a contour level of 1σ is visible in this crevice. This holds only for the dimer present in the asymmetric unit, while in the dimer generated by the crystallographic symmetry, this effect is possibly cancelled by the symmetry.

The overall CagD architecture allows many charged residues to protrude from the surface, without any hydrophobic patches exposed to the solvent, in agreement with the high solubility observed. The sequence of the unprocessed CagD including the N-terminal signal sequence shows a clear prevalence of positively charged residues over the negatively charged ones, conferring a basic pI to the entire protein. The processed and exported CagD looses many lysines present in the signal sequence, resulting in a general counterbalance between positive and negative charges, with a slight prevalence toward the latter. However, the charges are not uniformly distributed on the protein surface: an analysis of the electrostatic potential indicates that a prevalence of lysine and arginine residues confers an overall positive charge to the internal groove running between the two CagD monomers, starting from the central disulfide bridge which covalently links the two monomers and extending toward both the directions of the crevice (Fig. 4-4). It must be however remembered that our model lacks amino acids from 1 to 46, which were

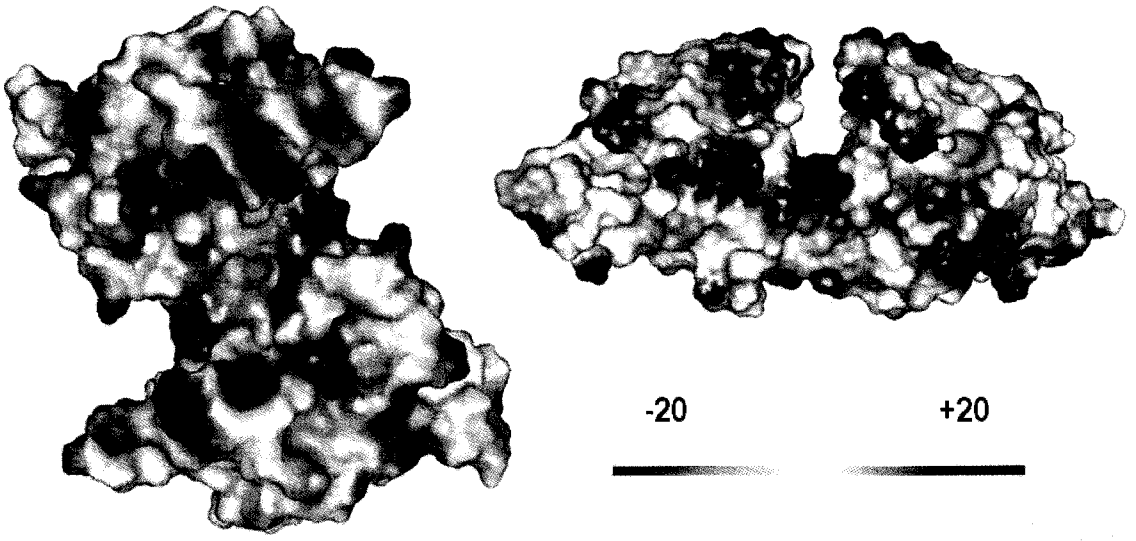

Figure 4-4. Two different views of the electrostatic potential surface of the CagD dimer, showing the distribution of positive charges in the crevice generated by dimerization. The potential surface was calculated with Pymol (71).

not identifiable in the electron-density and were processed in one of the monomers. When these regions are present, they are possibly located in this grove.

A long N-terminal portion of the molecule (46 amino acids other than the 32 comprising the predicted secretion signal) is disordered and is selectively degraded by a protease in one monomer. Residues involved in dimerization are characterized by the lowest temperature factors and the most clearly defined electron density regions, while regions far from the dimerization area are characterized by the highest B-factors and a more disordered electron density pattern. These observations suggest that the more conserved and less flexible regions are grouped in the core of the protein, while the extremities could be more prone to a series of movements and distortions upon protein-protein interactions and/or a protein-substrate complex formation.

4.2.3 Structure comparison

The CagD fold, a β-sheet flanked by α-helices, is not at all unique. However, a more accurate comparison of the three dimensional structure of the monomer with the entire PDB performed using the secondary structure comparison service SSM at the European Bioinformatics Institute (126) finds only four proteins with a Z-score between 2.5 and 1.9: the SycT chaperone of *Yersinia enterocolitica* type III secretion system (T3SS), the DNA binding domain of the phage T4 transcription factor MotA, the trimeric frataxin from the yeast *Saccharomyces cerevisiae,* and the C-terminus of outer surface lipoprotein B (OspB) of *Borrelia burgdorferi.* While the latter three can barely be related to the CagD role inside the pathogenicity island, the first one seems to suggest for CagD a chaperone function (Figure 4-5). The CagD monomer shares roughly the same

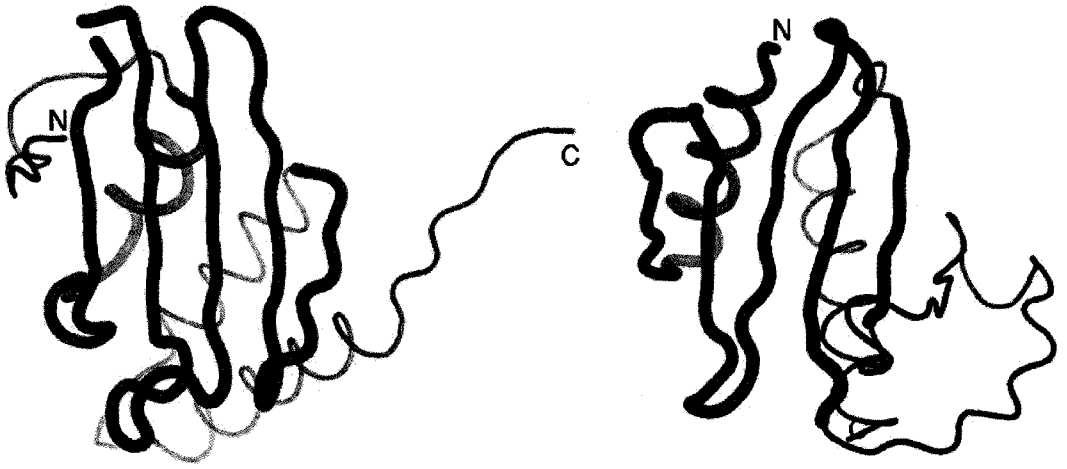

Figure 4-5. Ribbon drawings of CagD (left, light blue) and *Y. enterocolitica* SycT (right, green). Regions that superimpose well (the β-sheet and the first α-helix) are shown as larger tubes. The C-terminal region is dissimilar however, with the other two helices displaying different orientations.

topology of the SycT structure in the region including the N-terminal helix and the β-sheet element, while displaying remarkable difference in the orientation of the α-helices located at the C-terminus. Analogous to the *Yersinia* SycT chaperone, CagD presents all the main α-helical motifs grouped on just one side of the β-strands, whereas all the other T3SS chaperones display a third α-helix on the opposite side which is widely involved in the dimerization process (40, 135). However, the dimeric arrangement of CagD is quite different from SycT and that of other members of this family, suggesting that, starting from a topological proximity, they developed divergent ways to address different effector/substrate properties.

4.2.4 CagD localization

The subcellular localization of CagF was determined using differential detergent solubility (61). This protocol was further optimized to achieve complete separation of the inner and outer bacterial membranes. 0.1% sodium lauroyl sarcosine was used to achieve exclusive solublization of the inner membrane while 0.2% sodium lauroyl sarcosine was employed to obtain a clean outer membrane preparation. To begin the initial biochemical characterization of CagD, it was of interest to determine the location of CagD in the bacterial cell. Figure 4-6 shows CagD localized largely in the cytosolic fraction as well as the inner bacterial membrane. A small amount of the protein was also detectable in the periplasmic fraction, however due to the lack of a suitable periplasmic and cytosolic marker, this finding is merely suggestive. CagF was used as a marker for inner

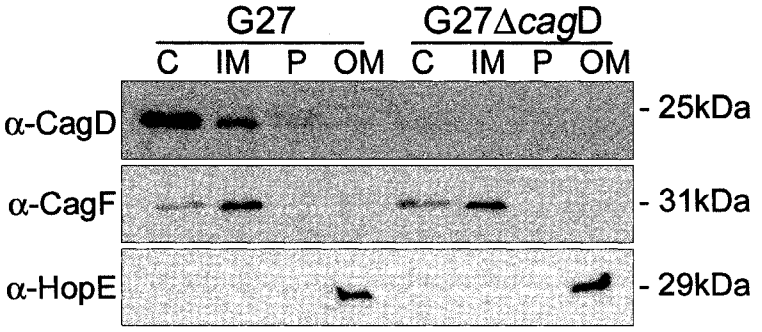

Figure 4-6. Subcellular bacterial localization of CagD. G27 wild-type and G27Δ*cag*D were fractionated into four major fractions: cytoplasm (C), inner membrane (IM), periplasm (P), and outer membrane (OM). The cytoplasm was purified by ultracentrifugation, periplasm by lysosyme treatment, and inner and outer membranes by differential solubility in 0.1% and 0.2% sarcosyl, respectively. Equal proportions of each fraction samples were analyzed. Immunodetection of CagD was conducted using rat α-CagD antisera. Immunoblots were probed with the control antibodies α-CagF (inner membrane) and α-HopE (outer membrane) to monitor the purity of the membrane fractions.

membrane protein separation. HopE, an outer membrane porin, served as an outer membrane marker and was reactive only to the outer membrane fraction. These controls show exclusive separation of the inner and outer membrane.

Consistent with these subcelluler fractionation results, CagD was also visualized within the bacteria by immunofluorescent microscopy (Figure 4-7). G27 when stained with CagD antiserum was not labeled during normal infection conditions. However, when the samples were permeablized with 0.2% NP-40, a distinct focal staining pattern was observed around the membrane of the bacteria in addition to a generalized staining of the cytosol (Figure 4-7). G27Δ*cag*D did not show any staining when permeablized (Figure 4-7), supporting the specificity of the staining pattern seen for the wild-type samples. This would suggest that CagD was not on the external surface of the bacteria, and instead was only recognized when antibodies were allowed access to the internal membrane compartments. As the subcellular fractionation data did not detect CagD in the outer membrane, the punctuate staining represents discrete inner membrane foci, likely accounting for the inner membrane and periplasmic localization described in Figure 4-6. The staining pattern for Δ*cag*D/D-FL was consistently localized to discrete focal regions within the bacterium rather than punctuate foci around the periphery of the membrane (Figure 4-7).

4.2.5 Effects of CagD mutants on CagA translocation

To further characterize whether CagD is a crucial component of the type IV secretion system we used the CagA tyrosine phosphorylation assay. As tyrosine-phosphorylation of CagA occurs only inside the host cell, this assay is a sensitive

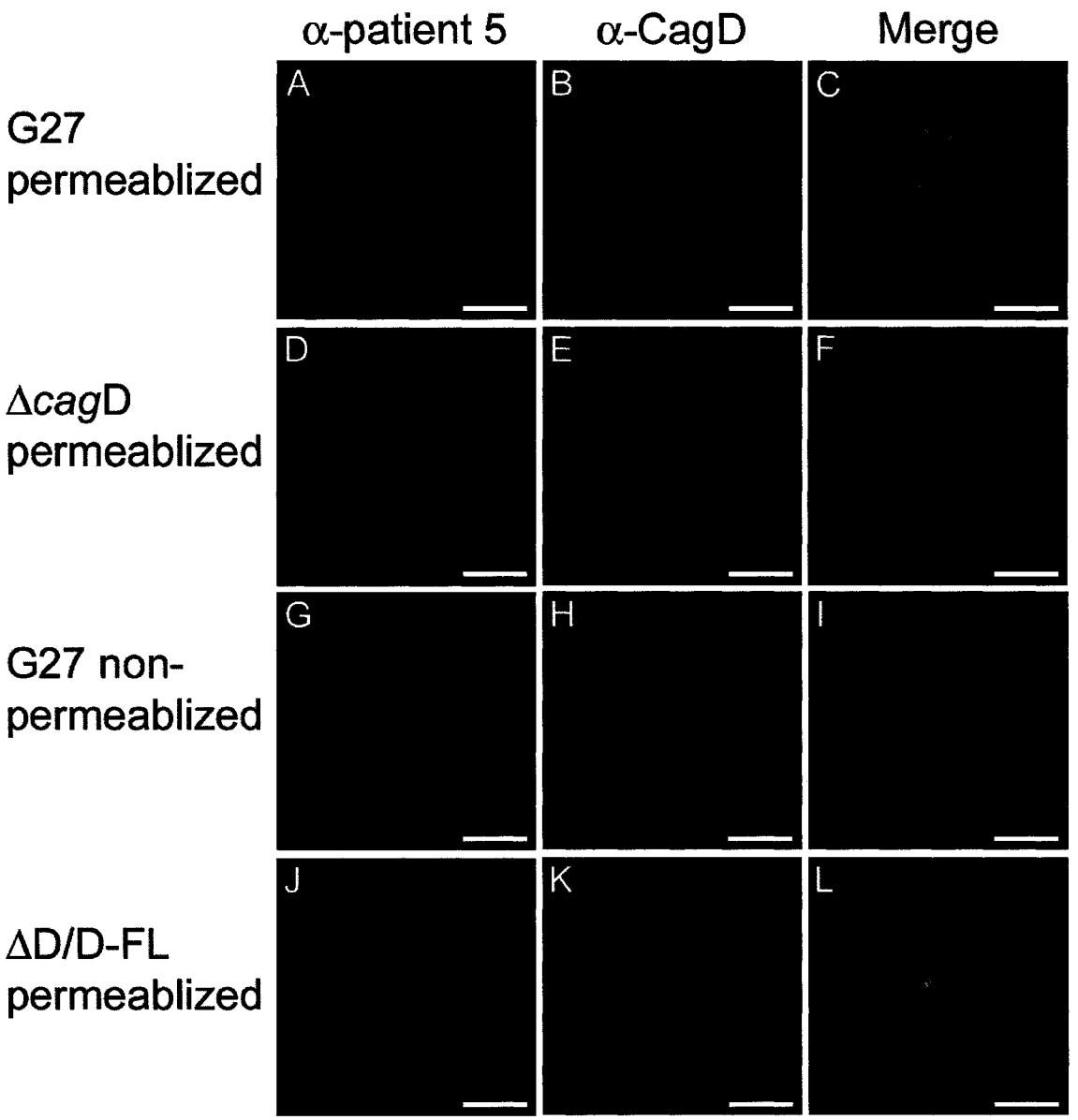

Figure 4-7. CagD forms punctuate foci around the bacterial membrane. AGS cells were infected with G27, G27Δ*cag*D, and Δ*cag*D/D-FL for 4 hours at an MOI of 10. Samples were permeablized with 0.1% NP-40 and *H. pylori* was visualized by immunofluorescence microcopy with serum from a convalescent patient, while CagD was visualized with rat α-CagD antiserum. Scale bars represent 2.5μm.

measure for CagA translocation. A previous report indicated that CagD is not absolutely required for CagA secretion but increases secretion efficiency when present (87). Therefore, it was of interest that we obtained contradictory findings when membrane containing fractions of AGS cells infected with various *H. pylori* strains were analyzed by immunobloting using the α-phosphotyrosine antibody (Figure 4-8). Wild-type G27 translocated CagA that was subsequently tyrosine phosphorylated in the AGS cell (Figure 4-8). Our previous work established that a Δ*cag*F isogenic mutant was unable to translocate CagA (61), and this served as a negative control in this assay. The phosphorylation pattern of uninfected cells was the same as the Δ*cag*F isogenic mutant (Figure 4-8). The Δ*cag*D strain showed identical results as the Δ*cag*F strain. To ensure that our *cag*D mutant did not have polar effects on downstream gene products, a CagD-Flag gene was expressed from the *rec*A gene site under the control of the *cag*A promotor. As seen in Figure 4-8, phosphorylated CagA was detected in the membrane-containing fraction for Δ*cag*D/D-FL, albeit at lower levels than wild-type. To test whether the C-terminal Flag-tag was interfering with protein function or possible dimer formation, the wild-type CagD protein was expressed in the same manner as the Flag construct. The Δ*cag*D/Dwt strain showed similar CagA phosphorylation levels as Δ*cag*D/D-FL (Figure 4-8). Both the wild-type and Flag-tagged *cag*D were under the control of the *cag*A promoter, as the promotor for *cag*D has yet to be identified. To test whether expression of CagD from a non-native promotor could have decreased effects on CagA translocation, CagD was reintroduced by homologous recombination into the native gene location yielding the rescued strain D*. D* appeared to translocate CagA similar to G27, suggesting that expression levels of CagD may be tightly controlled for this function.

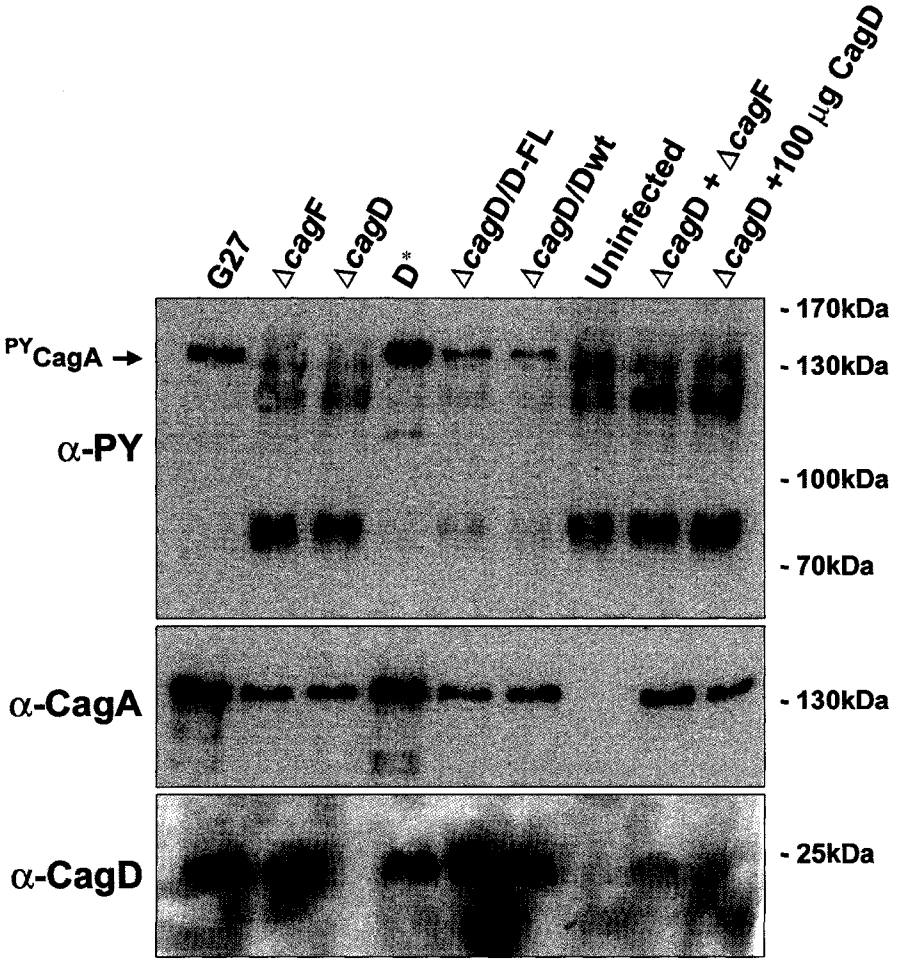

Figure 4-8. CagD is required for CagA phosphorylation. AGS cells were infected with various strains of *H. pylori* for 4 hours and fractionated into cytosol and RIPA buffer soluble fraction containing eukaryotic membranes. RIPA soluble fractions were separated by SDS-PAGE, transferred to PVDF membranes, and immunobloted with the α-PY antibody to detect phosphorylated proteins. Normal host protein phosphorylation patterns are depicted by uninfected cells. Immunoblots were also probed with α-CagA and α-CagD antibodies to confirm protein expression for each sample.

4.2.6 CagD does not interact with CagF or CagA

CagF and CagA were previously described to interact at the inner bacterial membrane; an interaction that was essential for CagA translocation (61, 163). The subcellular fractionation of CagD was similar to CagF as well as its necessity for CagA translocation; therefore we were interested to determine whether CagD interacted with CagA and CagF in a multi protein complex. The strains ΔF/F-FL and G27/A-FL were grown overnight in addition to G27 and lysed. α-Flag M2 beads were used to immunoprecipitate the corresponding Flag-tagged CagA and CagF from the lysates. Samples were analysed by SDS-PAGE and western blot for co-immunoprecipitation of CagD (Figure 4-9). Neither CagF-Flag nor CagA-Flag precipitated CagD from solution, suggesting that CagD does not interact with this complex. It should be noted that both CagF and CagA were able to reciprocally immunoprecipitate each other, confirming that the experiment was successful. G27 IPs were devoid of CagA, CagF, and CagD.

4.2.7 Extracellular localization of CagD

A previous proteomic analysis indicated that CagD was present in the bacterial culture supernatant, while other Cag proteins were not detected (201). We therefore tested whether we could confirm these findings and expand their scope. In fact, CagD could be immunoprecipitated in significant amounts from *H. pylori* supernatants of wild-type G27, Δ*cag*D/D-FL, as well as G27Δ*cag*E, G27Δ*cag*X, G27Δ*cag*Y, and G27Δcagβ (Figure 4-10). To ensure that release of CagD in the extracellular supernatant was not due to autolysis, we immunoprecipitated extracellular supernatants of Δ*cag*D/D-FL and ΔF/F-FL with α-Flag M2 agarose beads (Fig 4-10). As

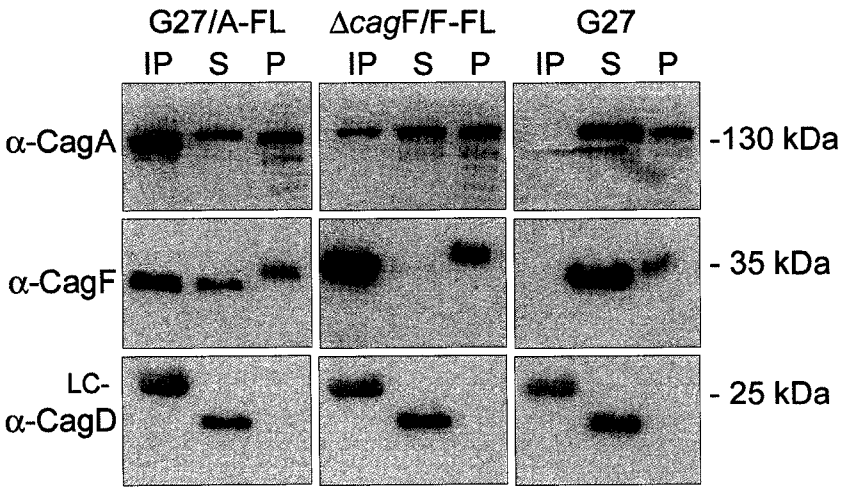

Figure 4-9. CagD does not interact with CagA or CagF. Flag-tagged CagF and CagA were immunoprecipitated from lysed overnight culture with α-Flag MS agarose beads. Samples were probed with α-CagA, α-CagF, and α-CagD to detect proteins in precipitation samples (IP), lysis supernatants (S), and bacterial pellets (P). LC indicates Ig light chain.

we have previously shown that CagF-Flag readily precipitates with the Flag antibody (Couturier 2006), if autolysis was occurring, CagF would be readily immunoprecipitated from the extracellular supernatant. CagD-FL precipitated readily from the extracellular supernatants, while CagF-FL was found exclusively in the bacterial pellet (Figure 4-10). These results suggest that CagD was likely not secreted by the type IV secretion system since each mutant for *cag* genes tested showed extracellular localization fo CagD. CagD was also not released unspecifically by bacterial lysis, suggesting that CagD was released by an unknown mechanism into the extracellular supernatant.

CagD was now established to be present in the extracellular space; therefore it was of interest to test whether CagD played its role in CagA translocation in the extracellular space during infection. To test this hypothesis, extracellular CagD produced by G27Δ*cag*F was tested for functional complementation ability during coinfection with G27Δ*cag*D. In this assay, G27Δ*cag*F would export CagD to the extracellular supernatant, while not being able to translocate CagA into host cells. Likewise, G27Δ*cag*D could not translocate CagA unless the extracellular CagD (released by CagF) was functionally complementing the secretion system from the exterior environment. If the extracellular CagD can complement the *cag*D mutant, CagA phosphorylation would be detected in the membrane fraction. AGS cells were co-infected with G27Δ*cag*F and G27Δ*cag*D and the CagA tyrosine phosphorylation assay was used to detect translocated and phosphorylated CagA (Figure 4-8). No tyrosine phosphorylated CagA was detected in this sample. It was possible that the levels of CagD released by G27Δ*cag*F were not sufficient to functionally complement CagA translocation in G27Δ*cag*D to detectable levels during infection. To test this hypothesis 100 μg of purified recombinant CagD was

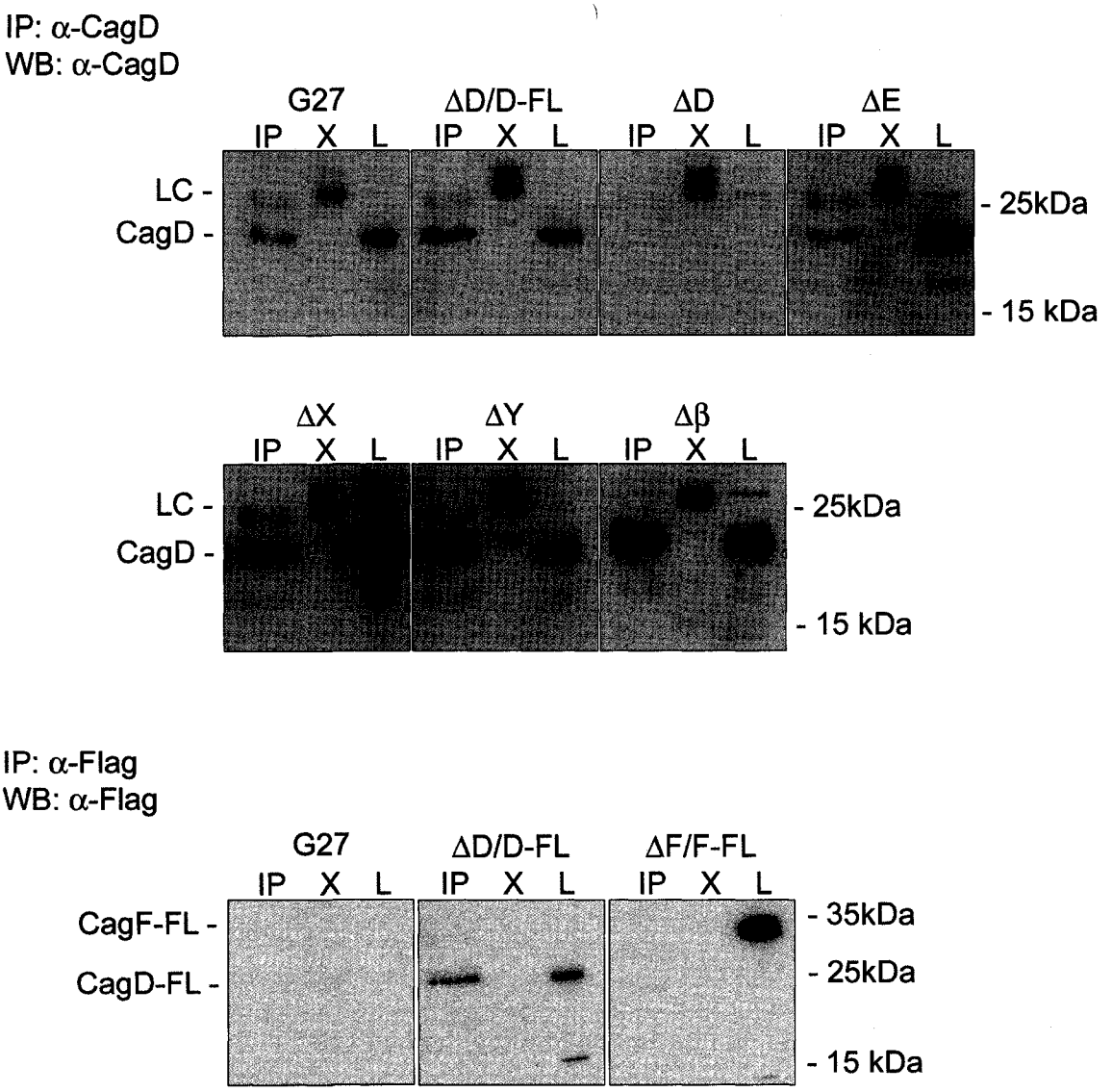

Figure 4-10. CagD is present in the supernatant of *H. pylori* cultures. Extracellular supernatants from various *H. pylori* strains were immunoprecipitated with the α-CagD antibody (top panel) or α-Flag antibody (lower panel). Immunoprecipitations were separated by SDS-PAGE, transferred to PVDF membranes, and detected by immunoblotting with the same antibody used for immunoprecipitation. (IP: immunoprecipitation sample, X: culture extracellular supernatant, L: bacterial lysate, LC: IgG light chain).

added to the infection medium and the infection with G27Δ*cag*D was allowed to proceed for 4 hours. Similar to the previous co-infection, no CagA phosphorylation was detected in this condition, suggesting CagD plays its role in CagA secretion inside the bacterium (Figure 4-9).

4.2.8 CagD co-fractionates with host membranes following infection

As significant amounts of CagD were precipitated from the extracellular supernatant, we hypothesized that extracellular CagD associated with host cell membranes during infection and this process may aid CagA translocation or provide alternative virulence functions. To investigate this hypothesis we performed eukaryotic cellular fractionation studies. AGS Cells were infected with *H. pylori* for 4 hours and fractionated by mechanical lysis into host cytosol, membrane, and the fraction containing the host insoluble fraction and the bacteria. Membrane and insoluble fractions were analyzed by SDS-PAGE analysis and immunobloting (Figure 4-11). The results showed that significant amounts of CagD co-fractionated with the host cell membranes. In agreement with the T4SS-independent extracellular localization of CagD, this association appeared independent of CagA translocation or components of the type IV secretion system (CagF) (Figure 4-11). Detection with α-CagA antibody was used as a positive control for T4SS dependent effector association with host membranes, c-MET was used as a general host membrane marker and loading control, and CagF and CagX were used as negative controls to show that CagD co-localization with membrane fractions was not due to bacterial membrane contamination.

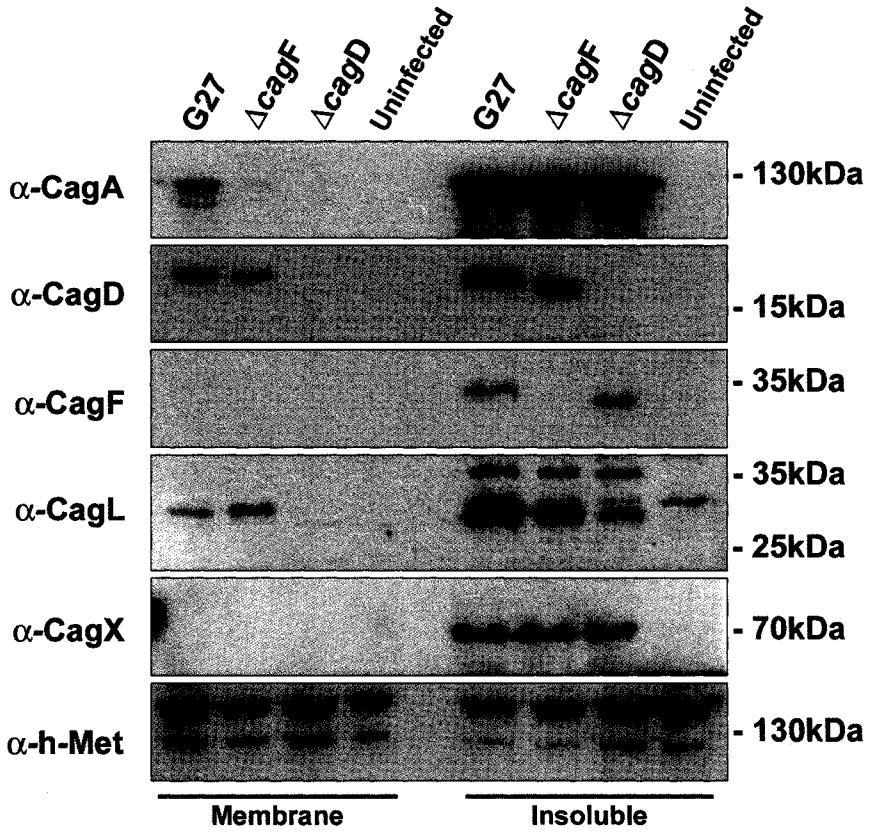

Figure 4-11. CagD is required for CagA translocation and associates with the eukaryotic membrane. AGS cells were infected with the wild-type strain G27 or its isogenic mutants G27Δ*cag*F and G27Δ*cag*D for 4 hours or left uninfected. Cells were then fractionated by syringe lysis. Host cell cytosol and membrane proteins were separated from the cellular fraction containing the bacteria, and the cytoskeleton proteins (Insol). Membrane and insoluble fractions were probed with antibodies for CagA, CagD, CagF, CagL, CagX, and h-Met.

4.2.9 CagD is involved in pilus assembly

Given the data acquired, it seemed reasonable to speculate that CagD may associate with the extracellular environment as a component of the type IV secretion pilus. CagL was recently shown to be an adhesin of the type IV secretion pilus that binds to host integrin and fractionates with the eukaryotic membrane (131); therefore we were interested to confirm whether CagL was also found in the host cell membrane fraction similar to CagD and whether it was still associated with the membrane in the absence of CagD. CagL was detected in the G27 infected membrane fraction as well as the insoluble fraction as expected. Interestingly, CagL was not present in the host cell membrane fraction during infection with G27Δ*cag*D, but did associate with the host cell membrane in the *cag*F mutant (Figure 4-11). To further confirm these findings, IL-8 induction was measured during infection with various strains as a reporter for pilus assembly and host cell contact. As shown in Figure 4-12, IL-8 induction was decreased for a *cag*D mutant, while a *cag*F mutant showed no drastic reduction. Both Δ*cag*D/Dwt and D* restored IL-8 induction levels, with D* achieving wild-type-like induction. Both ΔcagF and ΔcagF/F-FL showed no a limited decrease in IL-8 induction, supporting the CagL fractionation results that CagD is required for CagL fractionation with the host membrane. The *cag*E mutant, previously shown to abolish T4SS related IL-8 induction (87), showed IL-8 induction similar to uninfected cells (Figure 4-12).

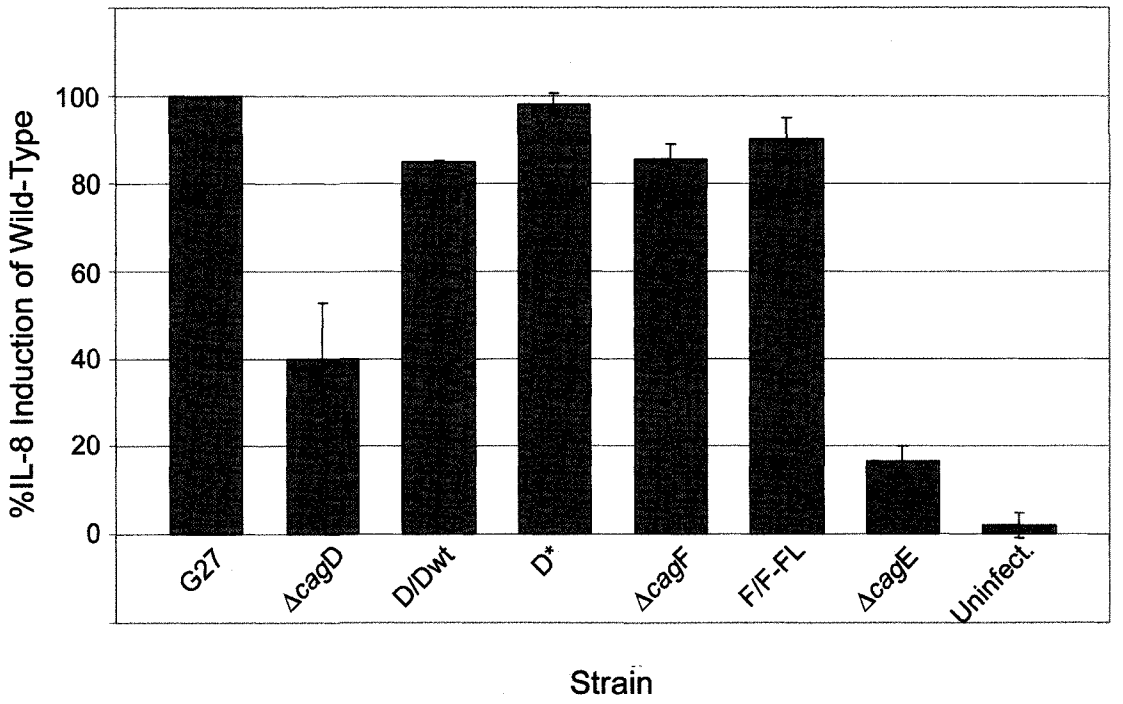

Figure 4-12. CagD is involved in pilus assembly. IL-8 levels post-24 hour infection of AGS cells for various mutants are expressed in relative percentage to wild-type G27 infection. Values represent means $\pm$ standard deviations for three independent trials for all samples except ΔcagE which is based on two independent samples. The bars on ΔcagE represent the difference in two samples rather than standard deviation.

4.3 Discussion

In addition to the conventional components that comprise T4SS, *H. pylori* encodes additional proteins that are required for CagA translocation including CagC to CagD, CagF to CagL, CagM, CagU, and Cagδ (87). We and others previously demonstrated a chaperone-like function for CagF, which is required for CagA secretion (61, 163). CagC was suggested to be a potential subunit of the type IV secretion pilus (10, 130) and CagL was identified as the pilus adhesin that is crucial for integrin binding (131). In this study we investigated the structure and function of the poorly described CagD protein. Crystallization data revealed that CagD forms a covalent homo-dimer, characterized by a molecular two-fold symmetry. Despite the fact that the fold of the monomer is relatively common, the protein topology does not coincide with that of other proteins of known structure. The organization of the dimer is quite peculiar and there are no other similar dimers in the Protein Data Bank. The most similar structure for the CagD monomer found in the data bank is that of the SycT chaperone protein of *Y. enterocolitica* type III secretion system (T3SS) (40, 135). This similarity is quite intriguing, since SycT is a chaperone of YopT, a cysteine protease that cleaves the membrane-anchor of Rho-GTPases in the host (194). SycT is a member of a family of T3SS chaperones, whose functions include preventing effector agglomeration, keeping the effector in a partially unfolded state, and helping to regulate the T3SS (161). All these chaperones are characterized by low molecular weight, low sequence similarity, low pI, and are homodimers (85). The similarity of the fold of CagD with that of SycT, though limited, suggests that it could play a similar role of chaperone for the secretion system of *H. pylori*.

To elucidate more about the localization and function of CagD we performed bacterial and cellular fractionation assays as well as fluorescence microscopy. Our data showed that in addition to a cytosolic pool, CagD partially associates with the inner membrane, where it is likely exposed to the periplasmic space. Such localization is supported by the strongly predicted N-terminal signal peptide of CagD, the presence of a minor amount of the protein in the periplasmic fraction, as well as disulphide bond formation detected in the crystal structure. However, it should be mentioned that our lack of suitable cytosol and periplasm markers does not allow for certainty of the periplasmic fraction. Due to the nature of the protocol, it is possible that the small amount of periplasmic localization detected was a result of cytosolic CagD leaking out of the cell. However, when we use this methodology for CagF, there is no detectable CagF in the periplasmic fraction. Since both proteins exist in cytosolic pools, this argues against cytoplasmic contamination. In agreement with these data, fluorescence microscopy during AGS cell infection visualized CagD at the bacterial membrane. Here, CagD appeared to localize in a spot-like pattern rather than exhibiting a homogenous distribution throughout bacteria. However, whether the spots co-localize with the T4SS could not be determined. We were unable to detect an interaction between CagD and CagF or CagA, which was not unexpected since the radiograph and Strep pull-down experiments for CagF did not have bands in the 20 kDa range (Figure 3-2A and 3-4A).

Furthermore, CagA tyrosine phosphorylation assays identified CagD as an essential component of the T4SS, since an isogenic *cag*D mutant was unable to translocate CagA. This result was in contradiction with previous findings that reported CagD having reduced CagA translocation efficiency (87). The reason for this

discrepancy remains unclear, however the fact that we were able to restore CagA translocation in the *cag*D mutant by re-introducing and expressing the *cag*D gene (wild-type and Flag-fusion) in trans, argues against a polar effect of our mutant on expression of downstream *cag* genes. The previous CagD deletion created by Fischer *et al.* was made by inserting a kanamycin resistance gene in the open reading frame. It is possible that a truncated version of CagD was expressed in their strain, possibly resulting in the partial restoration of CagA translocation described. Our mutant was a clean in frame deletion of the gene, and therefore more reliable for the purpose of these studies. Thus, our results show that CagD is a crucial component of the T4SS that is strictly required for CagA translocation into the host epithelial cells.

It was interesting to observe that both Δ*cag*D/Dwt and Δ*cag*D/D-FL displayed reduced CagA secretion while the D* rescue strain showed wild-type-like CagA phosphorylation. Both Δ*cag*D/Dwt and Δ*cag*D/D-FL have CagD expressed under the *cag*A promoter, which we have shown to be a highly active promoter for expression of Cag proteins from the *rec*A locus (61). Our results therefore suggest that CagD expression must be optimally regulated in order for efficient CagA translocation and phosphorylation events to take place. Consistent with this idea, the staining pattern for Δ*cag*D/D-FL using α-CagD resulted in a more conglomerate staining rather than peripheral foci staining as seen in G27. This may reflect CagD that is not being trafficked equally to its proper location due to low amounts or possible aggregation and inclusion due to overexpression.

In agreement with previous findings, we also identified significant amounts of CagD in the culture supernatants (201), which was not a result of general bacterial lysis,

suggesting a possible second function for CagD. However, since various core components of the T4SS were not required for the extracellular location of CagD, the export mechanism and the importance of this finding remain elusive. However it should be noted that T4SS-dependent secretion could not completely be excluded since we only tested a sub-set of mutants for core components. It is possible that a single Cag protein that is not implicated in CagA secretion could be involved in CagD secretion. Another possibility is that CagD is transported out of the bacteria by another secretory pathway in the absence of a functional *cag* T4SS. There are two additional T4SSs described in *H. pylori*: the ComB DNA uptake system and the less characterized *tfs*3 system. However the *tfs*3 can be ruled out, as strain G27 does not posses this gene cluster (17).

Interestingly, we found significant amounts of CagD co-fractionated with host cell membrane proteins during fractionations studies of infected AGS tissue culture cells. Since this co-fractionation was as well independent from the *cag* genes tested, our findings may indicate that CagD is released into the supernatant during host cell infection and then binds to the host cell surface. Alternatively, CagD may be incorporated into the type IV secretion pilus as an accessory component. This hypothesis could explain its co-fractionation with the host membrane and enrichment in culture supernatant. However, the fact that CagD is found in these fractions independent of the T4SS components tested is quite puzzling. Furthermore, because CagL was not detected in the eukaryotic membrane fraction and IL-8 induction was reduced in the *cag*D mutant, it appears that CagD is involved in the pilus assembly process. Admittedly, as IL-8 induction was only partially reduced, it is possible that CagL presentation was correspondingly reduced below the detection capabilities of the assay via the CagL western blot. Our investigation

by immunofluorescent microscopy was unable to detect surface exposed CagD; however the protein may not have been exposed for access to the antibody, as surface staining studies were not permeablized. Of interest, IL-8 induction was only partially restored by the Δ*cag*D/Dwt strain, while the D* strain restored IL-8 induction to wild-type levels. These results echo the trends seen for CagA secretion/phosphorylation. Though previously published results found CagD was only partially required for CagA translocation and IL-8 induction (87), our results together show that CagD is in fact absolutely necessary for CagA translocation and necessary for efficient pilus assembly.

Overall, these results suggest that CagD may serve as a unique multifunctional component of the T4SS which is likely involved in CagA secretion at the inner membrane (independent of the CagF-CagA protein interaction) and may be released into the supernatant to promote additional effects on the host cell. Whether these effects are required for CagA translocation or trigger CagA-independent virulence functions remains to be determined.

Chapter 5

Helicobacter pylori Produces Unique Filaments Upon Host Contact *In Vitro*

Portions of this chapter have been published as:

Couturier, M. R., and Stein, M. (2008) *Helicobacter pylori* produces unique filaments upon host contact *in vitro*. *Canadian Journal of Microbiology*, 54(7): 537-548.

5. *Helicobacter pylori* produces unique filaments upon host contact *in vitro*

5.1 Introduction

The gastric pathogen *Helicobacter pylori* (*H. pylori)* is a gram-negative, microaerophilic, polar flagellated bacterium that colonizes the harsh environment of the human stomach. *H. pylori* has been implicated in significant gastric maladies such as peptic ulcer disease, chronic gastritis, MALT lymphoma, and adenocarcinoma (142, 154, 155, 165, 207, 221). To date it is still unclear how *H. pylori* is transmitted from human to human, though the organism is thought to infect roughly half of the world's population (98, 207).

H. pylori has been documented as existing in two distinct morphological states in both standard laboratory culture and gastric mucosa of infected individuals (24, 51, 56, 151). The first morphologic state is the helicoid or spiral form. Helicoid *H. pylori* are short (1-3 μm in length) curved rods which are polar flagellated (4-6 flagella) and are the predominant state in exponential culture. The coccoid morphology represents the second morphologic state of *H. pylori.* Coccoids are typically 1-2 μm in diameter, may or may not possess flagella which typically wrap around the organism, and are commonly found in stationary phase or stressed culture (177, 180). Several investigations have further suggested that specific conditions such as temperature downshift (47, 149, 169), nutrient starvation (47), osmotic stress (16, 169), oxygen tension (76, 159), nitric oxide increase (59), and certain antibiotics (196) can contribute to the development of coccoid *H. pylori.* Furthermore, coccoid forms of *H. pylori* cannot currently be revived in standard laboratory culture. As a result, coccoid *H. pylori* are often referred to as viable-but-not-culturable. Debate continues as to the biological function and significance of the coccoid

phenotypic state. Several lines of investigation suggest that coccoid *H. pylori* can colonize and cause infection in mice (46, 195). Osmotic stress has also been shown to induce coccoid formation over time, and allow for binding to abiotic surfaces (15). Furthermore, the AmiA protein was identified as an essential factor for coccoid conversion and immune evasion, leading to the hypothesis that coccoids represent a persistant state of *H. pylori* (53). Therefore, it is plausible that the coccoid state serves as a "spore-like" stress-induced survival mechanism for transmission between hosts and/or a factor contributing to long-term survival and persistence in the stomach.

H. pylori assembles two known surface structures, the first major structure being the flagellum. *H. pylori* possess a single polar cluster of flagella which are used primarily for motility through the gastric mucosa (80). These flagella are unique from most other bacterial flagella in that they are coated in a sheath (96, 100). A second surface structure, the *cag* type IV secretion system, was recently identified by electron microscopy as well as by immunofluorescence microscopy (173, 210). This structure was shown to be comprised of the *cag* pathogenicity island encoded proteins CagT, CagX, CagY, CagC, and CagL (10, 131, 173, 210).

Here we describe the identification of bacterial surface appendages termed "filaments" that can be observed during co-cultivation of *H. pylori* with tissue culture cells. Filaments were unique structures from the previously known flagella and T4SS pilus. The filaments varied in length and increased in number over time as the bacteria progressively converted from helicoid to coccoid morphology. Importantly, filaments were partially composed of mannose-linked carbohydrates and were recognized by convalescent serum from human patients, lending support for *in vivo* relevance.

5.2 Results

5.2.1 Observation of novel bacterial filaments *in vitro*

We sought to use antiserum raised against complete *H. pylori* to visualize antigenic molecules on the bacterial surface during infection of AGS cells. This serum recognized bacteria on the surface of AGS cells during infection with *H. pylori* wild-type strain G27, and additionally two surface structures that were attached to the bacteria (Figure 5-1). The first structure (arrow head) resembled the bacterial flagella due to its characteristic polar localization, curvature, length, and abundance. The second structure (arrow) was observed less frequently and occurred on both helicoids and coccoids (Figure 5-1A-H'). These filamentous structures were consistently longer than flagella, often linear in appearance, and frequently connected two or more bacteria (Figure 5-1B-B' and D-E'). Filaments sometimes appeared to follow the curvature of eukaryotic cells or spanned the void between two adjacent cells. The longest observed structure measured 59 μm in length. Helicoid bacteria appeared to form filaments on the opposite pole from the flagella (Figure 5-1A); however these were not as common as those extending from coccoid bacteria, which typically appeared non-flagellated. The structures were not limited to strain G27, but were also formed by strains 87A300, N6, 26695, and J99 (Figure 5-2). While AGS cells were used for this study it should be noted that N87 cells were also used to reveal that filament development was not cell type specific (Figure 5-1B). Filaments could not be detected using various control conditions (Figure 5-1F-H') including the use of pre-immune serum from the mouse used to create the *H. pylori* antiserum, which strongly suggested that the filaments are bacterial derived and not

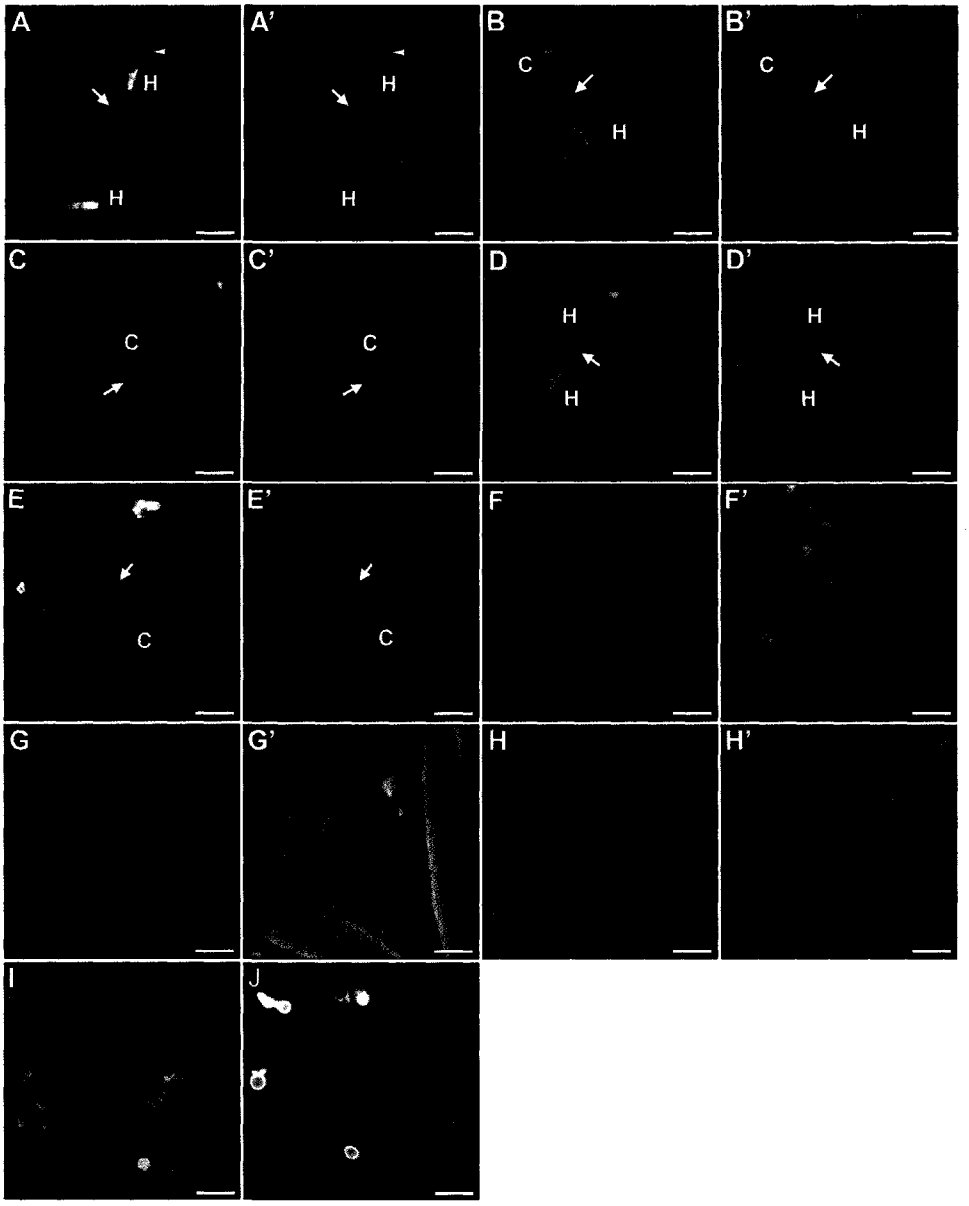

Figure 5-1. Various *H. pylori* strains form filaments during infection of AGS tissue culture cells. Strains G27 (A-B', I, and J), N6Δ*fla*AB (C and C'), G27Δ*cag*Y (D and D'), and G27Δ*com*B (E and E') were used to infect AGS cells for 4 hours, stained with *Helicobacter* mouse antiserum, and visualized by immunofluorescence (left panel of pair) and phase contrast microscopy (right panel of pair). Filaments are indicated by arrows and flagella are represented by arrowheads. Coccoid and helicoid bacteria are indicated by "C" and "H" respectively. Negative controls include: infected cells stained with only the secondary antibody (F and F'), uninfected AGS cells stained with *H. pylori* antiserum and secondary antibody (G and G'), infected cells stained with mouse pre-immune serum and secondary antibody (H and H'), and G27 incubated on polyethylene terephthalate membranes in infection medium for 4h in the absence of AGS cells (I). AGS cells in J were prefixed in paraformaldehyde and infected with G27 for 4 hours. Scale bars represent 5.0 μm (A-H') and 2.5 μm (I and J).

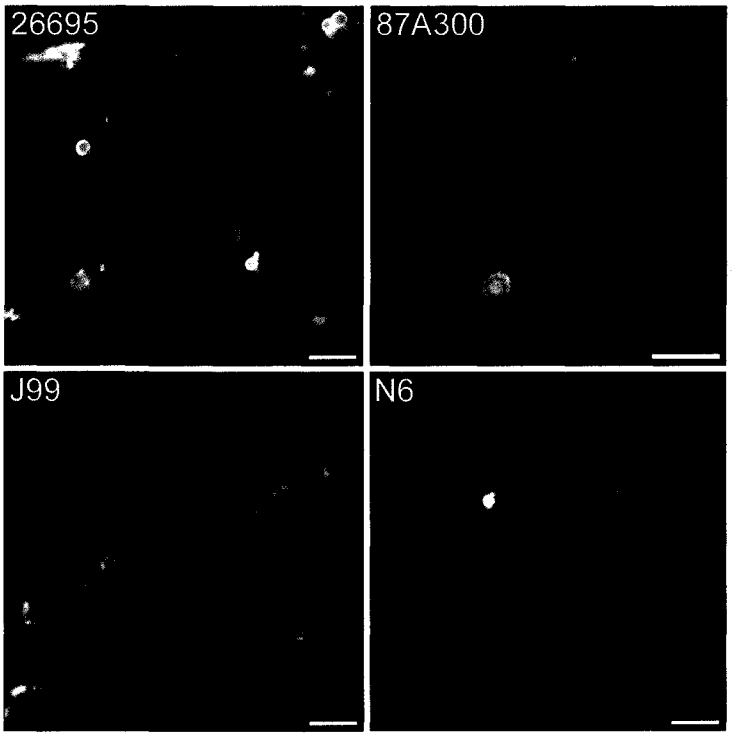

Figure 5-2. Filaments are formed by various wild-type strains of *H. pylori*. Strains 87A300 (source strain for α-*H. pylori* antiserum), J99 (sequenced strain), 26695 (sequenced strain), and N6 (flagella mutant background) were stained with α-*H. pylori* antiserum and visualized by immunofluorescence microscopy. Scale bars represent 5.0 μm (26695, J99, and N6) and 2.5 μm (87A300).

artifacts of staining or self antigen recognition. To exclude that the medium rather than host cell contact triggered filament formation we also infected the cells in the presence of various media. All tested conditions, including Brucella Broth and RPMI with 0, 5, or 10% FCS resulted in filament formation (Figure 5-3). However, when PET tissue culture inserts were employed to physically separate bacteria from eukaryotic cells while allowing passive movement of soluble molecules, there were no filaments detected (Figure 5-1I). Similarly, we did not observe filament formation during a 1 to 12 day time course, when *H. pylori* was incubated in the various media in the absence of host cells (Figure 5-1I, representative field). To test whether contact with host cells is sufficient to trigger filament formation, or whether metabolically active eukaryotic cells are required, we prefixed AGS cells with paraformaldehyde and infected the cells as before. The bacteria colonized the fixed cells readily but did not form filaments (Figure 5-1J). Therefore, our experiments suggest that direct contact with metabolically active eukaryotic cells is necessary for filament formation.

5.2.2 Filaments are formed by strains with known mutations in surface structures

In order to determine whether the filaments observed by immunofluorescence microscopy were abnormal flagella or type IV secretion complexes, we used mutant strains of *H. pylori* to infect AGS cells and assay for filaments as described above. The *H. pylori* flagella is the most obvious and visible structure seen on the surface of the bacteria. We infected AGS cells with the wild-type N6 strain and the flagellin double mutant N6Δ*fla*AB, which was previously shown to lack any flagella (120). Strain N6 formed flagellated helicoids and coccoids with filaments in a 4 hour infection (Figure 5-

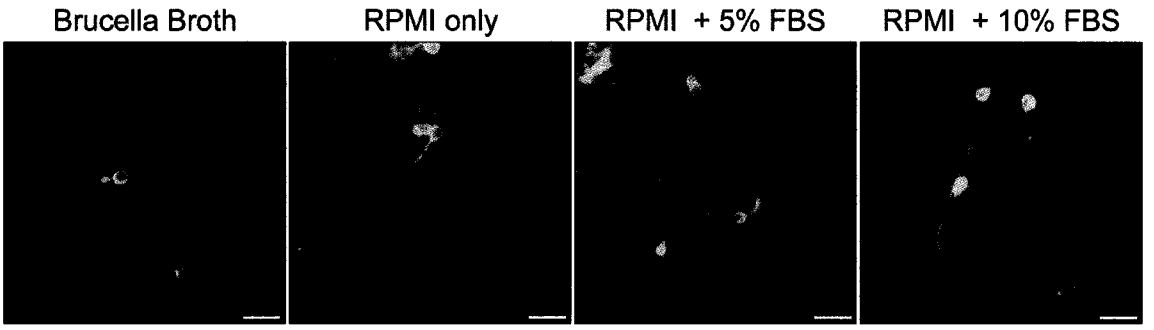

Figure 5-3. Filament formation is independent of media composition. G27 was used to infect AGS cells with various culture media including: Brucella broth liquid, RPMI, and RPMI supplemented with 5 or 10% FBS. Samples were stained α-*H. pylori* serum and visualized by immunofluorescence microscopy. Scale bars represent 5.0 μm.

2). N6Δ*fla*AB formed long filaments but did not synthesize flagella (Figure 5-1C-C'). This suggested that the structures were not atypical flagella. The second known bacterial surface structure, the *cag* type IV secretion complex, is comparatively smaller in size and only stains as foci by immunofluorescence microscopy (10, 173, 210). The filaments described in Figure 5-1 did not resemble the type IV secretion system sheathed pilus (173, 210). To ensure that the filaments were not abnormal manifestations of a type IV secretion system, we infected AGS cells with G27Δ*cag*Y, a structurally disrupted type IV secretion mutant. G27Δ*cag*Y was also able to form filaments (Figure 5-1D-D'). We further mutated the *com*B DNA uptake type IV secretion system, but the G27Δ*com*B strain which was lacking the *com*B8, *com*B9, and *com*B10 genes was also able to form filaments (Figure 5-1E-E'). A third type IV secretion system, *tfs*3, was not present in strain G27 and therefore could not account for the filaments reported here (17).

5.2.3 Filamentous structures are visualized by scanning electron microscopy

To further confirm that the filaments seen in the immunofluorescent microscopic analysis represented a physical structure, AGS cells infected for four hours were analyzed by scanning electron microscopy (SEM). Long bacterial filaments were visible along the surface of the AGS cells (red arrow) (Figure 5-4A), which were absent on uninfected AGS cells (Figure 5-4B). Eukaryotic structures on AGS cells with potentially similar appearance include filopodia (arrow head) and microvilli (white arrow) (Figure 5-4A-B), which have been shown previously by SEM (104). However, the extended microvilli appear shorter than our documented structures with a larger diameter. The filopodia are

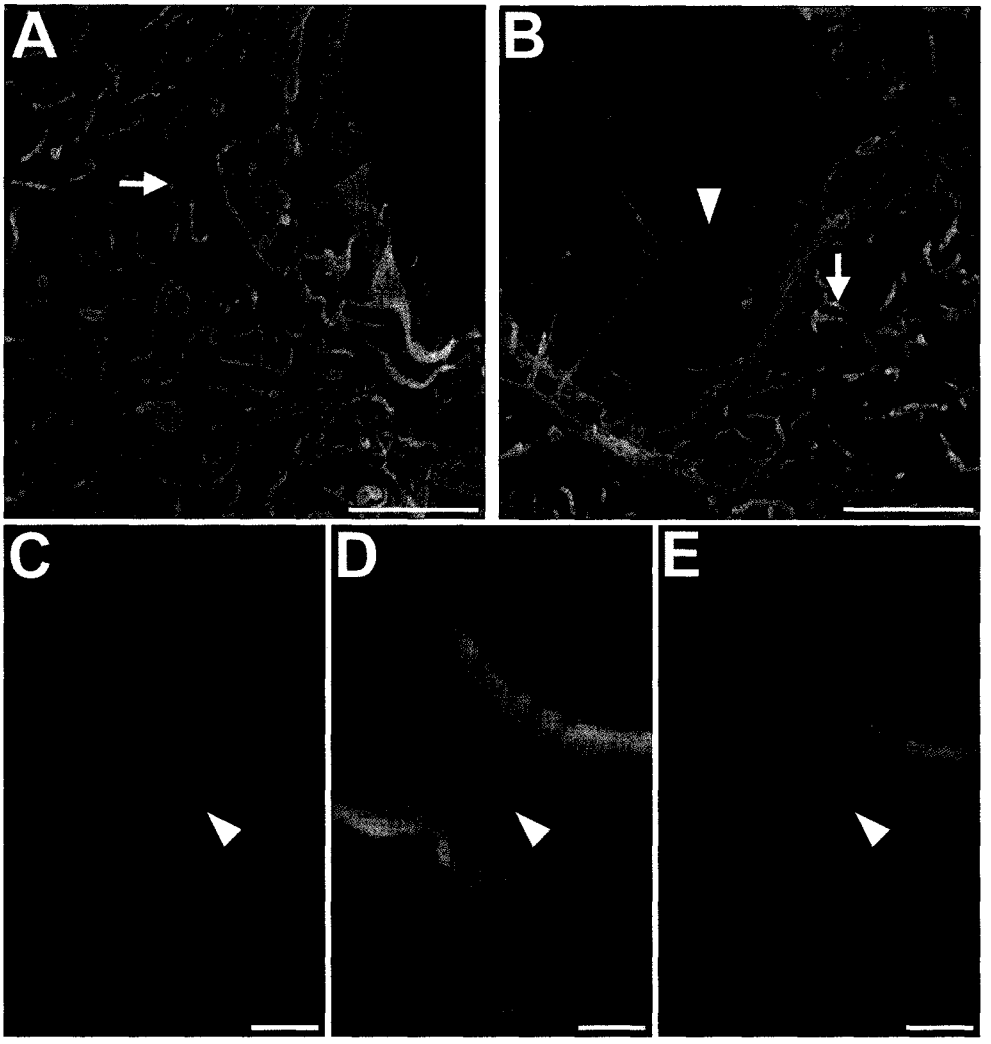

Figure 5-4. Visualization by scanning electron microscopy of long filamentous appendages on *H. pylori* unique from eukaryotic cellular structures (A and B). G27 filaments (red arrows) stretch across the surface of AGS cells connecting one or more bacteria (A). Filaments are absent on uninfected AGS cells (B). White arrows represent microvilli and arrowheads represent filopodia. Phase contrast microscopy reveals an abundance of filopodia (D). Filopodia did not stain with the α-*H. pylori* antiserum (C and E). Scale bars represent 7.5 μm (A-B) 2.5 μm (C-E).

often similar in length to the bacterial filaments but appear thicker and do not stain with the *H. pylori* antiserum (Figure 5-4C-E).

5.2.4 Coccoid *H. pylori* and filament formation increase over time during tissue culture infections

AGS cells infected with G27 were examined over a 24 hour period. Samples were fixed and analyzed at 1, 2, 3, 4, 8, and 24 hour time points by immunofluorescence microscopy. Bacteria were visually enumerated and scored based on morphology, presence of filaments, and whether the filaments connected two bacteria. Figure 5-5 shows a graphical representation of the scoring of *H. pylori* at each time point for three independent trials. The mean percentage of coccoid bacteria in the infection increased drastically over the first 4 hours to 81% (Figure 5-5A and Figure 5-6). Filament formation was not observed during the first two hours of infection, and maximally between 3 and 4 hours (Figure 5-5B). At 4 hours, 15.7% of bacteria possessed filaments. The abundance of bacteria-bacteria filaments also increased over time during the infections (Figure 5-5B). Between 4 and 8 hours, conversion to coccoid increased from 81% to 91% (Figure 5-5A and Figure 5-6), while during the same period a decrease in the number of filaments was evident (Figure 5-5B). This decrease appeared inverse to bacterial clustering. By 24 hours, bacteria were greater than 99% coccoid and too clustered for accurate statistical analysis (Figure 5-6). However, it should be noted that the actual numbers of coccoids may have been slightly lower than we reported, since enumerating by fluorescence microscopy involves a certain degree of inherent

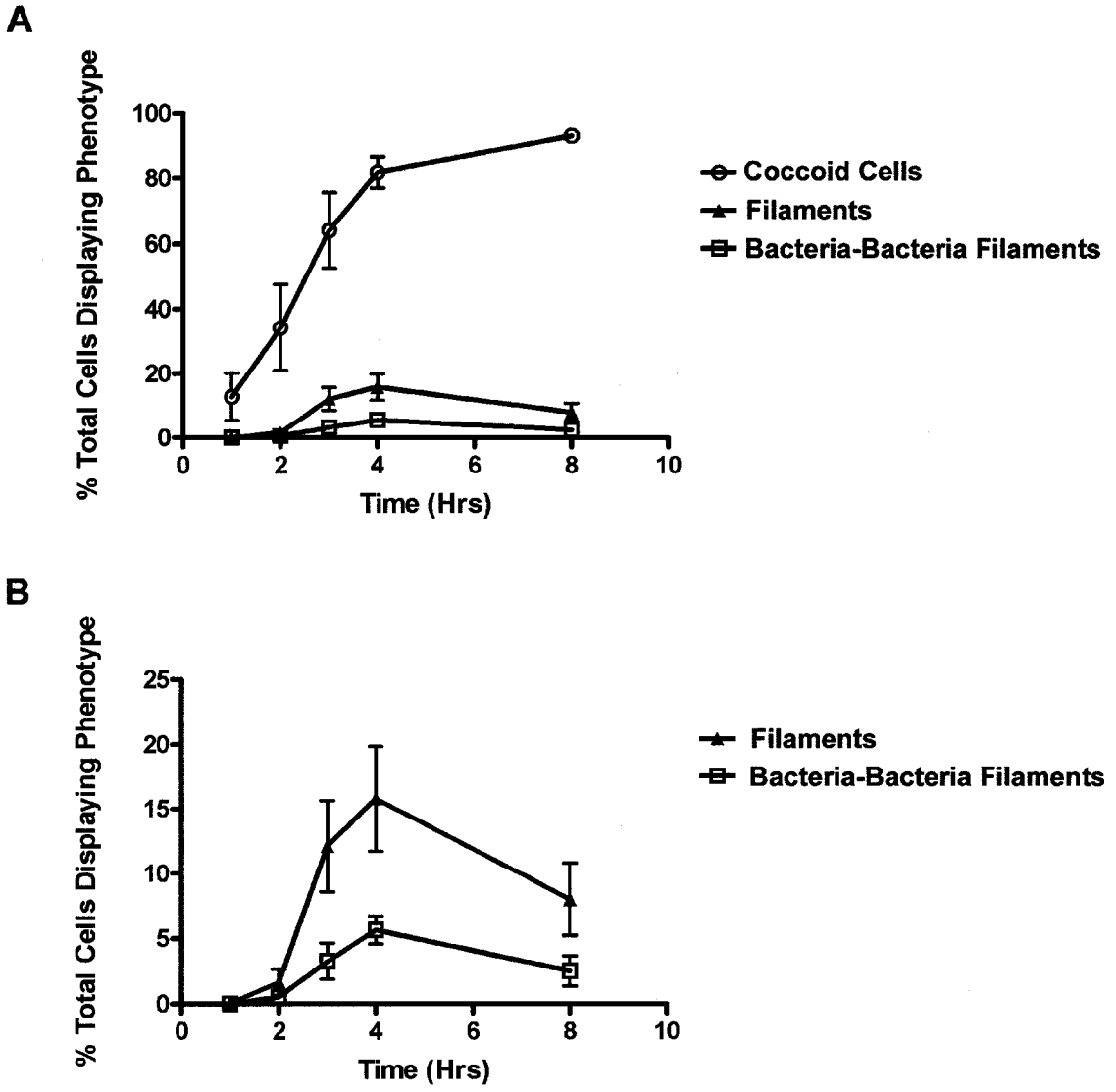

Figure 5-5. Enumeration and characterization of *H. pylori* G27 infection of AGS cells over an 8 hour time course on the basis of morphology (circle), presence of filaments (black triangle), and whether filaments connect 2 or more bacteria (square) (A). Data is displayed as a percentage of bacteria displaying each phenotype. Subsets of the data: filaments and connective filaments were displayed on a separate graph (B) for better resolution of the curves and error bars. Results represent means and standard deviation based on three independent experiments in which N≥ 1000 bacteria per timepoint were enumerated.

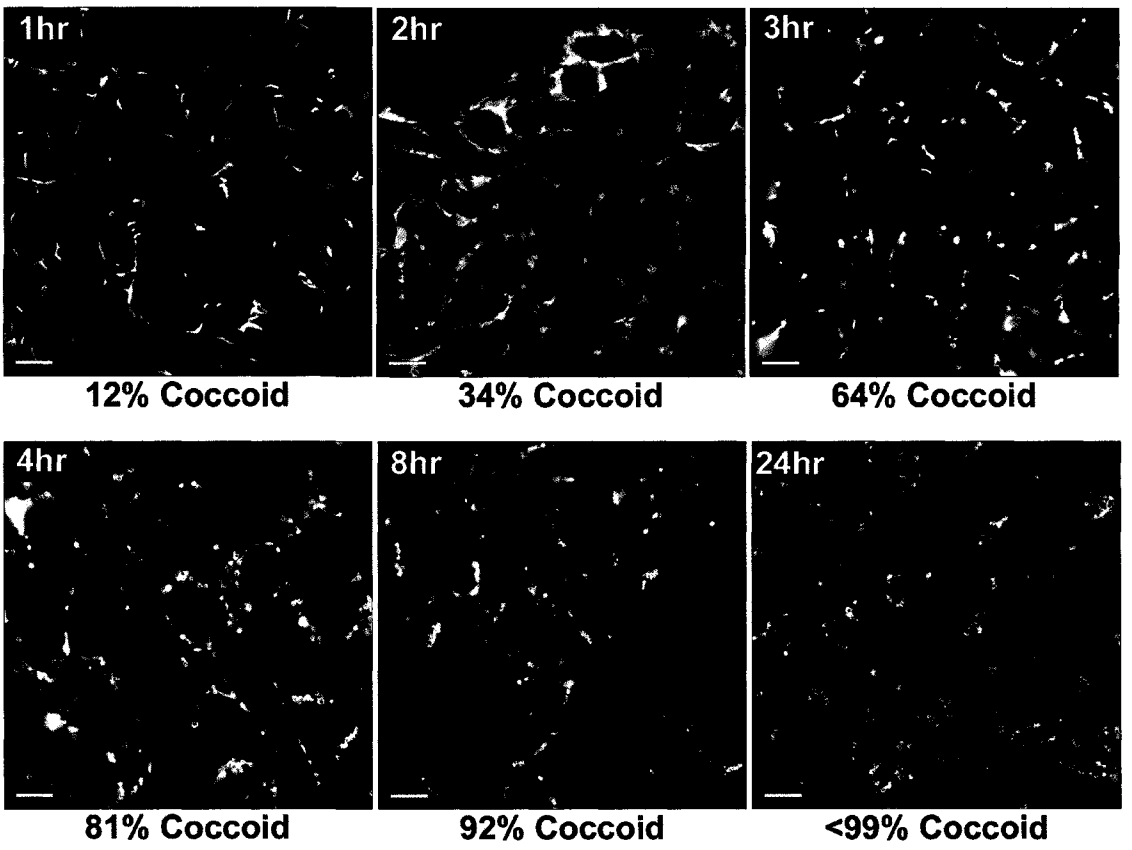

Figure 5-6. Immunofluorescent microscopic analysis of filament formation and coccoid conversion of *H. pylori* G27 over 24 hours of AGS cell infection. Images were generated by merging fluorescent images with phase contrast images to better analyze bacterial location. Scale bars represent 12.5μm.

human error. An example of this error can include incorrect scoring of helicoid bacteria that are perpendicular to the focal plane; ultimately appearing as coccoid.

5.2.5 Filaments are not composed of DNA or actin

To test whether the filaments contain extracellular DNA as a structural component, we stained samples with Hoechst 33342 and α-Helicobacter mouse serum and assayed for colocalization. Samples were fixed and processed for immunofluorescence microscopy. The DNA dye did not stain the filaments (Figure 5-7A). This detection threshold with DNA dyes in the presence of eukaryotic nuclear staining rendered these images difficult to interpret. To better confirm that DNA was not a structural component of filaments, we treated infected AGS cells with DNase for the final 30 minutes of a 4 hour infection. Filaments were not dissociated using a DNase treatment of 0.5 μg/ml, which was shown previously to dissolve extracellular DNA-composed neutrophil extracellular traps (Figure 5-7B) (37). These results support the idea that DNA is not a structural component of the filaments.

Retroviruses were recently shown to use eukaryotic filopodia as a bridge to traverse from an infected cell to an uninfected cell (197). We were interested to determine whether the long filaments seen were associating with actin derived filopodia or microvilli as a potential mechanism for movement after attachment to the host. Phalloidin was shown previously to label filopodia and actin enriched microvilli at the site of *H. pylori* attachment (202). AGS cells were infected with strain G27 for four hours. Then, actin was labeled with Alexa Fluor 568-Phalloidin and bacterial filaments

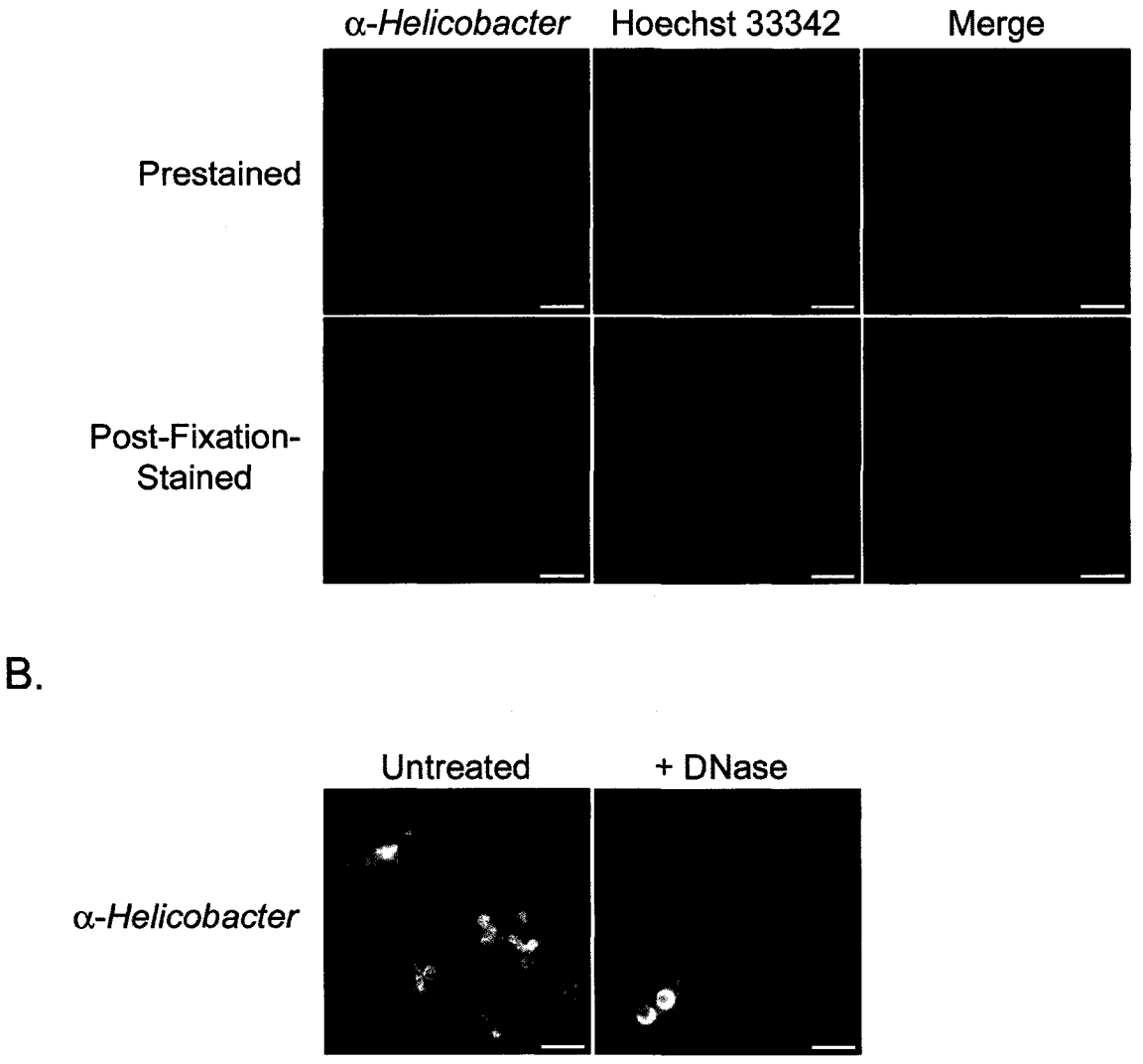

Figure 5-7. Filaments are not composed of DNA. *H. pylori* G27 infections of AGS cells were stained with Hoechst 33342 and α-*H. pylori* (A). Samples were stained before infection or after fixation with Hoechst 33342. Filaments were treated with 0.5 μg/ml RNase-free DNase to dissociate extracellular DNA (B). Scale bars represent 5.0 μm.

were stained with α-*H. pylori* antiserum and the Alexa Fluor-488 secondary antibody (Figure 5-8). Examination by immunofluorescence microscopy showed that filaments did not localize along actin containing structures, nor did they stain with phalloidin themselves, demonstrating that host actin was not incorporated in the filaments. Paired with the data in Figure 5-4, these results clearly demonstrate that the filaments are distinct from the eukaryotic cellular extensions.

5.2.6 Periodate oxidation reveals filaments are partially composed of carbohydrates

Both pili and flagella are bacterial surface structures that can be glycosylated (119). Therefore we sought to determine whether these newly discovered filaments also contained carbohydrates. We aimed to denature carbohydrates to determine whether the *H. pylori* antiserum could still recognize the filaments. Therefore, G27 infected AGS cells were treated with periodic acid and potassium borohydrate after paraformaldehyde fixation. All samples were stained with *H. pylori* antiserum. Untreated samples revealed typical bacterial and filament (arrow) staining (Figure 5-9). Samples treated with one round of periodate oxidation revealed normal bacterial staining; however filaments were not readily detectable. Samples treated with two rounds of periodate oxidation were completely devoid of detectable filaments, while the bacteria were still stained similar to untreated samples (Figure 5-9). This suggested that carbohydrates are a component of the filaments and the major antigenic determinant, while the serum was still able to stain other non-carbohydrate antigens on the bacterial surface without a noticeable loss in fluorescence.

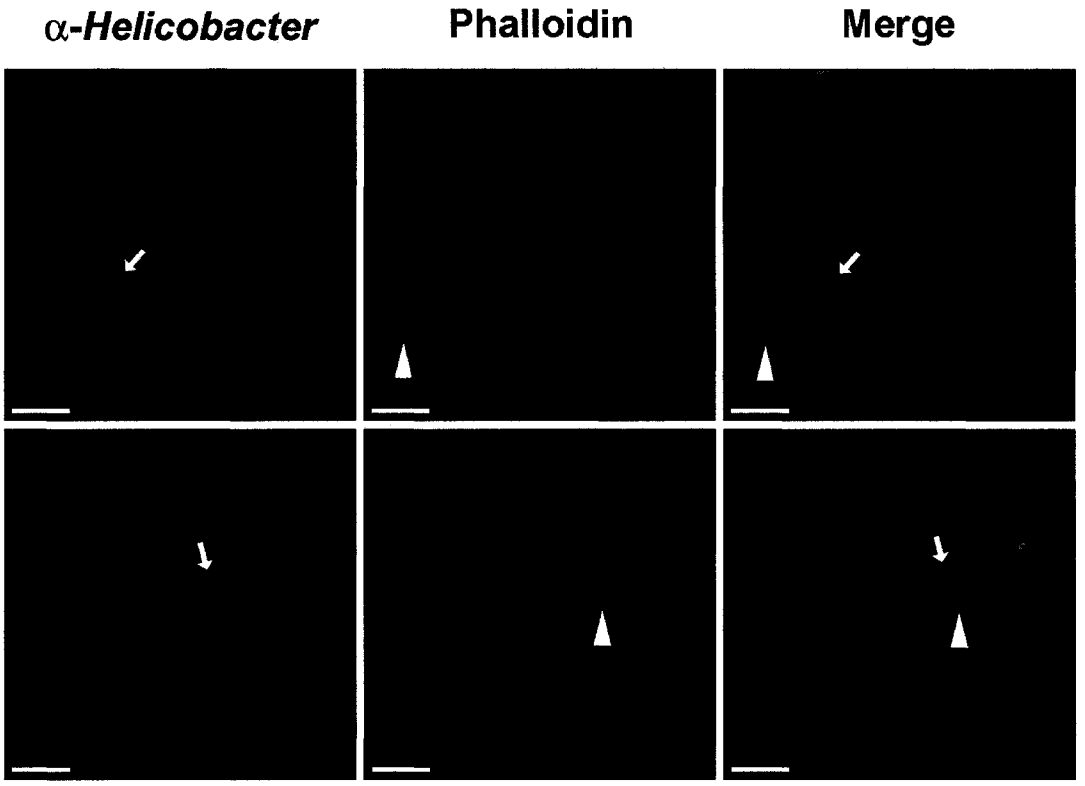

Figure 5-8. Filaments do not contain polymerized actin and do not co-localize with eukaryotic extracellular structures. (Left panels) Cells were permeablized with 0.2% NP-40 and stained with *H. pylori* antiserum and secondary Alexa Fluor-488 antibody. (Middle panels) The actin cytoskeleton labeled with Alexa Fluor-568 Phalloidin. (Right panels) Images were merged to show distinct staining of different surface structures. Bacterial filaments are indicated by arrows and eukaryotic filopodia are labeled with arrowheads. Scale bars represent 5.0 μm.

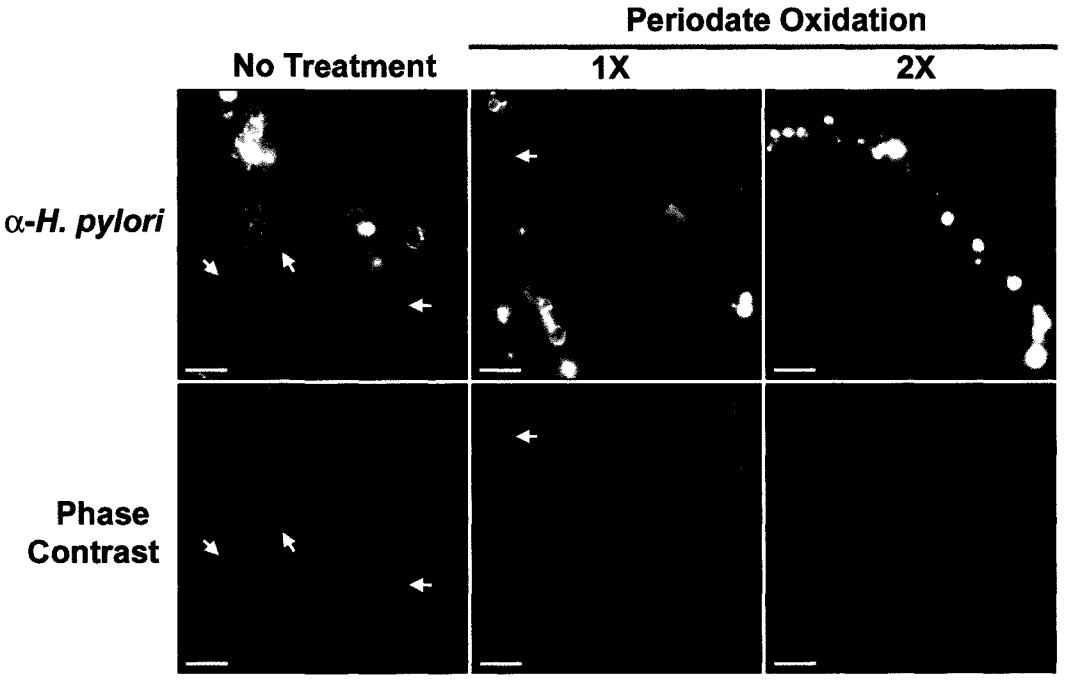

Figure 5-9. Antibody recognition of carbohydrates on *H. pylori* filaments. Fixed samples were either left untreated or treated with periodate and borohydrate once (1X) or twice (2X). All samples showed similar levels of fluorescence for bacteria as all images were captured at constant exposure lengths and fluorescent intensity. Corresponding phase contrast panels are shown. Scale bars represent 5.0 μm.

5.2.7 Filaments are stained with Concanavalin A (ConA)

The antigenic component of filaments was found to be carbohydrate in composition, therefore a lectin staining kit was used to detect various potential sugar linkages on the filaments. Of the lectins tested (ConA, WGA, RCA_{120}, PNA, SBA, UEA I, and DBA) only two lectins were able to recognize the bacteria; ConA and WGA (Figure 5-10). These results were consistent with previously described agglutination activities of ConA and WGA toward *H. pylori* (121). ConA recognized D-mannose containing sugars on the eukaryotic membrane, bacterial filaments, as well as the bacterial membrane. WGA however, only stained N-acetyl-D-glucosamine containing sugars on the bacterial and eukaryotic membranes. Samples were co-stained with α-*Helicobacter* mouse serum and colocalization with ConA was confirmed by merging the images (Figure 5-10). No colocalization was observed for WGA and α-*Helicobacter* staining.

5.2.8 *De novo* synthesis of proteins is not needed for filament formation

To determine whether filaments contain or require proteins synthesized upon contact with host cells, we employed chloramphenicol to arrest *de novo* protein synthesis. Bacterial cultures were treated 20 minutes pre-infection or during the infection via chloramphenicol supplemented infection medium. Control samples were left untreated. *H. pylori* treated with chloramphenicol were able to form filaments with no noticeable difference in morphology or relative abundance when viewed by immunofluorescent microscopic analysis (Figure 5-11A). This suggested that any proteins contained in or

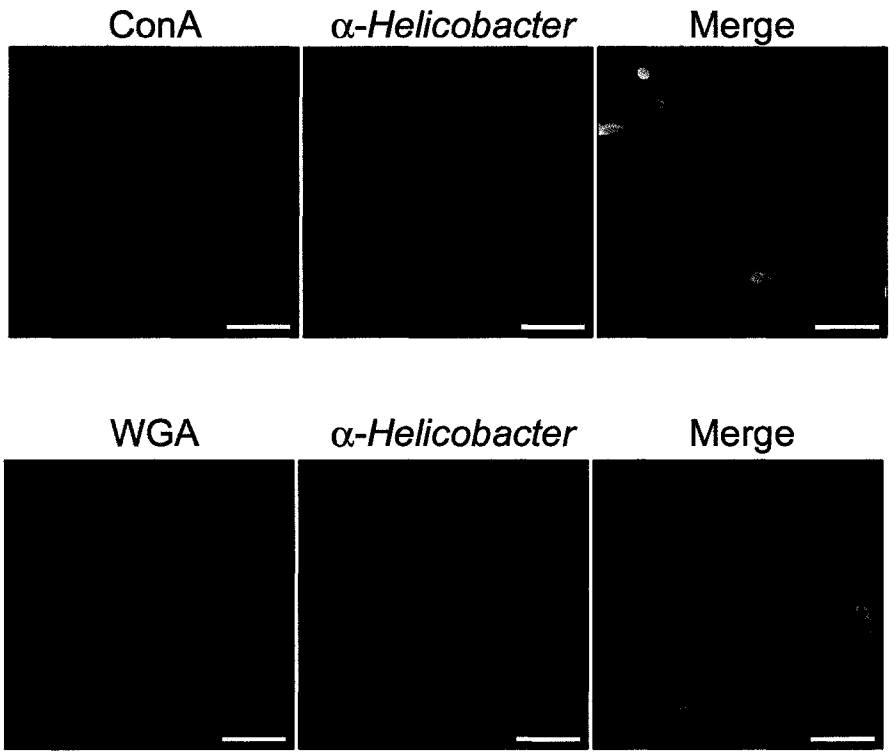

Figure 5-10. Lectin staining of G27 *H. pylori* infection of AGS cells. Samples were stained with α-*H. pylori* and either ConA or WGA. Images were merged to visualize co-staining of filaments. Scale bars represent 5.0 μm.

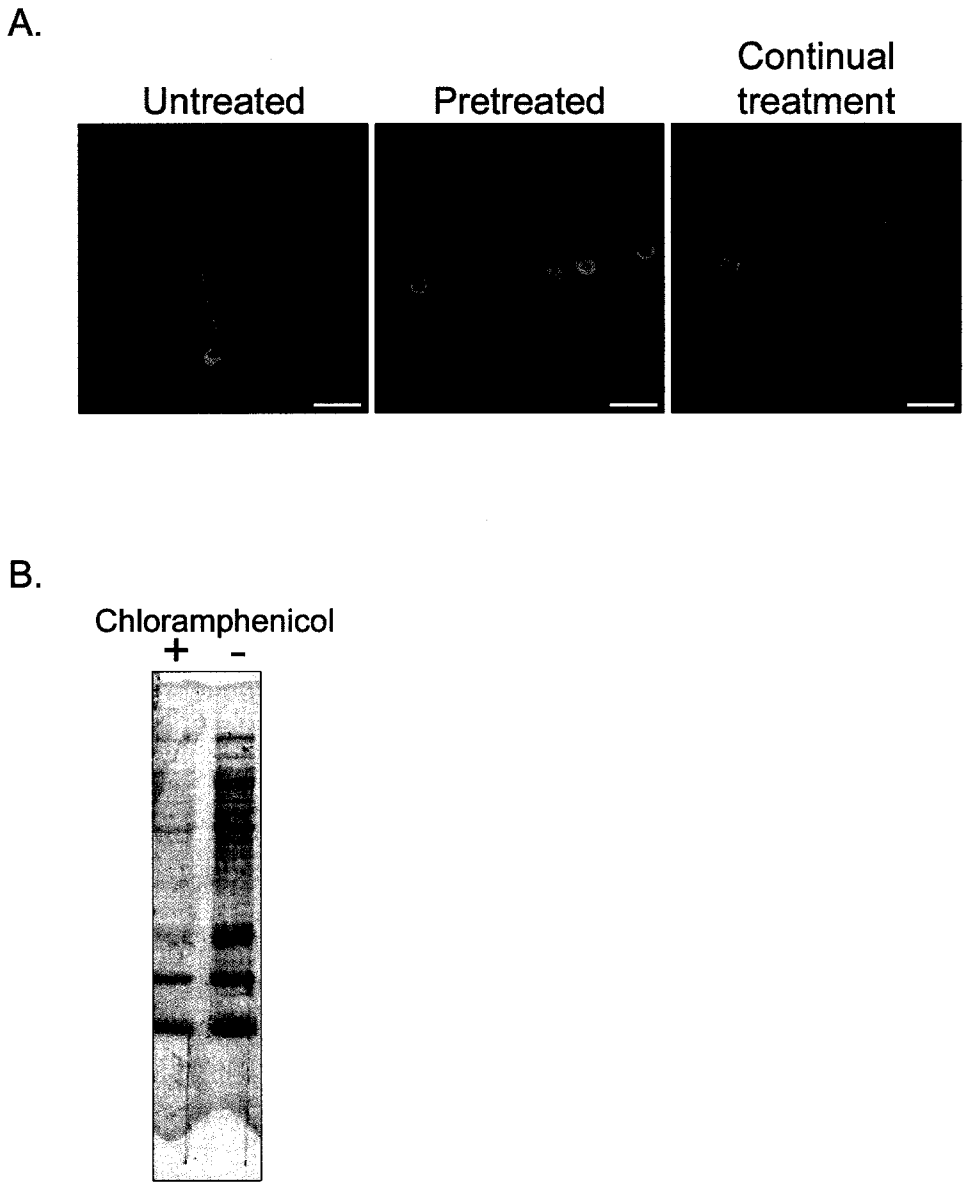

Figure 5-11. Chloramphenicol treatment of *H. pylori* abolishes *de* novo synthesis of proteins but does not inhibit filament formation. Infections were untreated, treated 30 minutes preinfection, or treated throughout the duration of the experiment with chloramphenicol (A) and visualized by immunofluorescence microscopy with α-*H. pylori* antiserum. Scale bars represent 5.0 μm. Lysates of chloramphenicol treated *H. pylori* incubated with ^{35}S methionine/cysteine analyzed by autoradiographic imaging (B).

required for the filaments are synthesized before contact with eukaryotic cells. ^{35}S methionine incorporation during the bacterial culture confirmed that the working concentration of chloramphenicol was sufficient to shut down *de novo* protein synthesis when bacterial lysates were visualized by radiographic analysis (Figure 5-11B).

5.2.9 *H. pylori* positive human sera recognize filaments *in vitro*

The carbohydrates and other possible molecules that comprise the filaments elicited an immune response in the mouse used to create the *H. pylori* antiserum. This suggested that the filaments may be immunogenic in humans as well. To test this hypothesis we stained infected AGS cells with various *H. pylori*-positive human patient sera including patients 90 and 5 (Figure 5-12). All tested sera stained *H. pylori* and the bacterial filaments as observed by immunofluorescence microscopy. Serum from patient 9 was used as a representative negative serum for *H. pylori* and this serum did not stain filaments or bacteria. Negative control staining is shown for each patient, which confirmed the specificity of each serum for the bacteria and the filaments. All sera used for this assay tested *H. pylori* positive or negative with biopsies and confirmed by western blot for antigenic recognition of *H. pylori* lysates.

5.3 Discussion

Non-flagellar bacterial appendages have been documented in both Gram-negative and Gram-positive bacteria by electron microscopy (78, 114, 228). These structures were termed either fimbriae or pili. Both terms are used synonymously to describe any bacterial surface appendage that is not an obvious flagella related structure (212). The

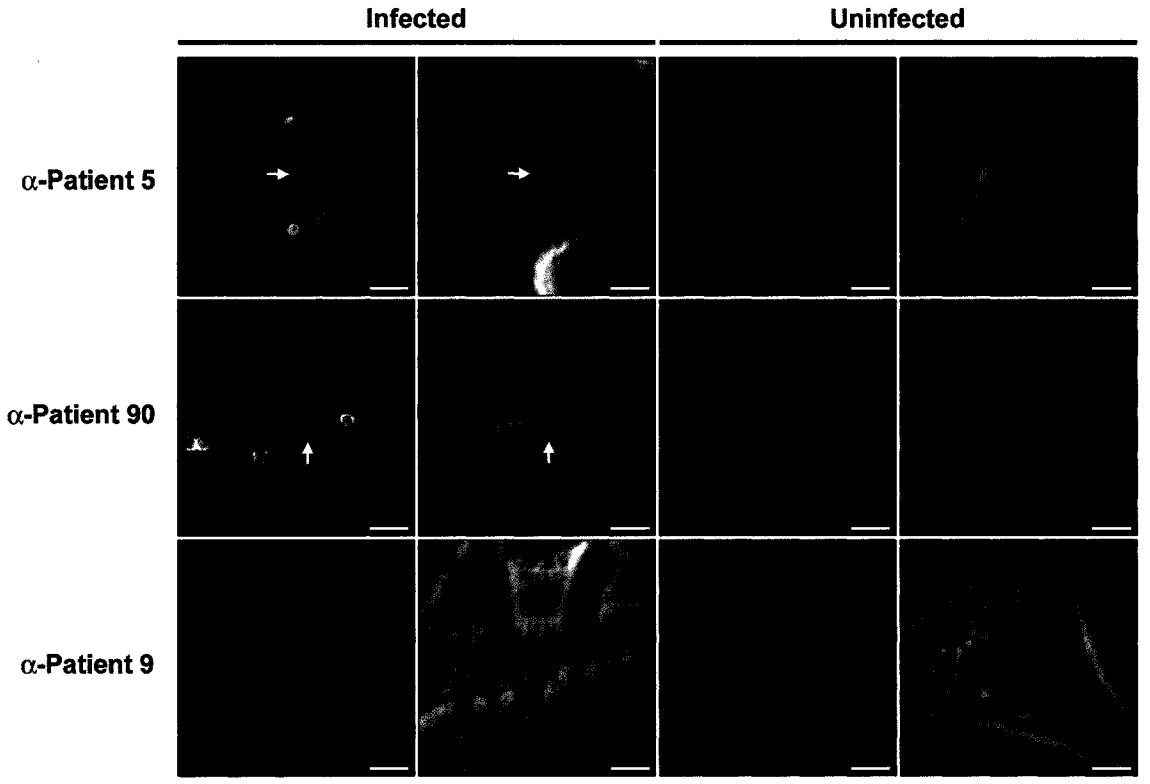

Figure 5-12. Recognition of filaments by *H. pylori*-positive human patient sera *in vitro*. AGS cells infected with strain G27 were stained with various *H. pylori* positive human sera (patients 5 and 90). All convalescent sera tested recognized filaments (arrows) *in vitro*. Serum from a confirmed healthy patient (patient 9) was used as a representative negative serum for *H. pylori*. Appropriate negative controls are shown, consisting of uninfected cells stained with both primary and secondary antibody antibodies. Scale bars represent 5.0 μm.

major groupings of fimbrial structures include: type I pili, type IV pili, curli pili, secretion/conjugation systems, and the recently described Gram-positive fibrils and pili (212). The length of fimbrial structures can range from 0.07 μm to 3 μm, with widths ranging from 2 nm to 10 nm (212). Fimbriae have been shown to provide bacteria with an array of functions such as host cell binding, aggregation, biofilm formation, motility, and DNA transfer (212).

A majority of *in vitro* experimentation in *H. pylori* has been conducted using only helicoid cultures of the organism. Though a great deal of work has been devoted to coccoid morphology, the morphology remains enigmatic as to its function in bacterial homeostasis and eukaryotic infection. However, the complex process of conversion from helicoid to coccoid form has been well documented using transmission electron microscopy (24, 177). We used both immunofluorescence microscopy as well as scanning electron microscopy to identify a unique filament on the surface of both helicoid and coccoid *H. pylori* which appear to form during morphologic conversion. Unlike the various fimbriae formed by other bacteria, these filaments far exceeded the previously observed lengths of 3 μm. The *H. pylori* filaments reached lengths of nearly 50 μm, roughly 15 times the length of helicoids (3 μm) and often connected between two or more bacteria. Extended microvilli and filopodial structures that resemble the bacterial filaments have been described to surround *H. pylori* attached to AGS tissue culture cells previously. However, we demonstrate clearly that these host cell structures are distinct from the bacterial filaments, which in contrast to host cell elongations do not contain actin. Furthermore, *H. pylori* antiserum generated in mice as well as sera from donors infected with *H. pylori* recognized the bacterial filaments, but not host cell

structures. As well, pre-immune sera from the mouse used to create the *Helicobacter* antiserum and serum from uninfected human donors failed to recognize any filaments, *H. pylori,* or self antigens.

The composition of the medium used to conduct the infections did not have an effect on filament formation; however the fact that direct host cell contact was required for filament formation was intriguing. In addition to direct contact, our results also suggest that direct contact with metabolically active eukaryotic cells is ultimately required for filament formation or visualization. This may suggest a complex interplay between host and pathogen which may be required for filaments to be induced. Conditioned media from an active infection was unable to trigger filament formation in a cell free environment, which further suggests that a soluble "trigger" is not likely for filament formation.

In liquid culture *H. pylori* typically reaches a majority of coccoid cells after several days of growth, with variable conditions such as pH, nutrients, oxygen, nitric oxide, temperature, antibiotics, and metals (24, 36, 59, 76, 144, 149, 177, 180, 215) leading to a more rapid conversion process. However, the conversion process of *H. pylori* during infection of eukaryotic cells *in vitro* has not been previously described. We documented that strain G27 using the described experimental conditions reached a majority of coccoid forms after only 4 hours with near complete conversion by 24 hours of infection *in vitro*. At 8 to 24 hours of infection, coccoid *H. pylori* also appeared to cluster on the apical surface of eukaryotic cells, which has been described for coccoid forms on abiotic surfaces in aqueous environments (16, 76). Therefore it is likely that the eukaryotic environment may drive coccoid formation and clustering. It should be noted

that the morphology was scored based on careful observation by immunofluorescence microscopy involving analysis of multiple planes of focus for each field of view. This avoided incorrect scoring of helicoid bacteria orientated perpendicular to the plane of view. Hence, the overall trend argues for increasing coccoid conversion rather than a coordinated rotation of helicoids away from the plane of focus.

Previous reports indicated the ability of *H. pylori* to form microcolonies (16). These microcolonies were able to colonize abiotic surfaces and grow as three-dimensional structures, which eventually merge to form layers that resemble biofilms (58). Our inability to detect the filaments in the absence of the host cell may indicate that there is a connection between the filaments and the previously described microcolony formation. In microcolonies, the filaments may not be visible due to the dense aggregation of the bacteria, whereas on host cells the bacterial movement and cellular motility might separate bacteria exposing the filaments. This may also explain why after prolonged infection periods (8 and 24 hours) the bacteria aggregated in clusters, while the filaments where not visible anymore. After the molecular identification of the filament components it will be of interest to test whether the filaments are involved in microcolony formation and aid in the colonization of abiotic surfaces.

The filaments we have described represent unique structures in *H. pylori.* Neither the type IV secretion system nor flagella of *H. pylori* could be attributed to these filaments. The overall abundance of filaments *in vitro* is striking, as is their statistically significant development over time course infection of tissue culture cells. Though we were unable to directly correlate coccoid conversion rate to filament formation rate, the

two events appear to be interdependent in that filament formation was only observed when coccoid conversion was taking place.

The ultimate composition of these filaments has not been established, however we were able to determine that a major component of the filament is carbohydrate-based, since periodate oxidation destroyed their antigenicity. The carbohydrate was further characterized by positive staining with the concanavalin A lectin. ConA specifically binds and recognizes polysaccharides at D-mannose residues. Wheat germ agglutinin (WGA) specifically recognizes carbohydrates at *N*-acetyl-D-glucosamine residues. WGA also stained *H. pylori*; however it did not recognize the filaments. Though uncommon in most prokaryotic organisms, evidence for D-mannosyl linkages has been documented, in Gram-positive (*Lactobacillus* spp., *Bifidobacterium* spp., *Streptococcus bovis*, *Enterococcus* spp. (123)), acid fast (*Mycobacterium tuberculosis* (73)), and Gram-negative bacteria (*H. pylori* (226), *Campylobacter fetus* (143), and *Campylobacter jejuni* (145)). Of particular interest to our findings, ConA and WGA were shown previously to agglutinate *H. pylori*, with greater agglutination activity seen for coccoids than helicoids (121). Furthermore, periodate treatment was shown to completely abolish agglutination activity of ConA and WGA for *H. pylori* (121). The ability for periodate oxidation and borohydrate reduction to disrupt carbohydrate recognition by lectins (including WGA) and antibodies has been described previously (99, 224). As filaments were stained with α-*Helicobacter* serum as well as ConA, this suggests not only that filaments contain D-mannose linked sugars, but also that the α-*Helicobacter* serum specifically recognizes an antigenic D-mannose-containing molecule that is a component of the filaments.

Since the filaments did not rely on or contain *de novo* synthesized proteins, and since *H. pylori* antiserum was created from a total lysate of bacteria grown overnight on solid medium, the antigenic components responsible for filament assembly and structure must be present in non-infecting bacteria. As carbohydrates are implicated in the structures, the lack of *de novo* synthesized proteins for filament formation is not all-together surprising. It is possible that the enzymes responsible for filament assembly and carbohydrate synthesis are normal metabolic proteins and would be resident in a culture grown bacterium. This possibility could explain the enigmatic ability of filaments to be formed in the absence of active protein expression.

Of utmost importance in our study is the recognition of the filaments *in vitro* using human *H. pylori* positive patient serum. The structural components of the filaments resulted in an immune response for each patient. Each convalescent serum recognized the structures, suggesting that the molecules are common in symptomatic patients. This not only suggests that the filament components are immunogenic, but that they may have *in vivo* relevance to *H. pylori* pathogenesis as well. Importantly, sera from uninfected individuals were completely negative for filament staining or bacterial staining. This supports the specificity of our results and suggests an *in vivo* relevant finding. As these structures are inexplicably tied to the coccoid conversion process (but can occur on helicoids as well), it is suggestive that the coccoid morphology may also play a role in *Helicobacter*-related disease.

This data has provided strong evidence for a previously unrecognized filamentous structure formed by *H. pylori in vitro.* These filaments appear to form during the conversion from the helicoid to coccoid state and were induced after contact with

eukaryotic cells. Future work is required to determine the precise molecular make-up of the filaments and the potential role in pathogenesis and infection.

Chapter 6

General Discussion

6. General discussion

6.1 Revisiting the T4SS and pathogenesis

The T4SSs of Gram-negative bacterial pathogens represent a paradox in bacterial homeostasis. In one sense, these macromolecular structures represent an immense material requirement in addition to a demanding energetic requirement for effector translocation. Due to the nature of the bacterial cell envelope, a specialized protein with lytic transglycosylase activity must deconstruct the murein layer in order to allow for a transmembrane complex to form in the first place (235). The multi-protein secretion system such as that described for VirB/VirD4 in *A. tumefaciens* (Figure 1-2) would then fill this destabilized region of the membrane. Conceivably the bacteria can only tolerate a certain amount of murein instability before deleterious effects may occur such as a stress response (236).

The other side of the paradox weighs whether the benefits of the functional secretion system balance or outweigh the energetic and materialistic requirements to assemble the structures. Taking into consideration the conjugation systems, an altruistic role can be ascribed to the donor bacteria since the energetic requirements on the donor are immense, while the recipient is conceivably benefiting from the conjugation event. Population biology would argue that this "bacterial sex" represents the basic propagation of genetic material, and therefore still benefits the donor. DNA uptake T4SSs can be viewed as beneficial to the organism synthesizing the T4SS as it involves energetic input but yields potential fitness (*e.g.* antibiotic resistance genes or an energy source) from DNA captured by the system. The effector translocation system however is an abstract grouping of the T4SS since most systems are known to be involved in some aspect of

host pathogenesis (44). It can be assumed that the various effects conferred by translocated effector molecules are advantageous to the bacterium since it would not be energetically favorable to assemble a secretion system and induce damage to the host if no gain to the bacterium is achieved.

In the case of *H. pylori*, the development of severe pathology in the form of adenocarcinoma due (in part) to chronic CagA translocation by the *cag* T4SS would (superficially) seem to be a non-advantageous result, since without medical intervention the host will likely die. However, as these cases are in the minority and are often compounded by host polymorphisms (7), one can assume that this effect is not intuitively the intended outcome of infection. Furthermore, life-spans of humans have increased greatly with the advent of antibiotic therapy and social sanitation. Therefore, it is possible that death of the host was rarely seen in the past, as most patients would not live long enough to die from the *H. pylori*-associated cancer. Interestingly, the conditions that exist in carcinomas would appear to be advantageous to *H. pylori,* as acid production is low or non-existant which alleviates stress on the bacteria and the need to synthesize urease to buffer the environment (102). If these conditions are in fact favorable for *H. pylori* and since adenocarcinoma is typically found later in life, it is conceivable that this disease state is a trade-off for the bacteria to live less dangerously while still allowing the host to persist long enough to spread the bacteria to new hosts.

The large proportion of *H. pylori* positive patients that are infected with strains possessing an in tact *cag*-PAI display chronic inflammation and often ulceration, while never developing cancer (102). In these conditions, both acid and gastrin are hyper secreted, and conceivably the bacteria are forced not only to combat the acidic

environment, but also the pro-inflammatory immune response (83). If this in fact represents a significant proportion of cases involving *cag*-PAI containing strains, one would assume that the progression toward adenocarcinoma would be the preferred disease state from a bacterial stand point (*i.e.* less stressful). However it would appear that *H. pylori* is more than capable of tolerating the stress of the human stomach since many strains of *H. pylori* do not possess T4SSs yet have developed successful chronic infection, often with no deleterious effects on the host (or no clinically presenting effects) (165). To date *H. pylori* remains the only bacteria known to colonize the harsh environment of the human stomach, suggesting that it has developed a niche in this environment that other bacteria have failed to exploit. The fact that 50% of the world's population is thought to be infected with *H. pylori*, and that fewer than 10% of those will ever become sick from the colonization, would suggest that *H. pylori* represents: an incidental pathogen, an emerging pathogen, or a pathogen that is evolving toward a commensal relationship with the human host (7). These ideas all culminate into a complex biological question: why would *H. pylori* need to encode a *cag* T4SS when non-*cag*-PAI strains can survive readily and why has it developed to be so complex compared to its orthologous counterparts? The first part of this question lends itself largely to philosophical discourse. However, to address the latter part of this question, a better understanding of these unique non-orthologous components of the *cag* T4SS is required.

6.2 *cag* T4SS model updated: A place for CagF and CagD

The schematic model of the VirB/VirD4 T4SS in *A. tumefaciens* is well established for both protein localization as well as protein interactions (Figure 1-2). In

contrast, the *cag* T4SS remains in its infancy with regards to determining the subcellular location of the components as well as the protein-protein interactions (Figure 1-4). The roles for most of these components remain unassigned, especially those components in the CagI region of the *cag*-PAI (Figure 1-3). Our studies have contributed to the understanding of the *cag* T4SS by characterizing two components of the secretion system that previously were only partially described (inaccurately in some cases) by previous investigators; CagF and CagD.

6.2.1 CagF: possible roles and future studies

We described CagF as an inner membrane/cytosolic protein that binds CagA at the inner membrane and is required for successful delivery of CagA into the secretion system (61). We also detirmined that CagF is not required for CagL localization on the host membrane or IL-8 induction, implicating that it is not involved in pilus assembly and integrin binding. An early report had described CagF as an outer membrane protein, and we were able to show this was an incorrect finding (Figure 3-6) (192). Our attempt to locate the interaction domain for CagF and CagA was unsuccessful due to the instability of various CagF deletion constructs. However, our recent studies were able to identify a second interacting partner with CagF; a coupling protein of unknown genomic origin. This finding may have further implications in our model, as coupling proteins are thought to have ATPase activity. Since the *cag* T4SS is not known to translocate DNA, it is of particular interest to know what role the coupling protein has developed in this system. As the current model shows (Figure 6-1), CagF may bind CagA at the inner membrane in order to deliver it to the secretion system, however it is possible that the coupling protein

then provides the necessary energy to shuttle CagA though the opening of the secretion channel, where it may then interact with other ATPases (Cagα and CagE) or structural components similar to the VirB/VirD4 system. The CagF-coupling protein interaction may in fact be indirect, conferred by CagA as an intermediate during the "passing off" of the substrate (Figure 6-1).

Future studies as to the role of CagF will require not only investigation into CagF, but into identifying the coupling protein identified by mass spectrometry through a detailed search of the finalized genome of G27. One possibility is that G27 has acquired another coupling protein through DNA uptake that is expressed and encorportaed into the *cag* T4SS. Cagβ as well may be implicated in this function as it is a coupling protein homolog, is part of the *cag* T4SS, and may also function in a redundant nature to the unidentified coupling protein. An antibody for Cagβ has not been published to date, and therefore a suitable antibody should be developed. However in tandem with antibody production, creation of a StrepII tagged construct of Cagβ would also be beneficial. The StrepII tag has proven useful for the CagF-Strep pull-down experiments, and therefore having a StrepII tag on Cagβ would allow for reciprocal pull-down experiments to be conducted. This would allow us to determine whether CagF interacts with Cagβ, and potentially identify other interacting partners. Creation of a Cagβ-Strep construct would also allow for direct interaction tests in *E. coli* by coexpressing CagF or CagA with Cagβ. In the same manner, a StrepII fusion of CagA would also allow for additional interacting partners to be identified. Understanding the nature of this complete interaction scheme would provide a better understanding of the first steps in CagA secretion.

6.2.2 CagD: Possible roles and future studies

CagD was described in our work as an *in vitro* dimer that shows limited tertiary structural similarity to the SycT T3SS chaperone in *Y. enterocolitica* and is absolutely necessary for CagA secretion. A previous report indicated that CagD was involved, but not essential for CagA secretion, however our results show otherwise (87). Furthermore, in accordance with proteomic studies of the culture supernatant, we showed that a portion of CagD was localized outside of the bacteria (201). We were further able to determine that CagD is not likely secreted by the *cag* T4SS, exerts its role in CagA secretion inside the bacteria, and associates with the host membrane during *in vitro* infection (Figure 6-1). Lastly, CagD appears to be involved in pilus assembly, as infection with a *cag*D mutant showed reduced IL-8 induction and did not yield CagL fractionation with the eukaryotic membrane. In this sense CagD may be involved in pilus assembly but not absolutely essential, as IL-8 induction was simply reduced (not abolished like the *cag*E mutant). It is possible that CagD is pilus-associated or that it is binding the host cell to provide additional cytologic effects. Though we were not able to identify CagD by immunofluorescence on the bacterial surface, it would be of interest to use immuno-SEM to try and detect the T4SS pilus with α-CagL and α-CagD using different sized gold particles. It would also be interesting to see if CagD is found on the eukaryotic membrane surface or not. This could readily be investigated as the CagL antibody is of rabbit origin while the CagD antibody is of rat origin. To test for possible cytologic effects on the host cell, CagD should also be transfected into AGS cells and assayed for visual morphologic effects, CagD localization inside of AGS cells, possible cytoskeletal rearrangements (actin and tubulin staining), as well as host gene expression changes.

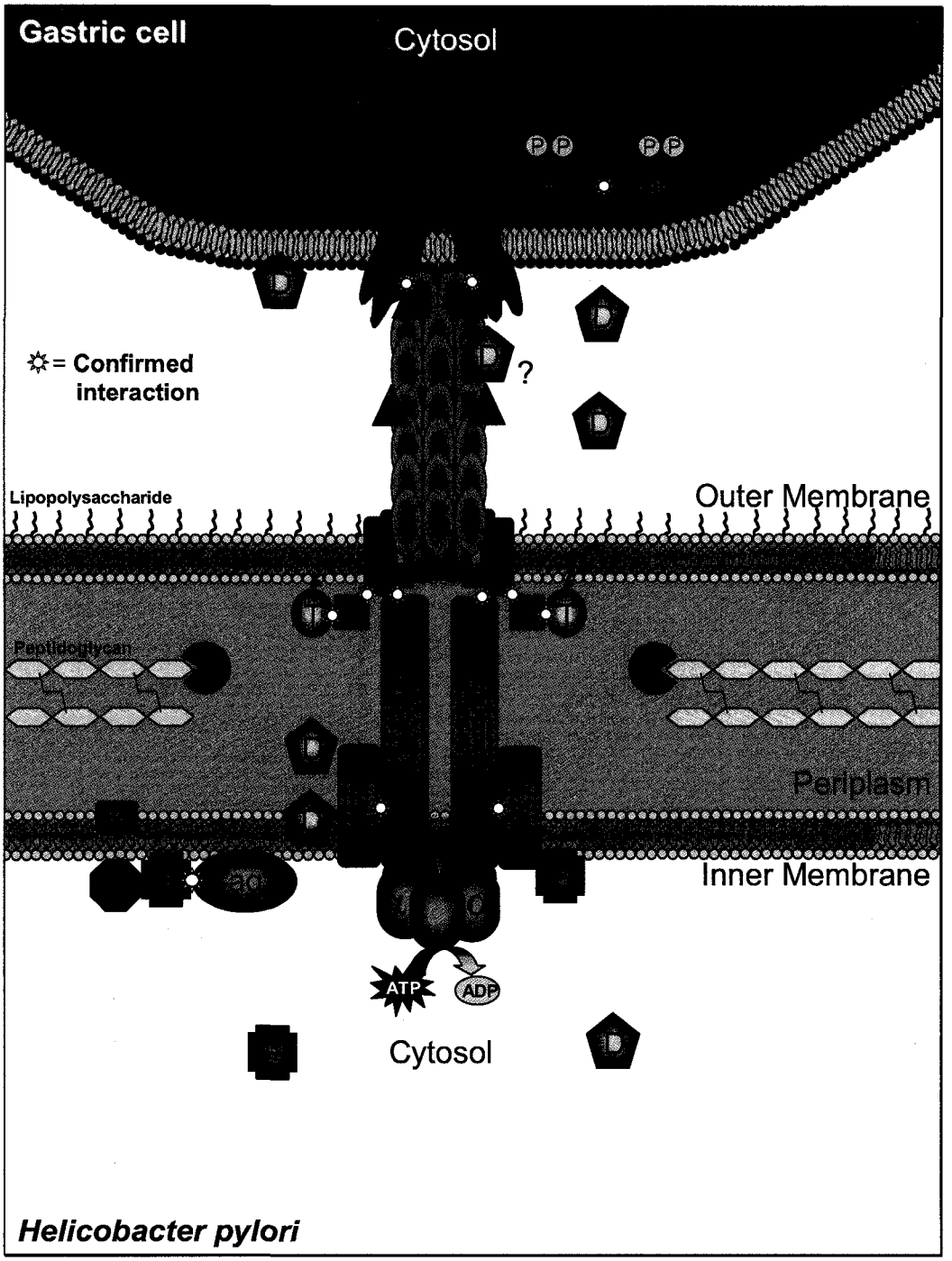

Figure 6-1. Updated schematic model of the *H. pylori cag* T4SS. All documented subcellular localizations for Cag proteins are depicted in a schematic model. Confirmed protein-protein interactions are indicated by yellow starbursts. Only proteins with documented interactions or localizations are included in this model. CagF and CagD localization and interactions are included in the updated model to reflect these studies.

Several attempts were made to pull down CagD and interacting partners, however both immunoprecipitation with the CagD antibody and the Flag-agarose beads failed to precipitate any interacting proteins when analyzed by silver stained SDS-PAGE gel. It is highly unlikely that CagD does not interact with any other prokaryotic proteins; however it would be of interest to immunoprecipitate CagD from an *in vitro* infection of AGS cells to determine if CagD interacts with any prokaryotic or eukaryotic proteins in this environment. These findings would be of the utmost importance and possibly provide insight into the function of CagD. Concerning the localization of CagD, it would be of further interest to determine the region of the protein required for prokaryotic membrane localization, secretion, IL-8 induction, CagL presentation, and eukaryotic membrane association. For this purpose, systematic deletions of the protein should be constructed, starting first with the predicted signal peptide to confirm that this region confers bacterial membrane association and continuing throughout the sequence of the protein. Initial studies would target the regions determined by crystallographic analysis to form the six individual β-strands and three α-helices. As well, individual point mutations in Cys120, Cys133, and Cys172 would be of interest to determine whether dimerization can be abolished, and whether this in turn abrogates CagA secretion or CagD extracellular localization. An advantage to having the crystal structure of CagD solved is that it allows for an informed direction for deletions, rather than random protein deletions such as those conducted previously for CagF.

A final experiment to definitively show that CagD is not secreted by the *cag* T4SS would be to transform the pSK+recx*cag*D plasmid into a Δ*cag*-PAI strain which lacks the entire secretion system. We previously screened a variety of individual mutants of the

cag T4SS to conclude that CagD was exported independent of the T4SS, however expressing CagD in a Δ*cag*-PAI strain would establish definitively that CagD is not secreted by the *cag* system. A Δ*cag*-PAI strain is available in our lab; however it does not behave like wild type *H. pylori* in growth rate, morphology, and physical consistency. For these reasons, it would be of interest to create a new Δ*cag*-PAI strain for this purpose.

6.3 Filaments: Preliminary description and future studies

H. pylori filaments were serendipitously discovered during the course of these studies. We were able to rule out the two previously described surface structures (flagella and T4SSs) by using mutants of both structures. Our preliminary analysis of the filments describes unique structures that are formed *in vitro* during the morphological conversion from helicoid to coccoid. Filaments appeared to often connect multiple bacteria together, and disappeared over the course of a 24 hour infection. We were able to determine that the filaments are partially composed of mannose-linked sugars that likely represent the major antigenic component of the structures. Of utmost importance, the structures were recognized by serum from convalescent human patients, lending evidence for an *in vivo* relevance. Given the observed tendency for filaments to interconnect bacteria and to disappear as bacteria cluster, it is attractive to speculate that filaments act as a retractile mechanism used to bring immobile bacteria together on a solid surface, possibly in response to cell density or stress.

The basic framework of this study has been conducted, however purification and identification of the filaments remains the major challenge and obstacle. It is highly likely that the filaments are composed of more than one component (protein,

glycoprotein, carbohydrate, or any of the above); however amyloid-like rope structures formed by pathogenic *E. coli* were recently shown to be composed of just two proteins, EspC and EspP (Personal communication, Jorge Giron, Banff Conference on Infectious Diseases, Banff, Alberta, 2008). These structures are even larger than filaments and were visible by the naked eye in liquid culture; therefore it is possible that filaments are composed of only a few components as well. One method to try and identify these structures would involve biotinylation of the *H. pylori* carbohydrates using biotin hydrazide throughout overnight culture. The bacteria would then be used to infect AGS cells for 4 hours to allow filaments to form. The infections could then by scraped and lysed, and all mannose containing carbohydrates could be precipitated with concanavalin A. The samples could then be separated by SDS-PAGE gel and analyzed by western blot with streptavidin conjugated to horseradish peroxidase to detect those mannose containing sugars that are biotinylated and therefore of bacterial origin. The corresponding regions of the SDS-PAGE could then be extracted for mass spectrometric identification. It is possible that glycoproteins would be detected in this output. Detection may be difficult if the carbohydrates are synthesized after infection, thereby limiting the amount of biotinylated sugars residues. All potential candidates could then be mutated in *H. pylori* and screened for filament formation. If any particular genes are attributed to formation, then the gene can be complemented to determine whether filament formation is regained. With this identification, an antibody can be made against the component to verify the identity definitively by immunofluorescence and electron microscopy. This would be a potentially large undertaking, but could yield extremely exciting results.

If there are no glycoproteins involved in filament structure, then directed mutagenesis of the putative GDP-mannose biosynthesis control gene (*man*C) would be a logical second line of investigation. This mutant would be screened by immunofluorescent microscopy to confirm a loss of fluorescence (by ConA and α-*H. pylori*). It would then be of interest to visualize this mutant by SEM to determine if the structures are abolished completely, or whether filaments are still formed, but simply lack the antigenic carbohydrate residues. This would provide more insight into the overall structural make-up of the filaments.

A second line of investigation should attempt to identify artificial conditions to trigger filament formation in the absence of eukaryotic cells. The type III secretion pilus in various pathogens can be induced by several triggers including: pH shift, calcium and iron depletion, host cell contact, as well as soluble hormones and immune defense factors secreted by the host (103). We have determined that host contact in an infection is required for filament formation *in vitro* whereas soluble host-derived molecules did not appear to trigger filament formation. Therefore an array of culture conditions, times, and metal chelators should be tested to try and identify an artificial condition that can trigger filament production in a cell-free environment. The ability to induce filaments in static culture on solid surface would allow for easier purification, in addition to reducing the need to use eukaryotic cells for each experiment. The ideal induction condition for filaments would trigger filament formation but not coccoid conversion. Though our data suggests the processes are interconnected, because a great debate exists as to the relevance of coccoid *H. pylori*, conducting experiments on "normal" bacteria would be favorable.

6.4 Final thoughts

The field of type IV secretion has made steady headway in the past decade despite a great deal of technical limitations and conflicting data from various investigators, perhaps none more than the *cag* T4SS. After nearly a decade of investigation, only one effector molecule remains identified for this system. Though CagA appears to be a multifunctional protein, it would be a return to reductionism to assume that this represents the only translocated effector in the complex *cag* T4SS. Like our research counterparts investigating the icm/dot T4SS in *Legionella pneumophila*, the time may have come for the rest of the *H. pylori* genome to be explored for potential translocated effector molecules. To date we (as a field) have limited our search mainly to those accessory proteins encoded by the *cag*-PAI, however hindsight is revealing that this may have been misdirected. The *cag* system in *H. pylori* appears to be a particularly complex T4SS in that it requires many additional components for effector translocation that are absent in other orthologous systems. To date it remains a mystery as to where the genes were acquired and we have only begun to appreciate the importance of these enigmatic components in *H. pylori* pathogenesis. Our work herein has contributed to this important understanding.

7 Appendix

7.1 Table A-1. Crystallographic structure determination and model analysis

Data collection				
Datasets	**Peak (crystal I)**	**Remote (crystal I)**	**Remote (crystal II)**	**Cu adduct**
Wavelength (Å)	0.97942	0.97420	0.97814	0.97621
Space group, cell parameters (Å, °)	C2, **a**=81.22, **b**=117.90, **c**=66.52, β=110.6			$P6_222$, **a=b**=65.03, **c**=156.16
Resolution range (Å)	63.37-2.50 (2.64-2.50)	63.89-2.20 (2.32-2.20)	62.26-2.20 (2.32-2-20)	78.09-2.70 (2.85 – 2.70)
Unique reflections [1]	19,417 (2,852)	28,578 (4,165)	30507 (4107)	5757 (796)
Multiplicity			7.3 (7.4)	10.3 (10.7)
Completeness (%)	96.7 (96.8)	96.3 (96.5)	99.2 (99.9)	99.9
<I/σ(I)>	9.0 (2.2)	7.1 (1.8)	16.6 (4.1)	7.5 (1.7)
R_{symm}	0.067(0.345)	0.066 (0.396)	0.088 (0.411)	0.079 (0.459)
Anomalous phasing	1.66	1.23	-	-
Figure of merit Centric/acentric	0.361/0.125			
Refinement statistics				
Resolution Used (Å)	10 – 2.2			6.0 – 2.75
Reflections (R_{free} set)	27780 (2778)			4959 (252)
R_{cryst}	0.237			0.261
R_{free}	0.306			0.307
Rmsd from ideal values				
Bond lengths (Å)	0.005			0.006
Bond angles	0.020 Å			1.2 °

[*] Values in parentheses are for outer resolution shell $R_{sym} = \Sigma_{hkl}|I_{hkl} - \langle I_{hkl} \rangle| / \Sigma_{hkl} I_{hkl}$

$ R factor = $\sum_{hkl}||F_o| - |F_c||/\sum_{hkl}|F_o|$ where $|F_o|$ and $|F_c|$ are the observed and calculated structure factor amplitudes for reflection hkl, applied to the work (R_{cryst}) and test (R_{free}) (5% omitted from refinement) sets, respectively

Bibliography

1. 1994. Schistosomes, liver flukes and *Helicobacter pylori*. IARC Working Group on the Evaluation of Carcinogenic Risks to Humans. Lyon, 7-14 June 1994. IARC Monogr Eval Carcinog Risks Hum **61:**1-241.

2. **Akopyants, N., Bukanov, N.O., Westblom, T.U., and Berg, D.E.** 1992. PCR-based RFLP analysis of DNA sequence diversity in the gastric pathogen *Helicobacter pylori*. Nucleic Acids Research **20:**6221-6225.

3. **Akopyants, N., Clifton, S.W., Kersulyte, D., Crabtree, J.E., Youree, B.E., Reece, C.A., Bukanov, N.O., Drazek, E.S., Roe, B.A., and Berg, D.E.** 1998. Analyses of the *cag* pathogenicity island of *Helicobacter pylori*. Molecular Microbiology **28:**37-53.

4. **Alm, R. A., L. S. Ling, D. T. Moir, B. L. King, E. D. Brown, P. C. Doig, D. R. Smith, B. Noonan, B. C. Guild, B. L. deJonge, G. Carmel, P. J. Tummino, A. Caruso, M. Uria-Nickelsen, D. M. Mills, C. Ives, R. Gibson, D. Merberg, S. D. Mills, Q. Jiang, D. E. Taylor, G. F. Vovis, and T. J. Trust.** 1999. Genomic-sequence comparison of two unrelated isolates of the human gastric pathogen *Helicobacter pylori*. Nature **397:**176-80.

5. **Altschul, S. F., W. Gish, W. Miller, E. W. Myers, and D. J. Lipman.** 1990. Basic local alignment search tool. J Mol Biol **215:**403-10.

6. **Aly, K. A., and C. Baron.** 2007. The VirB5 protein localizes to the T-pilus tips in *Agrobacterium tumefaciens*. Microbiology **153:**3766-75.

7. **Amieva, M. R., and E. M. El-Omar.** 2008. Host-bacterial interactions in *Helicobacter pylori* infection. Gastroenterology **134:**306-23.

8. **Amieva, M. R., Vogelmann, R., Covacci, A., Tompkins, L.S., Nelson, W.J., and Falkow, S.** 2003. Disruption of the apical-junction complex by *Helicobacter pylori* CagA. Science **300:**1430-1434.

9. **Andersen-Nissen, E., K. D. Smith, K. L. Strobe, S. L. Barrett, B. T. Cookson, S. M. Logan, and A. Aderem.** 2005. Evasion of Toll-like receptor 5 by flagellated bacteria. Proc Natl Acad Sci U S A **102:**9247-52.

10. **Andrzejewska, J., S. K. Lee, P. Olbermann, N. Lotzing, E. Katzowitsch, B. Linz, M. Achtman, C. I. Kado, S. Suerbaum, and C. Josenhans.** 2006. Characterization of the pilin ortholog of the *Helicobacter pylori* type IV cag pathogenicity apparatus, a surface-associated protein expressed during infection. J Bacteriol **188:**5865-77.

11. **Aras, R. A., W. Fischer, G. I. Perez-Perez, M. Crosatti, T. Ando, R. Haas, and M. J. Blaser.** 2003. Plasticity of repetitive DNA sequences within a bacterial (Type IV) secretion system component. J Exp Med **198:**1349-60.

12. **Asahi, M., Awuma, T., Ito, Y., Suto, H., Nagai, Y., Tsubokawa, M., Tohyama, Y., Maeda, S., Omata, M., Suzuki, T., and Sasakawa, C.** 2000. *Heliobacter pylori* CagA protein can be tyrosine phosphorylated in the gastric epithelial cells. Journal of Experimental Medicine **191:**593-602.

13. **Atherton, J. C., P. Cao, R. M. Peek, Jr., M. K. Tummuru, M. J. Blaser, and T. L. Cover.** 1995. Mosaicism in vacuolating cytotoxin alleles of *Helicobacter pylori*. Association of specific vacA types with cytotoxin production and peptic ulceration. J Biol Chem **270:**17771-7.

14. **Atmakuri, K., Cascales, E., and Christie, P.J.** 2004. Energetic components VirD4, VirB11 and VirB4 mediate early DNA transfer reactions required for bacterial type IV secretion. Molecular Microbiology **54:**1199-1211.

15. **Azevedo, N. F., C. Almeida, L. Cerqueira, S. Dias, C. W. Keevil, and M. J. Vieira.** 2007. Coccoid form of *Helicobacter pylori* as a morphological manifestation of cell adaptation to the environment. Appl Environ Microbiol.

16. **Azevedo, N. F., A. P. Pacheco, C. W. Keevil, and M. J. Vieira.** 2006. Adhesion of water stressed *Helicobacter pylori* to abiotic surfaces. J Appl Microbiol **101:**718-24.

17. **Backert, S., T. Kwok, and W. Konig.** 2005. Conjugative plasmid DNA transfer in *Helicobacter pylori* mediated by chromosomally encoded relaxase and TraG-like proteins. Microbiology **151:**3493-503.

18. **Backert, S., and T. F. Meyer.** 2006. Type IV secretion systems and their effectors in bacterial pathogenesis. Curr Opin Microbiol **9:**207-17.

19. **Backert, S., Moese, S., Selbach, M., Brinkmann, V., and Meyer, T.F.** 2001. Phosphorylation of tyrosine 972 of the *Helicobacter pylori* CagA protein is essential for induction of a scattering phenotype in gastric epithelial cells. Molecular Microbiology **42:**631-644.

20. **Bacon, D. J., R. A. Alm, D. H. Burr, L. Hu, D. J. Kopecko, C. P. Ewing, T. J. Trust, and P. Guerry.** 2000. Involvement of a plasmid in virulence of *Campylobacter jejuni* 81-176. Infect Immun **68:**4384-90.

21. **Baik, S., Kim, K., Song, S., Kim, D., Jun, J., Lee, S., Song, J., Park, J., Kang, H., Lee, W., Cho, M., Youn, H., Ko, G., and Rhee, K.** 2004. Proteomic analysis

of the sarcosine-insoluble outer membrane fraction of *Helicobacter pylori*. Journal of Bacteriology **186:**949-995.

22. **Baron, C.** 2006. VirB8: a conserved type IV secretion system assembly factor and drug target. Biochem Cell Biol **84:**890-9.

23. **Bayliss, R., R. Harris, L. Coutte, A. Monier, R. Fronzes, P. J. Christie, P. C. Driscoll, and G. Waksman.** 2007. NMR structure of a complex between the VirB9/VirB7 interaction domains of the pKM101 type IV secretion system. Proc Natl Acad Sci U S A **104:**1673-8.

24. **Benaissa, M., P. Babin, N. Quellard, L. Pezennec, Y. Cenatiempo, and J. L. Fauchere.** 1996. Changes in *Helicobacter pylori* ultrastructure and antigens during conversion from the bacillary to the coccoid form. Infect Immun **64:**2331-5.

25. **Berger, B. R., and P. J. Christie.** 1994. Genetic complementation analysis of the *Agrobacterium tumefaciens* virB operon: virB2 through virB11 are essential virulence genes. J Bacteriol **176:**3646-60.

26. **Bergman, M. P., A. Engering, H. H. Smits, S. J. van Vliet, A. A. van Bodegraven, H. P. Wirth, M. L. Kapsenberg, C. M. Vandenbroucke-Grauls, Y. van Kooyk, and B. J. Appelmelk.** 2004. *Helicobacter pylori* modulates the T helper cell 1/T helper cell 2 balance through phase-variable interaction between lipopolysaccharide and DC-SIGN. J Exp Med **200:**979-90.

27. **Best, L. M., S. J. Veldhuyzen van Zanten, P. M. Sherman, and G. S. Bezanson.** 1994. Serological detection of *Helicobacter pylori* antibodies in children and their parents. J Clin Microbiol **32:**1193-6.

28. **Bhasin, M., Garg, A., and Raghava, G.P.S.** 2005. PSLpred: prediction of subcellular localization of bacterial proteins. Bioinformatics **In press**.

29. **Blaser, M. J.** 2005. An endangered species in the stomach. Sci Am **292:**38-45.

30. **Blaser, M. J., and J. C. Atherton.** 2004. *Helicobacter pylori* persistence: biology and disease. J Clin Invest **113:**321-33.

31. **Blocker, A., Komoriya, K., and Aizawa, S.** 2003. Type III secretion systems and bacterial flagella: insights into their function from structural similarities. Proceedings of the National Academy of Sciences of the United States of America **100:**3027-3030.

32. **Boonjakuakul, J. K., D. R. Canfield, and J. V. Solnick.** 2005. Comparison of *Helicobacter pylori* virulence gene expression *in vitro* and in the Rhesus macaque. Infect Immun **73:**4895-904.

33. **Boonjakuakul, J. K., M. Syvanen, A. Suryaprasad, C. L. Bowlus, and J. V. Solnick.** 2004. Transcription profile of *Helicobacter pylori* in the human stomach reflects its physiology *in vivo*. J Infect Dis **190:**946-56.

34. **Bourzac, K. M., L. A. Satkamp, and K. Guillemin.** 2006. The *Helicobacter pylori cag* pathogenicity island protein CagN is a bacterial membrane-associated protein that is processed at its C terminus. Infect Immun **74:**2537-43.

35. **Brandt, S., Kwok, T., Hartig, R., Konig, W., and Backert, S.** 2005. NF-{kappa}B activation and potentiation of proinflammatory responses by the *Helicobacter pylori* CagA protein. Proceedings of the National Academy of Sciences of the United States of America **102:**9300-9305.

36. **Brenciaglia, M. I., A. M. Fornara, M. M. Scaltrito, and F. Dubini.** 2000. *Helicobacter pylori*: cultivability and antibiotic susceptibility of coccoid forms. Int J Antimicrob Agents **13:**237-41.

37. **Brinkmann, V., U. Reichard, C. Goosmann, B. Fauler, Y. Uhlemann, D. S. Weiss, Y. Weinrauch, and A. Zychlinsky.** 2004. Neutrophil extracellular traps kill bacteria. Science **303:**1532-5.

38. **Buhrdorf, R., Förster, C., Haas, R., and Fischer, W.** 2003. Topological analysis of a putative *virB8* homologue essential for the *cag* type IV secretion system in *Helicobacter pylori*. International Journal of Medical Microbiology **293:**213-217.

39. **Burnens, A. P., J. Stanley, R. Morgenstern, and J. Nicolet.** 1994. Gastroenteritis associated with *Helicobacter pullorum*. Lancet **344:**1569-70.

40. **Buttner, C. R., G. R. Cornelis, D. W. Heinz, and H. H. Niemann.** 2005. Crystal structure of *Yersinia enterocolitica* type III secretion chaperone SycT. Protein Sci **14:**1993-2002.

41. **Caruso, R., F. Pallone, and G. Monteleone.** 2007. Emerging role of IL-23/IL-17 axis in *H pylori*-associated pathology. World J Gastroenterol **13:**5547-51.

42. **Cascales, E., and P. J. Christie.** 2004. *Agrobacterium* VirB10, an ATP energy sensor required for type IV secretion. Proceedings of the National Academy of Sciences of the United States of America **101:**17228-17233.

43. **Cascales, E., and P. J. Christie.** 2004. Definition of a bacterial type IV secretion pathway for a DNA substrate. Science **304:**1170-1173.

44. **Cascales, E., and P. J. Christie.** 2003. The versatile bacterial type IV secretion systems. Nature Reviews Microbiology **1:**137-149.

45. **Cavelli-Sforza, L., Lederberg, J., and Lederberg, E.** 1953. An infective factor controlling sex compatibility in *B. coli.* Journal of Genetic Microbiology **8:**89-103.

46. **Cellini, L., N. Allocati, D. Angelucci, T. Iezzi, E. Di Campli, L. Marzio, and B. Dainelli.** 1994. Coccoid *Helicobacter pylori* not culturable *in vitro* reverts in mice. Microbiol Immunol **38:**843-50.

47. **Cellini, L., I. Robuffo, N. M. Maraldi, and G. Donelli.** 2001. Searching the point of no return in *Helicobacter pylori* life: necrosis and/or programmed death? J Appl Microbiol **90:**727-32.

48. **Cendron, L., Seydel, A., Angelini, A., Battistutta, R., and Zanotti, G.** 2004. Crystal structure of CagZ, a protein from the *Helicobacter pylori* pathogenicity island that encodes for a type IV secretion system. Journal of Molecular Biology **340:**881-889.

49. **Cendron, L., E. Tasca, T. Seraglio, A. Seydel, A. Angelini, R. Battistutta, C. Montecucco, and G. Zanotti.** 2007. The crystal structure of CagS from the *Helicobacter pylori* pathogenicity island. Proteins **69:**440-3.

50. **Cesini, S., Lange, C., Xiang, Z., Crabtree, J.E., Ghiara, P., Borodovsky, M., Rappouli, R., and Covacci, A.** 1996. *cag,* a pathogenicity island of *Helicobacter pylori,* encodes type-I specific and disease-associated virulence factors. Proceedings of the National Academy of Sciences of the United States of America **93**.

51. **Chan, W. Y., P. K. Hui, K. M. Leung, J. Chow, F. Kwok, and C. S. Ng.** 1994. Coccoid forms of *Helicobacter pylori* in the human stomach. Am J Clin Pathol **102:**503-7.

52. **Chang, Y. J., M. S. Wu, J. T. Lin, R. G. Pestell, M. J. Blaser, and C. C. Chen.** 2006. Mechanisms for *Helicobacter pylori* CagA-induced cyclin D1 expression that affect cell cycle. Cell Microbiol **8:**1740-52.

53. **Chaput, C., C. Ecobichon, N. Cayet, S. E. Girardin, C. Werts, S. Guadagnini, M. C. Prevost, D. Mengin-Lecreulx, A. Labigne, and I. G. Boneca.** 2006. Role of AmiA in the morphological transition of *Helicobacter pylori* and in immune escape. PLoS Pathog **2:**e97.

54. **Christie, P. J.** 2004. Type IV secretion: the *Agrobacterium* VirB/D4 and related conjugation systems. Biochim Biophys Acta **1694:**219-34.

55. **Christie, P. J., and J. P. Vogel.** 2000. Bacterial type IV secretion: conjugation systems adapted to deliver effector molecules to host cells. Trends in Microbiology **8:**354-360.

56. **Chun, H. J., D. K. Park, C. H. Park, J. H. Park, Y. T. Jeen, S. H. Um, S. W. Lee, J. H. Choi, C. D. Kim, H. S. Ryu, J. H. Hyun, Y. S. Chae, and C. S. Uhm.** 2002. Electron microscopic evaluation of adhesion of *Helicobacter pylori* to the gastric epithelial cells in chronic gastritis. Korean J Intern Med **17:**45-50.

57. **Churin, Y., Al-Ghoul, L., Kepp, O., Meyer, T.F., Birchmeier, W., and Naumann, M.** 2003. *Helicobacter pylori* CagA protein targets the c-MET receptor and enhances the motogenic response. Journal of Cell Biology **161:**249-255.

58. **Cole, S. P., J. Harwood, R. Lee, R. She, and D. G. Guiney.** 2004. Characterization of monospecies biofilm formation by *Helicobacter pylori*. J Bacteriol **186:**3124-32.

59. **Cole, S. P., V. F. Kharitonov, and D. G. Guiney.** 1999. Effect of nitric oxide on *Helicobacter pylori* morphology. J Infect Dis **180:**1713-7.

60. **Copass, M., G. Grandi, and R. Rappuoli.** 1997. Introduction of unmarked mutations in the *Helicobacter pylori vac*A gene with a sucrose sensitivity marker. Infect Immun **65:**1949-52.

61. **Couturier, M. R., E. Tasca, C. Montecucco, and M. Stein.** 2006. Interaction with CagF is required for translocation of CagA into the host via the *Helicobacter pylori* type IV secretion system. Infect Immun **74:**273-81.

62. **Covacci, A.** 2000. *Helicobacter pylori* pathogenicity: the bacterium and the host. Eur J Gastroenterol Hepatol **12:**1050-2.

63. **Covacci, A., Cesini, S., Bugnoli, M., Petracca, R., Burroni, D., Macchia, G., Massone, A., Papini, E., Xiang, Z., Figura, N., and Rappouli, R.** 1993. Molecular characterization of the 128-kDa immunodominant antigen of *Helicobacter pylori* associated with cytotoxicity and duodenal ulcer. Proceedings of the National Academy of Sciences of the United States of America **90:**5791-5795.

64. **Cover, T. L., and M. J. Blaser.** 1992. Purification and characterization of the vacuolating toxin from *Helicobacter pylori*. J Biol Chem **267:**10570-5.

65. **Czero, M., Wallin, E., Simon, I., von Heijne, G., and Elofsson, A.** 1997. Prediction of transmembrane alpha-helices in prokaryotic membrane proteins: the Dense Alignment Surface method. Protein Engineering **10:**673-676.

66. **D'Elios, M. M., A. Amedei, A. Cappon, G. Del Prete, and M. de Bernard.** 2007. The neutrophil-activating protein of *Helicobacter pylori* (HP-NAP) as an immune modulating agent. FEMS Immunol Med Microbiol **50:**157-64.

67. **Dang, T. A., and Christie, P.J.** 1997. The VirB4 ATPase of *Agrobacterium tumefaciens* is a cytoplasmic membrane protein exposed at the periplasmic surface. Journal of Bacteriology **179:**453-462.

68. **Dang, T. A., Zhou, X.R., Graf, B., and Christie, P.J.** 1999. Dimerization of the *Agrobacterium tumefaciens* VirB4 ATPase and the effect of ATP binding cassette mutations on the assembly and function of the T-DNA transporter. Molecular Microbiology **32.**

69. **Day, A. S., and P. M. Sherman.** 2002. Accuracy of office-based immunoassays for the diagnosis of *Helicobacter pylori* infection in children. Helicobacter **7:**205-9.

70. **Delahay, R. M., G. D. Balkwill, K. A. Bunting, W. Edwards, J. C. Atherton, and M. S. Searle.** 2008. The highly repetitive region of the *Helicobacter pylori* CagY protein comprises tandem arrays of an alpha-helical repeat module. J Mol Biol **377:**956-71.

71. **Delano, W. L.** 2007. MacPyMOL, p. A PyMOL-based Molecular Graphics Application for MacOS X.

72. **Dillard, J. P., and Seifert, H.S.** 2001. A variable genetic island specific for *Neisseria gonorrhoeae* is involved in providing DNA for natural transformation and is found more often in disseminated infection isolates. Molecular Microbiology **41:**263-277.

73. **Dobos, K. M., K. Swiderek, K. H. Khoo, P. J. Brennan, and J. T. Belisle.** 1995. Evidence for glycosylation sites on the 45-kilodalton glycoprotein of *Mycobacterium tuberculosis*. Infect Immun **63:**2846-53.

74. **Dobrindt, U., Hochhut, B., Hentschel, U., and Hacker, J.** 2004. Genomic islands in pathogenic and environmental organisms. Nature Reviews Microbiology **2:**414-424.

75. **Doig, P., Exner, M.M., Hancock, R.E., and Trust, T.J.** 1995. Isolation and characterization of a conserved porin protein from *Helicobacter pylori*. Journal of Bacteriology **177:**5447-5452.

76. **Donelli, G., P. Matarrese, C. Fiorentini, B. Dainelli, T. Taraborelli, E. Di Campli, S. Di Bartolomeo, and L. Cellini.** 1998. The effect of oxygen on the growth and cell morphology of *Helicobacter pylori*. FEMS Microbiol Lett **168:**9-15.

77. **Draper, O., R. Middleton, M. Doucleff, and P. C. Zambryski.** 2006. Topology of the VirB4 C terminus in the *Agrobacterium tumefaciens* VirB/D4 type IV secretion system. J Biol Chem **281:**37628-35.

78. **Duguid, J. P., I. W. Smith, G. Dempster, and P. N. Edmunds.** 1955. Non-flagellar filamentous appendages (fimbriae) and haemagglutinating activity in *Bacterium coli*. J Pathol Bacteriol **70:**335-48.

79. **Dyrlov Bendtsen, J., Neilson, H., von Heijne, G., and Brunak, S.** 2004. Improved prediction of signal peptides: SignalP 3.0. Journal of Molecular Biology **340:**783-795.

80. **Eaton, K. A., S. Suerbaum, C. Josenhans, and S. Krakowka.** 1996. Colonization of gnotobiotic piglets by *Helicobacter pylori* deficient in two flagellin genes. Infect Immun **64:**2445-8.

81. **Eisenbrandt, R., M. Kalkum, E. M. Lai, R. Lurz, C. I. Kado, and E. Lanka.** 1999. Conjugative pili of IncP plasmids, and the Ti plasmid T pilus are composed of cyclic subunits. J Biol Chem **274:**22548-55.

82. **El-Omar, E. M., K. Oien, A. El-Nujumi, D. Gillen, A. Wirz, S. Dahill, C. Williams, J. E. Ardill, and K. E. McColl.** 1997. *Helicobacter pylori* infection and chronic gastric acid hyposecretion. Gastroenterology **113:**15-24.

83. **el-Omar, E. M., I. D. Penman, J. E. Ardill, R. S. Chittajallu, C. Howie, and K. E. McColl.** 1995. *Helicobacter pylori* infection and abnormalities of acid secretion in patients with duodenal ulcer disease. Gastroenterology **109:**681-91.

84. **Falush, D., T. Wirth, B. Linz, J. K. Pritchard, M. Stephens, M. Kidd, M. J. Blaser, D. Y. Graham, S. Vacher, G. I. Perez-Perez, Y. Yamaoka, F. Megraud, K. Otto, U. Reichard, E. Katzowitsch, X. Wang, M. Achtman, and S. Suerbaum.** 2003. Traces of human migrations in *Helicobacter pylori* populations. Science **299:**1582-5.

85. **Feldman, M. F., and G. R. Cornelis.** 2003. The multitalented type III chaperones: all you can do with 15 kDa. FEMS Microbiol Lett **219:**151-8.

86. **Ferrero, R. L., V. Cussac, P. Courcoux, and A. Labigne.** 1992. Construction of isogenic urease-negative mutants of *Helicobacter pylori* by allelic exchange. J Bacteriol **174:**4212-7.

87. **Fischer, W., Püls, J., Buhrdorf, R., Gebert, B., Odenbreit, S., and Haas, R.** 2001. Systematic mutagenesis of the *Helicobacter pylori cag* pathogenicity island: essential genes for CagA translocation in host cells and induction of interlukin-8. Molecular Microbiology **42:**1337-1348.

88. **Fox, J. G., C. C. Chien, F. E. Dewhirst, B. J. Paster, Z. Shen, P. L. Melito, D. L. Woodward, and F. G. Rodgers.** 2000. *Helicobacter canadensis* sp. nov. isolated from humans with diarrhea as an example of an emerging pathogen. J Clin Microbiol **38:**2546-9.

89. **Franco, A. T., D. A. Israel, M. K. Washington, U. Krishna, J. G. Fox, A. B. Rogers, A. S. Neish, L. Collier-Hyams, G. I. Perez-Perez, M. Hatakeyama, R. Whitehead, K. Gaus, D. P. O'Brien, J. Romero-Gallo, and R. M. Peek, Jr.** 2005. Activation of beta-catenin by carcinogenic *Helicobacter pylori*. Proc Natl Acad Sci U S A **102:**10646-51.

90. **Frankel, S., Sohn, R., and Leinwand, L.** 1991. The use of sarkosyl in generating soluble protein after bacterial expression. Proceedings of the National Academy of Sciences of the United States of America **88:**1192-1196.

91. **Fulkerson, J. F., and Mobley, H.T.** 2000. Membrane topology of the NixA nickel transporter of *Helicobacter pylori*: two nickel transport-specific motifs within transmembrane helices II and III. Journal of Bacteriology **182:**1722-1730.

92. **Gal-Mor, O., and B. B. Finlay.** 2006. Pathogenicity islands: a molecular toolbox for bacterial virulence. Cell Microbiol **8:**1707-19.

93. **Gardy, J. L., Laird, M.R., Chen, F., Rey, S., Walsh, C.J., Ester, M., and Brinkman, F.S.L.** 2005. PSORTb v.2.0: expanded prediction of bacterial protein subcellular localization and insights gained from comparative proteome analysis. Bioinformatics **21:**617-623.

94. **Gasteiger, E., Hoogland, C., Gattiker, A., Duvaud, S., Wilkins, M.R., Appel, R. and D., Bairoch, A.** 2005. *Protein identification and Analysis Tools on the ExPASy Server*, p. 571-607. *In* J. M. Walker (ed.), The Proteomics Protocols Handbook. Humana Press.

95. **Gauthier, A., Puente, J.L., and Finlay, B.B.** 2003. Secretion of the Enteropathogenic *Escherichia coli* type III secretion system requires components of the type III apparatus for assembly and localization. Infection and Immunity **71:**3310-3319.

96. **Geis, G., H. Leying, S. Suerbaum, U. Mai, and W. Opferkuch.** 1989. Ultrastructure and chemical analysis of *Campylobacter pylori* flagella. J Clin Microbiol **27:**436-41.

97. **Geis, G., S. Suerbaum, B. Forsthoff, H. Leying, and W. Opferkuch.** 1993. Ultrastructure and biochemical studies of the flagellar sheath of *Helicobacter pylori*. J Med Microbiol **38:**371-7.

98. **Go, M. F.** 2002. Review article: natural history and epidemiology of *Helicobacter pylori* infection. Alimentary Pharmacology and Therapeutics **16:**3-15.

99. **Goldstein, I. J., D. A. Blake, S. Ebisu, T. J. Williams, and L. A. Murphy.** 1981. Carbohydrate binding studies on the Bandeiraea simplicifolia I isolectins. Lectins which are mono-, di-, tri-, and tetravalent for N-acetyl-D-galactosamine. J Biol Chem **256:**3890-3.

100. **Goodwin, C. S., R. K. McCulloch, J. A. Armstrong, and S. H. Wee.** 1985. Unusual cellular fatty acids and distinctive ultrastructure in a new spiral bacterium (*Campylobacter pyloridis*) from the human gastric mucosa. J Med Microbiol **19:**257-67.

101. **Hacker, J., Blum-Oehler, G., Mühldorfer, I., and Tschäpe, H.** 1996. Pathogenicity islands of virulent bacteria: structure, function and impact on microbial evolution. Molecular Microbiology **23:**1089.

102. **Hatakeyama, M.** 2006. *Helicobacter pylor*i CagA -- a bacterial intruder conspiring gastric carcinogenesis. Int J Cancer **119:**1217-23.

103. **He, S. Y., K. Nomura, and T. S. Whittam.** 2004. Type III protein secretion mechanism in mammalian and plant pathogens. Biochim Biophys Acta **1694:**181-206.

104. **Heczko, U., V. C. Smith, R. Mark Meloche, A. M. Buchan, and B. B. Finlay.** 2000. Characteristics of *Helicobacter pylori* attachment to human primary antral epithelial cells. Microbes Infect **2:**1669-76.

105. **Higashi, H., R. Tsutsumi, A. Fujita, S. Yamazaki, M. Asaka, T. Azuma, and M. Hatakeyama.** 2002. Biological activity of the *Helicobacter pylori* virulence factor CagA is determined by variation in the tyrosine phosphorylation sites. Proc Natl Acad Sci U S A **99:**14428-33.

106. **Higashi, H., Tsutsumi, R., Muto, S., Sugiyama, T., Azuma, T., Asaka, M., and Hatakeyama, M.** 2002. SHP-2 tyrosine phosphatase as an intracellular target of *Helicobacter* CagA protein. Science **295:**683-686.

107. **Higashi, H., Tsutsumi, R., Muto, S., Sugiyama, T., Azuma, T., Asaka, M., and Hatakeyama, M.** 2001. SHP-2 tyrosine phosphatase as an intracellular target of *Helicobacter* CagA protein. Science **295:**683-686.

108. **Higashi, H., K. Yokoyama, Y. Fujii, S. Ren, H. Yuasa, I. Saadat, N. Murata-Kamiya, T. Azuma, and M. Hatakeyama.** 2005. EPIYA motif is a membrane-targeting signal of *Helicobacter pylori* virulence factor CagA in mammalian cells. J Biol Chem **280:**23130-7.

109. **Hilleringmann, M., W. Pansegrau, M. Doyle, S. Kaufman, M. L. MacKichan, C. Gianfaldoni, P. Ruggiero, and A. Covacci.** 2006. Inhibitors of *Helicobacter pylori* ATPase Cagalpha block CagA transport and *cag* virulence. Microbiology **152:**2919-30.

110. **Hofreuter, D., Odenbreit, S., and Haas, R.** 2001. Natural transformation competence of *Helicobacter pylori* is mediated by the basic components of a type IV secretion system. Molecular Microbiology **41:**379-391.

111. **Hofreuter, D., Odenbreit, S., Puls, J., Schwan, D., and Haas, R.** 2000. Genetic competence in *Helicobacter pylori*: mechanisms and biological implications. Research in Microbiology **151:**487-491.

112. **Hohlfeld, S., I. Pattis, J. Puls, G. V. Plano, R. Haas, and W. Fischer.** 2006. A C-terminal translocation signal is necessary, but not sufficient for type IV secretion of the *Helicobacter pylori* CagA protein. Mol Microbiol **59:**1624-37.

113. **Höppner, C., Liu, Z., Domke, N., Binns, A.N., Baron, C.** 2004. VirB1 orthologs from *Brucella suis* and pKM101 complement defects of the lytic transglycosolase required for efficient type IV secretion from *Agrobacterium tumefaciens*. Journal of Bacteriology **186:**1415-1422.

114. **Houwink, A. L., and I. W. van.** 1950. Electron microscopical observations on bacterial cytology; a study on flagellation. Biochim Biophys Acta **5:**10-44.

115. **Jakubowski, S. J., E. Cascales, V. Krishnamoorthy, and P. J. Christie.** 2005. *Agrobacterium tumefaciens* VirB9, an outer-membrane-associated component of a type IV secretion system, regulates substrate selection and T-pilus biogenesis. J Bacteriol **187:**3486-95.

116. **Jakubowski, S. J., V. Krishnamoorthy, E. Cascales, and P. J. Christie.** 2004. *Agrobacterium tumefaciens* VirB6 domains direct the ordered export of a DNA substrate through a type IV secretion System. J Mol Biol **341:**961-77.

117. **Jakubowski, S. J., V. Krishnamoorthy, and P. J. Christie.** 2003. *Agrobacterium tumefaciens* VirB6 protein participates in formation of VirB7 and VirB9 complexes required for type IV secretion. J Bacteriol **185:**2867-78.

118. **Jones, A. L., E. M. Lai, K. Shirasu, and C. I. Kado.** 1996. VirB2 is a processed pilin-like protein encoded by the *Agrobacterium tumefaciens* Ti plasmid. J Bacteriol **178:**5706-11.

119. **Jonson, A. B., S. Normark, and M. Rhen.** 2005. Fimbriae, pili, flagella and bacterial virulence. Contrib Microbiol **12:**67-89.

120. **Josenhans, C., A. Labigne, and S. Suerbaum.** 1995. Comparative ultrastructural and functional studies of *Helicobacter pylori* and *Helicobacter mustelae* flagellin

mutants: both flagellin subunits, FlaA and FlaB, are necessary for full motility in Helicobacter species. J Bacteriol **177:**3010-20.

121. **Khin, M. M., J. S. Hua, H. C. Ng, T. Wadstrom, and H. Bow.** 2000. Agglutination of *Helicobacter pylori* coccoids by lectins. World J Gastroenterol **6:**202-209.

122. **Kidd, M., and I. M. Modlin.** 1998. A century of *Helicobacter pylori*: paradigms lost-paradigms regained. Digestion **59:**1-15.

123. **Kim, S. Y., Y. Ogawa, and Y. Adachi.** 2006. Canine intestinal lactic acid bacteria agglutinated with concanavalin A. J Vet Med Sci **68:**1351-4.

124. **Krause, S., Barcena, M., Pansegrau, W., Lurtz, J., Carano, J.M., and Lanka, E.** 2000. Sequence-related protein export NTPases encoded by the conjugative transfer region of RP4 and by the *cag* pathogenicity island of *Helicobacter pylori* share similar hexameric ring structures. Proceedings of the National Academy of Sciences of the United States of America **97:**3067-3072.

125. **Krause, S., Pansegrau, W., Lurz, R., de la Cruz, F., and Lanka, E.** 2000. Enzymology of type IV macromolecule secretion systems: the conjugative transfer regions of plasmids RP4 and R388 and the *cag* pathogenicity island of *Helicobacter pylori* encode structurally and functionally related nucleoside triphosphate hydrolases. Journal of Bacteriology **182:**2761-2770.

126. **Krissinel, E., and K. Henrick.** 2004. Secondary-structure matching (SSM), a new tool for fast protein structure alignment in three dimensions. Acta Crystallogr D Biol Crystallogr **60:**2256-68.

127. **Kuipers, E. J., D. A. Israel, J. G. Kusters, and M. J. Blaser.** 1998. Evidence for a conjugation-like mechanism of DNA transfer in *Helicobacter pylori*. J Bacteriol **180:**2901-5.

128. **Kumar, R. B., and A. Das.** 2002. Polar location and functional domains of the *Agrobacterium tumefaciens* DNA transfer protein VirD4. Mol Microbiol **43:**1523-32.

129. **Kusters, J. G., A. H. van Vliet, and E. J. Kuipers.** 2006. Pathogenesis of Helicobacter pylori infection. Clin Microbiol Rev **19:**449-90.

130. **Kutter, S., R. Buhrdorf, J. Haas, W. Schneider-Brachert, R. Haas, and W. Fischer.** 2008. Protein subassemblies of the *Helicobacter pylori* Cag type IV secretion system revealed by localization and interaction studies. J Bacteriol **190:**2161-71.

131. **Kwok, T., D. Zabler, S. Urman, M. Rohde, R. Hartig, S. Wessler, R. Misselwitz, J. Berger, N. Sewald, W. Konig, and S. Backert.** 2007. *Helicobacter exploits* integrin for type IV secretion and kinase activation. Nature **449:**862-6.

132. **Lai, E. M., and C. I. Kado.** 1998. Processed VirB2 is the major subunit of the promiscuous pilus of *Agrobacterium tumefaciens*. J Bacteriol **180:**2711-7.

133. **Lederberg, J., and Tatum., E.L.** 1946. Gene recombination in *Escherichia coli*. Nature **158:**558.

134. **Llosa, M., Gomis-Rüth, F.X., Coll, M., and de la Cruz, F.** 2002. Bacterial conjugation: a two-step mechanism for DNA transport. Molecular Microbiology **45:**1-8.

135. **Locher, M., B. Lehnert, K. Krauss, J. Heesemann, M. Groll, and G. Wilharm.** 2005. Crystal structure of the *Yersinia enterocolitica* type III secretion chaperone SycT. J Biol Chem **280:**31149-55.

136. **Marshall, B. J., and J. R. Warren.** 1984. Unidentified curved bacilli in the stomach of patients with gastritis and peptic ulceration. Lancet **1:**1311-5.

137. **McNulty, C. A., J. C. Dent, A. Curry, J. S. Uff, G. A. Ford, M. W. Gear, and S. P. Wilkinson.** 1989. New spiral bacterium in gastric mucosa. J Clin Pathol **42:**585-91.

138. **Middleton, R., K. Sjolander, N. Krishnamurthy, J. Foley, and P. Zambryski.** 2005. Predicted hexameric structure of the *Agrobacterium* VirB4 C terminus suggests VirB4 acts as a docking site during type IV secretion. Proc Natl Acad Sci U S A **102:**1685-90.

139. **Mimuro, H., Suzuki, T., Tanaka, J., Ashi, M., Haas, R., and Sasakawa, C.** 2002. Grb2 is a key mediator of *Helicobacter pylori* CagA protein activities. Molecular Cell **10:**745-755.

140. **Moese, S., M. Selbach, V. Brinkmann, A. Karlas, B. Haimovich, S. Backert, and T. F. Meyer.** 2007. The *Helicobacter pylori* CagA protein disrupts matrix adhesion of gastric epithelial cells by dephosphorylation of vinculin. Cell Microbiol **9:**1148-61.

141. **Moese, S., Selbach, M., Zimmy-Arndt, U., Jungblut, P.R., Meyer, T.F., and Backert, S.** 2001. Identification of a tyrosine-phosphorylated 35kDa carboxy-terminal fragment (p35CagA) of the *Helicobacter pylori* CagA protein in phagocytic cells: processing or breakage? Proteomics **1:**618-629.

142. **Montecucco, C., and Rappuoli, R.** 2001. Living dangerously: how *Helicobacter pylori* survives in the human stomach. Nature Reviews Molecular Cell Biology **2:**457-466.

143. **Moran, A. P., D. T. O'Malley, T. U. Kosunen, and I. M. Helander.** 1994. Biochemical characterization of *Campylobacter fetus* lipopolysaccharides. Infect Immun **62:**3922-9.

144. **Mouery, K., B. A. Rader, E. C. Gaynor, and K. Guillemin.** 2006. The stringent response is required for *Helicobacter pylori* survival of stationary phase, exposure to acid, and aerobic shock. J Bacteriol **188:**5494-500.

145. **Muldoon, J., A. S. Shashkov, A. P. Moran, J. A. Ferris, S. N. Senchenkova, and A. V. Savage.** 2002. Structures of two polysaccharides of *Campylobacter jejuni* 81116. Carbohydr Res **337:**2223-9.

146. **Murata-Kamiya, N., Y. Kurashima, Y. Teishikata, Y. Yamahashi, Y. Saito, H. Higashi, H. Aburatani, T. Akiyama, R. M. Peek, Jr., T. Azuma, and M. Hatakeyama.** 2007. *Helicobacter pylori* CagA interacts with E-cadherin and deregulates the beta-catenin signal that promotes intestinal transdifferentiation in gastric epithelial cells. Oncogene **26:**4617-26.

147. **Nagai, H., Cambronne, E.D., Kagan, J.C., Amor, J.C., Kahn, R.A., and Roy, C.R.** 2005. A C-terminal translocation signal required for Dot/Icm-dependent delivery of the *Legionella* RalF protein to host cells. Proceedings of the National Academy of Sciences of the United States of America **102:**826-831.

148. **Nielson, H., Engelbrecht, J., Brunak, S., and von Heijne, G.** 1997. Identification of prokaryotic and eukaryotic signal peptides and prediction of their cleavage sites. Protein Engineering **10:**1-6.

149. **Nilsson, H. O., J. Blom, W. Abu-Al-Soud, A. A. Ljungh, L. P. Andersen, and T. Wadstrom.** 2002. Effect of cold starvation, acid stress, and nutrients on metabolic activity of *Helicobacter pylori.* Appl Environ Microbiol **68:**11-9.

150. **Nishi, T., K. Okazaki, K. Kawasaki, T. Fukui, H. Tamaki, M. Matsuura, M. Asada, T. Watanabe, K. Uchida, N. Watanabe, H. Nakase, M. Ohana, H. Hiai, and T. Chiba.** 2003. Involvement of myeloid dendritic cells in the development of gastric secondary lymphoid follicles in *Helicobacter pylori*-infected neonatally thymectomized BALB/c mice. Infect Immun **71:**2153-62.

151. **Noach, L. A., T. M. Rolf, and G. N. Tytgat.** 1994. Electron microscopic study of association between *Helicobacter pylori* and gastric and duodenal mucosa. J Clin Pathol **47:**699-704.

152. **O'Toole, P. W., M. C. Lane, and S. Porwollik.** 2000. *Helicobacter pylori* motility. Microbes Infect **2:**1207-14.

153. **Odenbreit, S., Gebert, B., Puls, J., Fischer, W., and Haas, R.** 2001. Interaction of *Helicobacter pylori* with professional phagocytes: role of the *cag* pathogenicity island and translocation, phosphorylation, and processing of CagA. Cellular Microbiology **3:**21-31.

154. **Odenbreit, S., Püls, J., Sedlmaier, B., Gerland, E., Fischer, W., and Haas, R.** 2000. Translocation of *Helicobacter pylori* CagA into gastric epithelial cells by type four secretion. Science **287:**1497-1500.

155. **Ogura, K., Maeda, S., Nakao, M., Watanabe, T., Tada, M., Kyutoku, T., Yoshida, H., Shiratori, Y., and Omata, M.** 2000. Virulence factors of *Helicobacter pylori* responsible for gastric diseases in Mongolian gerbil. Journal of Experimental Medicine **192:**1601-1610.

156. **Ohnishi, N., H. Yuasa, S. Tanaka, H. Sawa, M. Miura, A. Matsui, H. Higashi, M. Musashi, K. Iwabuchi, M. Suzuki, G. Yamada, T. Azuma, and M. Hatakeyama.** 2008. Transgenic expression of *Helicobacter pylori* CagA induces gastrointestinal and hematopoietic neoplasms in mouse. Proc Natl Acad Sci U S A **105:**1003-8.

157. **Oyarzabal, O. A., R. Rad, and S. Backert.** 2007. Conjugative transfer of chromosomally encoded antibiotic resistance from *Helicobacter pylori* to *Campylobacter jejuni*. J Clin Microbiol **45:**402-8.

158. **Papini, E., B. Satin, C. Bucci, M. de Bernard, J. L. Telford, R. Manetti, R. Rappuoli, M. Zerial, and C. Montecucco.** 1997. The small GTP binding protein rab7 is essential for cellular vacuolation induced by *Helicobacter pylori* cytotoxin. Embo J **16:**15-24.

159. **Park, A. M., Q. Li, K. Nagata, T. Tamura, K. Shimono, E. F. Sato, and M. Inoue.** 2004. Oxygen tension regulates reactive oxygen generation and mutation of *Helicobacter pylori*. Free Radic Biol Med **36:**1126-33.

160. **Parsonnet, J., G. D. Friedman, D. P. Vandersteen, Y. Chang, J. H. Vogelman, N. Orentreich, and R. K. Sibley.** 1991. *Helicobacter pylori* infection and the risk of gastric carcinoma. N Engl J Med **325:**1127-31.

161. **Parsot, C., Hamiaux, C., and Page, A.** 2003. The various and varying roles of specific chaperones in type III secretion systems. Current Opinion in Microbiology **6:**7-14.

162. **Parsot, C., Hamiaux, C., and Page, A.** 2002. The various and varying roles of specific chaperones in type III secretion systems. Current Opinion in Microbiology **6:**7-14.

163. **Pattis, I., E. Weiss, R. Laugks, R. Haas, and W. Fischer.** 2007. The *Helicobacter pylori* CagF protein is a type IV secretion chaperone-like molecule that binds close to the C-terminal secretion signal of the CagA effector protein. Microbiology **153:**2896-909.

164. **Peck, B., Ortkamp, M., Diehl, K.D., Hundt, E., and Knapp, B.** 1999. Conservation, localization and expression of HopZ, a protein involved in adhesion of *Helicobacter pylori*. Nucleic Acids Research **27:**3325-3333.

165. **Peek Jr., R. M., and Blaser, M.J.** 2002. *Helicobacter pylori* and gastrointestinal tract adenocarcinomas. Nature Reviews Cancer **2:**28-37.

166. **Poppe, M., S. M. Feller, G. Romer, and S. Wessler.** 2007. Phosphorylation of Helicobacter pylori CagA by c-Abl leads to cell motility. Oncogene **26:**3462-72.

167. **Portal-Celhay, C., and G. I. Perez-Perez.** 2006. Immune responses to *Helicobacter pylori* colonization: mechanisms and clinical outcomes. Clin Sci (Lond) **110:**305-14.

168. **Postle, K., and R. J. Kadner.** 2003. Touch and go: tying TonB to transport. Mol Microbiol **49:**869-82.

169. **Queralt, N., and R. Araujo.** 2007. Analysis of the Survival of *H. pylori* Within a Laboratory-based Aquatic Model System Using Molecular and Classical Techniques. Microb Ecol.

170. **Ren, S., H. Higashi, H. Lu, T. Azuma, and M. Hatakeyama.** 2006. Structural basis and functional consequence of *Helicobacter pylori* CagA multimerization in cells. J Biol Chem **281:**32344-52.

171. **Rieder, G., Fischer, W., and Haas, R.** 2005. Interaction of *Helicobacter pylori* with host cells: function of secreted and translocated molecules. Current Opinion in Microbiology **8:**67-73.

172. **Rohde, M., Püls, J., Buhrdorf, R., Fischer, W., and Haas, R.** 2003. A novel sheathed surface organelle of the *Helicobacter pylori cag* type IV secretion system. Molecular Microbiology:1-16.

173. **Rohde, M., Püls, J., Buhrdorf, R., Fischer, W., and Haas, R.** 2003. A novel sheathed surface organelle of the *Helicobacter pylori cag* type IV secretion system. Molecular Microbiology **49:**219-234.

174. **Romaniuk, P. J., Zoltowska, B., Trust, T.J., Lane, D.J., Olsen, G.J., Pace, N.R., and Stahl, D.A.** 1987. *Campylobacter pylori*, the spiral bacterium associated with human gastritis, is not a true *Campylobacter* sp. Journal of Bacteriology **169:**2137-2141.

175. **Saadat, I., H. Higashi, C. Obuse, M. Umeda, N. Murata-Kamiya, Y. Saito, H. Lu, N. Ohnishi, T. Azuma, A. Suzuki, S. Ohno, and M. Hatakeyama.** 2007. *Helicobacter pylori* CagA targets PAR1/MARK kinase to disrupt epithelial cell polarity. Nature **447:**330-3.

176. **Sadakane, Y., K. Kusaba, Z. Nagasawa, I. Tanabe, S. Kuroki, and J. Tadano.** 1999. Prevalence and genetic diversity of *cag*D, *cag*E, and *vac*A in Helicobacter pylori strains isolated from Japanese patients. Scand J Gastroenterol **34:**981-6.

177. **Saito, N., K. Konishi, F. Sato, M. Kato, H. Takeda, T. Sugiyama, and M. Asaka.** 2003. Plural transformation-processes from spiral to coccoid *Helicobacter pylori* and its viability. J Infect **46:**49-55.

178. **Salama, N., K. Guillemin, T. K. McDaniel, G. Sherlock, L. Tompkins, and S. Falkow.** 2000. A whole-genome microarray reveals genetic diversity among *Helicobacter pylori* strains. Proc Natl Acad Sci U S A **97:**14668-73.

179. **Sambrook, J., Fritsch, E.F., and Maniatis, T.** 1989. Molecular cloning: a laboratory manual, 2nd ed. Cold Spring Harbor Laboratory Press, Cold Spring Harbor, New York.

180. **Sato, F., N. Saito, K. Konishi, E. Shoji, M. Kato, H. Takeda, T. Sugiyama, and M. Asaka.** 2003. Ultrastructural observation of *Helicobacter pylori* in glucose-supplemented culture media. J Med Microbiol **52:**675-9.

181. **Savvides, S. N., H. J. Yeo, M. R. Beck, F. Blaesing, R. Lurz, E. Lanka, R. Buhrdorf, W. Fischer, R. Haas, and G. Waksman.** 2003. VirB11 ATPases are dynamic hexameric assemblies: new insights into bacterial type IV secretion. Embo J **22:**1969-80.

182. **Savvides, S. N., Yeo, H., Beck, M.R., Blaesing, F., Lurz, R., Lanka, E., Buhrdorf, R., Fischer, W., Haas, R., and Waksman, G.** 2003. VirB11 ATPases are dynamic hexameric assemblies: new insights into bacterial type IV secretion. EMBO Journal **22:**1969-1980.

183. **Schroder, G., and E. Lanka.** 2005. The mating pair formation system of conjugative plasmids-A versatile secretion machinery for transfer of proteins and DNA. Plasmid **54:**1-25.

184. **Schulein, R., Guye, P., Rhomberg, T.A., Schmid, M.C., Schröder, G., Vergunst, A.C., Carena, I., and Dehio, C.** 2005. A bipartite signal mediates the transfer of type IV secretion substrates of *Bartonella henselae* into human cells. Proceedings of the National Academy of Sciences of the United States of America **102:**856-861.

185. **Segal, E. d., Cha, J., Lo, J., Falkow, S., and Tompkins, L.S.** 1999. Altered states: involvement of phosphorylated CagA in the induction of host cellular growth changes by *Helicobacter pylori*. Proceedings of the National Academy of Sciences of the United States of America **96:**14559-14564.

186. **Segal, E. D., J. Shon, and L. S. Tompkins.** 1992. Characterization of *Helicobacter pylori* urease mutants. Infect Immun **60:**1883-9.

187. **Selbach, M., S. Moese, S. Backert, P. R. Jungblut, and T. F. Meyer.** 2004. The *Helicobacter pylori* CagA protein induces tyrosine dephosphorylation of ezrin. Proteomics **4:**2961-8.

188. **Selbach, M., S. Moese, C. R. Hauck, T. F. Meyer, and S. Backert.** 2002. Src is the kinase of the *Helicobacter pylori* CagA protein *in vitro* and *in vivo*. J Biol Chem **277:**6775-8.

189. **Selbach, M., S. Moese, R. Hurwitz, C. R. Hauck, T. F. Meyer, and S. Backert.** 2003. The *Helicobacter pylori* CagA protein induces cortactin dephosphorylation and actin rearrangement by c-Src inactivation. Embo J **22:**515-28.

190. **Selbach, M., S. Moese, T. F. Meyer, and S. Backert.** 2002. Functional analysis of the *Helicobacter pylori* cag pathogenicity island reveals both VirD4-CagA-dependent and VirD4-CagA-independent mechanisms. Infect Immun **70:**665-71.

191. **Seubert, A., Hiestand, R., de la Cruz, F., and Dehio, C.** 2003. A bacterial conjugation machinery recruited for pathogenesis. Molecular Microbiology **49:**1253-1266.

192. **Seydel, A., Tasca, E., Berti, D., Rappuoli, R., Del Giudice, G., and Montecucco, C.** 2002. Characterization and immunogenicity of the CagF protien of the *cag* pathogenicity island of *Helicobacter pylori*. Infection and Immunity **70:**6568-6470.

193. **Shamaei-Tousi, A., Cahill, R., and Frankel, G.** 2004. Interaction between protein subunits of the type IV secretion system of *Bartonella henselae*. Journal of Bacteriology **186:**4796-4801.

194. **Shao, F., P. O. Vacratsis, Z. Bao, K. E. Bowers, C. A. Fierke, and J. E. Dixon.** 2003. Biochemical characterization of the Yersinia YopT protease: cleavage site and recognition elements in Rho GTPases. Proc Natl Acad Sci U S A **100:**904-9.

195. **She, F. F., J. Y. Lin, J. Y. Liu, C. Huang, and D. H. Su.** 2003. Virulence of water-induced coccoid *Helicobacter pylori* and its experimental infection in mice. World J Gastroenterol **9:**516-20.

196. **She, F. F., D. H. Su, J. Y. Lin, and L. Y. Zhou.** 2001. Virulence and potential pathogenicity of coccoid *Helicobacter pylori* induced by antibiotics. World J Gastroenterol **7:**254-8.

197. **Sherer, N. M., M. J. Lehmann, L. F. Jimenez-Soto, C. Horensavitz, M. Pypaert, and W. Mothes.** 2007. Retroviruses can establish filopodial bridges for efficient cell-to-cell transmission. Nat Cell Biol **9:**310-5.

198. **Shimomura, H., S. Hayashi, K. Yokota, K. Oguma, and Y. Hirai.** 2004. Alteration in the composition of cholesteryl glucosides and other lipids in *Helicobacter pylori* undergoing morphological change from spiral to coccoid form. FEMS Microbiol Lett **237:**407-13.

199. **Shirasu, K., and C. I. Kado.** 1993. Membrane location of the Ti plasmid VirB proteins involved in the biosynthesis of a pilin-like conjugative structure on *Agrobacterium tumefaciens*. FEMS Microbiol Lett **111:**287-94.

200. **Shirasu, K., Koukolikova-Nicola, Z., Hohn, B., Kado, C.I.** 1994. An inner-membrane-associated virulence protein essential for T-DNA transfer from *Agrobacterium tumefaciens* to plants exhibits ATPase activity and similarities to conjugative transfer genes. Molecular Microbiology **11:**581-588.

201. **Smith, T. G., J. M. Lim, M. V. Weinberg, L. Wells, and T. R. Hoover.** 2007. Direct analysis of the extracellular proteome from two strains of *Helicobacter pylori*. Proteomics **7:**2240-5.

202. **Smoot, D. T., J. H. Resau, T. Naab, B. C. Desbordes, T. Gilliam, K. Bull-Henry, S. B. Curry, J. Nidiry, J. Sewchand, K. Mills-Robertson, and et al.** 1993. Adherence of *Helicobacter pylori* to cultured human gastric epithelial cells. Infect Immun **61:**350-5.

203. **Stanley, J., D. Linton, A. P. Burnens, F. E. Dewhirst, S. L. On, A. Porter, R. J. Owen, and M. Costas.** 1994. *Helicobacter pullorum* sp. nov.-genotype and

phenotype of a new species isolated from poultry and from human patients with gastroenteritis. Microbiology **140 (Pt 12):**3441-9.

204. **Stein, M., Bagnoli, F., Halenbeck, R., Rappouli, R., Fantl, W.J., and Covacci, A.** 2002. c-Src/Lyn kinases activate *Helicobacter pylori* CagA through tyrosine phosphorylation of the EPIYA motifs. Molecular Microbiology **43:**971-980.

205. **Stein, M., Rappuoli, R., and Covacci, A.** 2000. Tyrosine phosphorylation of the *Helicobacter pylori* CagA antigen after *cag*-driven host cell translocation. Proceedings of the National Academy of Sciences of the United States of America **97:**1263-1268.

206. **Su, B., P. M. Hellstrom, C. Rubio, J. Celik, M. Granstrom, and S. Normark.** 1998. Type I *Helicobacter pylori* shows Lewis(b)-independent adherence to gastric cells requiring *de novo* protein synthesis in both host and bacteria. J Infect Dis **178:**1379-90.

207. **Suerbaum, S., and Michetti, P.** 2002. *Helicobacter pylori* infection. New England Journal of Medicine **347:**1175-1179.

208. **Suzuki, M., H. Mimuro, T. Suzuki, M. Park, T. Yamamoto, and C. Sasakawa.** 2005. Interaction of CagA with Crk plays an important role in *Helicobacter pylori*-induced loss of gastric epithelial cell adhesion. J Exp Med **202:**1235-47.

209. **Tammer, I., S. Brandt, R. Hartig, W. Konig, and S. Backert.** 2007. Activation of Abl by *Helicobacter pylori*: a novel kinase for CagA and crucial mediator of host cell scattering. Gastroenterology **132:**1309-19.

210. **Tanaka, J., Suzuki, T., Mimuro, H., and Sasakawa, C.** 2003. Structural definition on the surface of *Helicobacter pylori* type IV secretion apparatus. Cellular Microbiology **5:**395-404.

211. **Tato, I., Zunzunegui, S., de la Cruz, F., and Cabezon, E.** 2005. TrwB, the coupling protein involved in DNA transport during bacterial conjugation, is a DNA-dependent ATPase. Proceedings of the National Academy of Sciences of the United States of America **102:**8156-8161.

212. **Telford, J. L., M. A. Barocchi, I. Margarit, R. Rappuoli, and G. Grandi.** 2006. Pili in gram-positive pathogens. Nat Rev Microbiol **4:**509-19.

213. **Terradot, L., Durnell, N., Li, D., Ory, J., Labinge, A., Legrain, P., Colland, F., and Waksman, G.** 2004. Biochemical characterization of protein complexes from the *Helicobacter pylori* protein interaction map: strategies for complex formation and evidence for novel interactions within type IV secretion systems. Molecular and Cellular Proteomics **3:**809-819.

214. **Tomb, J. F., O. White, A. R. Kerlavage, R. A. Clayton, G. G. Sutton, R. D. Fleischmann, K. A. Ketchum, H. P. Klenk, S. Gill, B. A. Dougherty, K. Nelson, J. Quackenbush, L. Zhou, E. F. Kirkness, S. Peterson, B. Loftus, D. Richardson, R. Dodson, H. G. Khalak, A. Glodek, K. McKenney, L. M. Fitzegerald, N. Lee, M. D. Adams, E. K. Hickey, D. E. Berg, J. D. Gocayne, T. R. Utterback, J. D. Peterson, J. M. Kelley, M. D. Cotton, J. M. Weidman, C. Fujii, C. Bowman, L. Watthey, E. Wallin, W. S. Hayes, M. Borodovsky, P. D. Karp, H. O. Smith, C. M. Fraser, and J. C. Venter.** 1997. The complete genome sequence of the gastric pathogen *Helicobacter pylori*. Nature **388:**539-47.

215. **Tominaga, K., N. Hamasaki, T. Watanabe, T. Uchida, Y. Fujiwara, O. Takaishi, K. Higuchi, T. Arakawa, E. Ishii, K. Kobayashi, I. Yano, and T. Kuroki.** 1999. Effect of culture conditions on morphological changes of *Helicobacter pylori*. J Gastroenterol **34 Suppl 11:**28-31.

216. **Tonello, F., W. G. Dundon, B. Satin, M. Molinari, G. Tognon, G. Grandi, G. Del Giudice, R. Rappuoli, and C. Montecucco.** 1999. The *Helicobacter pylori* neutrophil-activating protein is an iron-binding protein with dodecameric structure. Mol Microbiol **34:**238-46.

217. **Totten, P. A., C. L. Fennell, F. C. Tenover, J. M. Wezenberg, P. L. Perine, W. E. Stamm, and K. K. Holmes.** 1985. *Campylobacter cinaedi* (sp. nov.) and *Campylobacter fennelliae* (sp. nov.): two new *Campylobacter* species associated with enteric disease in homosexual men. J Infect Dis **151:**131-9.

218. **Tsutsumi, R., Higashi, H., Higuchi, M., Okada, M., and Hatakeyama, M.** 2003. Attenuation of *Helicobacter pylori* CagA x SHP-2 signaling by interaction between CagA and C-terminal Src kinase. Journal of Biological Chemistry **278:**3664-3670.

219. **Tsutsumi, R., A. Takahashi, T. Azuma, H. Higashi, and M. Hatakeyama.** 2006. Focal adhesion kinase is a substrate and downstream effector of SHP-2 complexed with *Helicobacter pylori* CagA. Mol Cell Biol **26:**261-76.

220. **Tummuru, M. K., Cover, T.L., and Blaser, M.J.** 1993. Cloning and expression of a high-molecular-mass major antigen of *Helicobacter pylori:* evidence of linkage to cytotoxin production. Infection and Immunity **61:**1799-1809.

221. **Uemura, N., Okamoto, S., Yamamoto, S., Matsumura, N., Yamaguchi, S., Yamakido, M., Taniyama, K., Sasaki, N., and Schlemper, R.** 2001. *Helicobacter pylori* infection and the development of gastric cancer. New England Journal of Medicine **345:**784-789.

222. **Vergunst, A. C., Schrammeijer, B., Den Dulk-Ras, A., De Vlaam, C.M.T., Regensburg-Tuink, T.J.G., and Hooykaas, P.J.J.** 2000. VirB/D4-dependent protein translocation from *Agrobacterium* into plant cells. Science **290:**979-982.

223. **Wang, Y., K. P. Roos, and D. E. Taylor.** 1993. Transformation of *Helicobacter pylori* by chromosomal metronidazole resistance and by a plasmid with a selectable chloramphenicol resistance marker. J Gen Microbiol **139:**2485-93.

224. **Woodward, M. P., W. W. Young, Jr., and R. A. Bloodgood.** 1985. Detection of monoclonal antibodies specific for carbohydrate epitopes using periodate oxidation. J Immunol Methods **78:**143-53.

225. **Wotherspoon, A. C., C. Ortiz-Hidalgo, M. R. Falzon, and P. G. Isaacson.** 1991. *Helicobacter pylori*-associated gastritis and primary B-cell gastric lymphoma. Lancet **338:**1175-6.

226. **Wu, B., Y. Zhang, R. Zheng, C. Guo, and P. G. Wang.** 2002. Bifunctional phosphomannose isomerase/GDP-D-mannose pyrophosphorylase is the point of control for GDP-D-mannose biosynthesis in *Helicobacter pylori.* FEBS Lett **519:**87-92.

227. **Xiang, Z., Censini, S., Bayeli, R.B., Telford, J.L, Figura, N., Rappouli, R., and Covacci, A.** 1995. Analysis of expression of CagA and VacA virulence factors in 43 strains of *Helicobacter pylori* reveals that clinical isolates can be

divided into two major types and that CagA is not necessary for expression of the vacuolating cytotoxin. Infection and Immunity **63:**94-98.

228. **Yanagawa, R., K. Otsuki, and T. Tokui.** 1968. Electron microscopy of fine structure of *Corynebacterium renale* with special reference to pili. Jpn J Vet Res **16:**31-7.

229. **Yeo, H., and G. Waksman.** 2004. Unveiling molecular scaffolds of the type IV secretion system. Journal of Bacteriology **186:**1919-1926.

230. **Yeo, H. J., S. N. Savvides, A. B. Herr, E. Lanka, and G. Waksman.** 2000. Crystal structure of the hexameric traffic ATPase of the *Helicobacter pylori* type IV secretion system. Mol Cell **6:**1461-72.

231. **Yokoyama, K., Higashi, H., Ishikawa, S., Fujii, Y., Kondo, S., Kato, H., Azuma, T., Wada, A., Hirayama, T., Aburatani, H., and Hatakeyama, M.** 2005. Functional antagonism between *Helicobacter pylori* CagA and vacuolating toxin VacA in control of the NFAT signaling pathway in gastric epithelial cells. Proceedings of the National Academy of Sciences of the United States of America **102:**9661-9666.

232. **Yoshida, M., Wakatsuki, Y., Kobayashi, Y., Itoh, T., Murakami, K., Mizoguchi, A., Usui, T., Chiba, T., and Kita, T.** 1999. Cloning and characterization of a novel membrane-associated antigenic protein of *Helicobacter pylori*. Infection and Immunity **67:**286-293.

233. **Yoshiyama, H., and T. Nakazawa.** 2000. Unique mechanism of Helicobacter pylori for colonizing the gastric mucus. Microbes Infect **2:**55-60.

234. **Yuan, Q., A. Carle, C. Gao, D. Sivanesan, K. A. Aly, C. Hoppner, L. Krall, N. Domke, and C. Baron.** 2005. Identification of the VirB4-VirB8-VirB5-VirB2 pilus assembly sequence of type IV secretion systems. J Biol Chem **280:**26349-59.

235. **Zahrl, D., M. Wagner, K. Bischof, M. Bayer, B. Zavecz, A. Beranek, C. Ruckenstuhl, G. E. Zarfel, and G. Koraimann.** 2005. Peptidoglycan degradation by specialized lytic transglycosylases associated with type III and type IV secretion systems. Microbiology **151:**3455-67.

236. **Zahrl, D., M. Wagner, K. Bischof, and G. Koraimann.** 2006. Expression and assembly of a functional type IV secretion system elicit extracytoplasmic and cytoplasmic stress responses in *Escherichia coli*. J Bacteriol **188:**6611-21.

237. **Zeaiter, Z., D. Cohen, A. Musch, F. Bagnoli, A. Covacci, and M. Stein.** 2008. Analysis of detergent-resistant membranes of *Helicobacter pylori* infected gastric adenocarcinoma cells reveals a role for MARK2/Par1b in CagA-mediated disruption of cellular polarity. Cell Microbiol **10:**781-94.

238. **Zhong, Q., S. H. Shao, L. L. Cui, R. H. Mu, X. L. Ju, and S. R. Dong.** 2007. Type IV secretion system in *Helicobacter pylori*: a new insight into pathogenicity. Chin Med J (Engl) **120:**2138-42.

239. **Zupan, J. R., Ward, D., and Zambryski, P.** 1998. Assembly of the VirB transport complex for DNA transfer from *Agrobacterium tumefaciens* to plant cells. Current Opinion in Microbiology **1:**649-655.

240. **Zusman, T., G. Yerushalmi, and G. Segal.** 2003. Functional similarities between the icm/dot pathogenesis systems of *Coxiella burnetii* and *Legionella pneumophila*. Infect Immun **71:**3714-23.